TETRAVALENT METAL PHOSPHONATE-PHOSPHATE HYBRIDS AS CATALYST SUPPORTS AND ION EXCHANGE MATERIALS

A Dissertation

by

RITA MARIE SILBERNAGEL

Submitted to the Office of Graduate and Professional Studies of
Texas A&M University
in partial fulfillment of the requirements for the degree of

DOCTOR OF PHILOSOPHY

Chair of Committee,	Abraham Clearfield
Co-Chair of Committee,	Janet Bluemel
Committee Members,	Charles M. Folden III
	Oleg Ozerov
Head of Department,	Simon North

May 2016

Major Subject: Chemistry

ABSTRACT

This work centers on recycling of Rh catalysts and utilizing ion exchange to separate nuclear waste. In the area of Rh-type catalyst supports, non-porous zirconium phosphate nanoplatelets (ZrP) were utilized to provide sufficient outside surface area while still being easily separable from the reaction mixtures. First, a phosphine linker containing an ethoxysilyl group, $(EtO)_3Si(CH_2)_3PPh_2$, is reacted with ZrP. Addition of Wilkinson's catalyst $ClRh(PPh_3)_3$ to the phosphine-modified ZrP gives the immobilized catalyst. In the absence of pore diffusion, the catalytic hydrogenation of 1-dodecene using the Rh-type immobilized catalyst proceeds with unprecedented speed and the catalyst can be recovered and recycled 15 times.

New materials were synthesized that are comprised of Zr/Sn phosphonate-phosphate hybrids. The general formula for these materials is $M(O_3PC_6H_4PO_3)_{1-x/2}(APO_4)_x \bullet nH_2O$, where M = Zr^{4+}, Sn^{4+}; A = H, Na, K; and x = 0, 0.5, 0.8, 1.0, 1.33, 1.6. These materials have a preference for ions of high charge (3+, 4+) over those with lower charge (1+, 2+). From this charge-based affinity and pH modification, separations can be achieved with Nd^{3+}/Cs^{+} separation factors $\geq$ 100. The stability of these materials to 3.18 MGy gamma radiation was also observed with performance and structure retained. Greater than 99% removal of radioactive Am(III) from solution was obtained. Similar materials have also been utilized to explore rare earth recovery from Compact Fluorescent Lamps and Cr(VI) removal from wastewater solutions.

DEDICATION

The work is dedicated to my family and friends for their support and encouragement throughout the years.

ACKNOWLEDGEMENTS

I would like to thank my committee chairs, Dr. Abraham Clearfield and Dr. Janet Bluemel, and my committee members, Dr. Folden and Dr. Ozerov, for their guidance and effort throughout my time at Texas A&M. To Drs. Folden and Ozerov, I have always respected you and am honored that you agreed to be part of my committee.

Special thanks to Thomas Shehee, David Hobbs, and Donald Reed who were my hosts and mentors at Savannah River and Los Alamos National Laboratories. Thank you for welcoming me into your homes and offering your expertise in the area of nuclear chemistry. I am forever grateful for your contributions.

I want to acknowledge the Clearfield and Bluemel group members from the past and present. They have offered a large range of knowledge, support, and companionship. I especially would like to point out the publication collaborators: Caroline Martin, Agustin Diaz, Eric Steffensmeier, Brian Mosby, and Yuwei Kan.

I would also like to acknowledge Loren Press, Jessica DeMott, Billy McCulloch, Rodrigo Ramirez, Joseph Baker, Jacqueline Pope, Marisa Alfonso, Jon Burns, Alex Kosanovich, Atashi Mukherjee-Bell, Bryan Foley, and Kevin Gagnon who offered their research guidance.

I have been fortunate for many undergraduates who have spent time working in the Clearfield laboratory with me (earliest to latest): Hannah Galvan, Renee Gomez, Josh Levin, Caroline Martin, Alyssa Smith, and Randinu Pulukkody. Thank you for your time and hard work. I enjoyed working with each of you.

I want to extend my gratitude to the US Department of Energy Nuclear Engineering University Program initiative, which provided the bulk of my research and funding for the past three years.

Thank you to Ron Carter for help in securing the Aggie Green Fund recycling grant. You are such an asset to this department. Thank you for all that you do.

I must include Dr. Michelle Driessen from the University of Minnesota Chemistry Department. I remember telling you in year two how my environmental science degree did not have enough chemistry background and you suggested that I pursue a degree in chemistry. I remember actually laughing out loud at the idea. Thanks for making my wheels turn. Who would have thought that I would have made it this far?

I want to thank my family for their support throughout the years. To my mom and dad who kept telling everyone I was getting a Master's Degree in Chemistry: It is nice to know that failing out of here would have still made you proud!! It is amazing to be the first person in my entire lineage to receive a PhD but I certainly will not be the last.

Dr. Janet Bluemel, I am thoroughly fortunate to have you as my co-advisor. You have been crucial to my success here at Texas A&M, which has undoubtedly landed me placement in the competitive BASF PhD Professional Development Program. Your insight and knowledge propelled me forward and I am very thankful.

Finally, I gratefully acknowledge Dr. Abraham Clearfield. Thank you for your support and belief in me throughout the years. I have yet to meet a more compassionate and positive individual. Working with you throughout my time here has been a real gift and I know that my success is directly linked with your trust in my abilities. Thank you.

NOMENCLATURE

ACS	Alyssa Smith, Undergrad Technician
An	Actinides
BNL	Brookhaven National Laboratory
CFL	Compact Fluorescent Lamp
CHM	Caroline Martin, Undergrad Technician
CP	Cross Polarization
DOE	Department of Energy
EA	Elemental Analysis
EXAFS	Extended X-ray Absorbance Fine Structure
Gray	SI Unit of Absorbed Dose
HRMAS	High Resolution Magic Angle Spinning
ICP-MS	Inductively Coupled Plasma-Mass Spectrometer
K_d	Dissociation Constant for Measuring Ion Uptake
LANL	Los Alamos National Laboratory
Ln	Lanthanides
MAS	Magic Angle Spinning
MGy	Megagray, 10^6 Gray.
NEUP	Nuclear Engineering University Program
PDF	Atomic Pair Distribution Function Theory
PXRD	Powder X-ray Diffraction

REE	Rare Earth Elements
RMS	Rita Marie Silbernagel
RP	Randinu Pulukkody, Undergrad Technician
SEM	Scanning Electron Microscope
SF	Separation Factor
SRNL	Savannah River National Laboratory
TA	TA Instruments, Maker of TGA
TEM	Transmission Electron Microscope
TGA	Thermogravimetric Analysis
ZrP	Zirconium Phosphate

TABLE OF CONTENTS

Page

LIST OF FIGURES

Page

LIST OF TABLES

Page

CHAPTER I

INTRODUCTION

1.1 Summary of Research Accomplishments

Research described herein is centered on recycling of scarce or environmentally hazardous materials in hopes of generating a renewable method for power and chemical feedstock production. My passion for recycling is evident in my research and private life. I successfully wrote a grant and received funding from the Aggie Green Fund to install convenient, color-coded recycling containers for cans, bottles, and paper and they are present within Chemistry, Reed McDonald, and Heldenfels buildings.

The first project of my research was a collaborative study between Drs. Bluemel and Clearfield on utilizing zirconium phosphate as a support material for a recyclable Wilkinson's catalyst and is described in Chapter II. This Rh-type immobilized catalyst was able to be recycled 15 times in a batchwise manner with little change in catalytic performance.

The second focus of my work was with Dr. Clearfield, in collaboration with Savannah River and Los Alamos National Laboratories. This work involved use of Zr/Sn(IV) phosphonates for the recycling of nuclear waste, which is featured in Chapters III and

IV. New materials were synthesized that were shown to be stable toward gamma radiation and were able to remove 99% of radioactive Americium-241 from solution.

Continued work with these materials resulted in new applications from Cr(VI) removal from wastewater (Chapter IV), and rare earth recovery from Compact Fluorescent Lamps (CFLs), which is discussed in Chapter V. Additional studies on traditional phosphonate-phosphate hybrids are listed in Appendix A.

1.2 Utilizing Zirconium Phosphate as a Support for Immobilized Wilkinson's Catalyst

α-Zirconium phosphate ($Zr(HPO_4)_2 \bullet H_2O$) is a layered inorganic material[1,2] with applications as a solid support for immobilized catalysts[3], as well as ion exchange materials[4], drug delivery[5,6], and nanocomposites[7,8]. Chapter II will focus on the use of α-zirconium phosphate (ZrP) as a solid support for immobilized Wilkinson's catalyst, $ClRh(PPh_3)_3$. Immobilized catalysts combine the advantages of homogeneous and heterogeneous catalysts by binding a homogeneous catalyst with a linker to a solid support, as seen in Figure 1. In this light, $ClRh(PPh_3)_3$ is immobilized on ZrP through use of an ethoxysilyl group, $(EtO)_3Si(CH_2)_3PPh_2$ (1). The addition of 1 to ZrP results in silyl-modified ZrP (1i). Upon addition of $ClRh(PPh_3)_3$ to 1i, the catalytic hydrogenation of 1-dodecene was studied at room temperature. The immobilized catalyst could be recycled 15 times in a batchwise manner.[3]

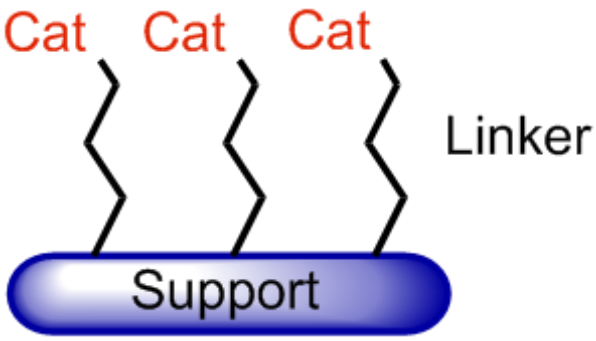

Figure 1: A diagram of an immobilized catalyst linked to a solid support.

As the catalysis progressed, the support changed its color from salmon-pink to dark gray, thus suggesting the formation of Rh nanoparticles,[9] which was confirmed by TEM analyses. Due to the flat platelet surface and low porosity, ZrP is an ideal support material because the linker and catalysts are readily available and easy to locate for the substrate on the surface, which allows for improved speed compared to other highly porous supports with diffusion issues. The impact of this study is the development of a recyclable Wilkinson-type catalyst, which allows for fast catalytic runs and a simple separation of the product from Wilkinson's catalyst.

1.3 Preparation and Characteristics of Zr/Sn Phosphonate-Phosphate Hybrids for the Separation of Nuclear Waste

During fission of U-235 in generating commercial nuclear power, actinides and lanthanides are produced and at least 95% of the spent fuel can be recycled. A diagram of the fuel before and after irradiation is shown in Figure 2.[10]

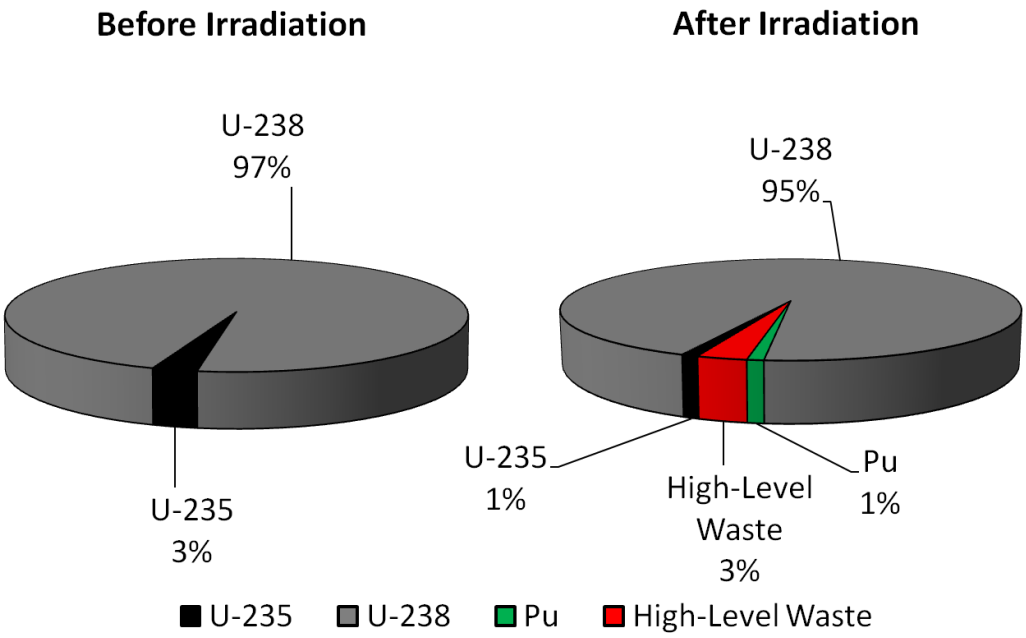

Figure 2: Fuel before and after irradiation from commercial nuclear power.

The 3% high-level radioactive waste contains 95% of the radioactive content.[11] This high-level waste consists of 0.1% minor actinides (such as Am, Cm), 0.9% lanthanides, and 2% are other fission products (such as Sr, Cs, Tc).[11] The objective is to cleanly separate the lanthanides and Cm from the reusable actinides to facilitate recycling for continued nuclear power generation.[12] In order to achieve this, radiolytically robust solvents and materials are required for separations through use of solvent extraction and/or ion exchange.

A possible separation method involves using Zr/Sn (IV) phosphonate-phosphate ion exchangers[13-17], which are versatile Unconventional Metal-Organic Frameworks (UMOFs) of the general composition $M(O_3PC_6H_4PO_3)_{1-x/2}(APO_4)_x \bullet nH_2O$, M = Zr^{4+},

Sn^{4+} and A = H, Na, K. They are three-dimensional porous solids that are stable in air up to 450 ºC. A study analyzing the varying ratio of phosphonate ($O_3PC_6H_4PO_3$) to phosphate (HPO_4) of H-Zr compounds is discussed in Chapter III.[18] These materials show varying ion preference depending on the amount of phosphate addition. The tradition preference for ion exchange has been 3+ ions over ions of lower charge (1+, 2+); however, as additional phosphate is added, the preference for ions of 1+ charge is enhanced but still not larger than the affinity for 3+ ions.

Even more startling, is the performance of H-Zr/H-Sn samples without phosphate added. Surprisingly, these complex materials also remove 3+ ions from solution, which illustrates that the phosphate is not the only mechanism for ion exchange. In Chapter IV, their analytical characteristics and applications for actinide uptake and radiolytic stability will be demonstrated.[19] The impact of this study is the development of an inexpensive, simple way in which to separate the lanthanides from the actinides found in the spent nuclear fuel rods and to recover a portion of the usable fuel for a closed fuel cycle.

Many different varieties of the Zr/Sn samples have been prepared and are listed in Appendix A. Included is full PXRD and TGA analysis and a full table of samples with microprobe, TGA, and EA data.

1.4 Early Studies on the Utilization of H/Na-Zr Phosphonate-Phosphates for Cr(VI) Removal and Rare Earth Recovery from Compact Fluorescent Lamps

The Zr/Sn Phosphonate-Phosphates have shown ability for separations based on charge, with a preference for 3+ ions. In this light, we have probed several ions for removal from water including Cr^{3+}, which had 99% removal at a concentration of $1x10^{-4}$ M and a pH = 3 solution. In order to expand this knowledge to a possible Cr (III/VI) separation scheme, we also tested for Cr(VI) uptake. Cr(VI) is unlike anything ever tested previously with these materials. Cr(VI) typically exists as an anion at pH = 3 ($HCrO_4^-$ or $Cr_2O_7^{2-}$).[20] Sodium chromate ($Na_2Cr_2O_7$) will change forms depending upon the pH and concentration of the solution.[20] The H-Zr x = 0 phosphonate sample without phosphate was the only material able to achieve 99% uptake of $5x10^{-4}$ M Cr(VI) at pH = 3. During the uptake of Cr(VI), the yellow liquid became colorless and the white H-Zr solid turned yellow, thus showing presence of Cr(VI) and not Cr(III), which is blueish-green. The mechanism for Cr(VI) uptake is not well understood and will be expanded upon at a later time. This is the first case of anion uptake and is part of a preliminary study on the unusual behavior of the H-Zr phosphonate, as discussed in Chapter IV.

As an extension of our work with the uptake of lanthanides in spent fuel, we also reviewed other applications related to rare earth uptake. One such example of rare earth recovery is from phosphors present in Compact Fluorescent Lamps (CFLs). They account for 12% of the rare earth market and contain a large portion of critical yttrium.[21]

Due to mercury present in the lamps, collection is already required by law; thus, making rare earth recycling possible after mercury removal. Once the lanthanides are solubilized, they were exposed to the Na-Zr x = 1 phosphonate-phosphate hybrid and were able to achieve 99% removal of Y and Eu from CFL waste. Work on this project is discussed in Chapter V.

Future directions for each of these projects are briefly discussed in Chapter VI. The radioactive separations will continue into the next year as part of our three year funding initiative through the NEUP. Potential provisional patents may be applied for surrounding the Cr(VI) and rare earth recovery work.

CHAPTER II

WILKINSON-TYPE RH HYDROGENATION CATALYST IMMOBILIZED ON ZIRCONIUM PHOSPHATE NANOPLATELETS*

2.1 Overview

Immobilized catalysts can be obtained by using a linker to bind a homogeneous catalyst to a solid support. Ideally, immobilized catalysts combine the advantages of homogeneous and heterogeneous catalysts. Porous supports such as silica result in optimal recyclability, however, the catalytic reactions are slowed down by pore diffusion within the silica particles. Here, non-porous zirconium phosphate nanoplatelets (ZrP) are used as support material to bridge the gap between homogeneous and immobilized catalysts. ZrP nanoplatelets provide sufficient outside surface area, while still being easily separable from the reaction mixtures. First, a phosphine linker containing an ethoxysilyl group, $(EtO)_3Si(CH_2)_3PPh_2$ (1), is reacted with ZrP to give the phosphine-modified 1i. Addition of Wilkinson's catalyst $ClRh(PPh_3)_3$ to 1i gives, via ligand exchange, the immobilized catalyst 1i-Rh. In the absence of pore diffusion the catalytic hydrogenation of 1-dodecene using 1i-Rh proceeds with unprecedented speed and the catalyst can be recovered and recycled 15 times. In the course of the catalytic reaction

---

* Reproduced in part with permission from Silbernagel, R.; Diaz, A.; Steffensmeier, E.; Clearfield, A. Blümel, J. *J. Mol. Catal. A: Chem.* **2014**, *394*, 217-223. http://dx.doi.org/10.1016/j.molcata.2014.07.005

the mononuclear species forms catalytically active Rh nanoparticles on the surface. Finally it is demonstrated that $ClRh(PPh_3)_3$ can be bound to ZrP directly without linker. However, the catalytic activity of the resulting material ZrP-Rh does not quite match the favorable characteristics of 1i-Rh.

2.2 Introduction to Research

Immobilized catalysts combine in principle the advantages of homogeneous and heterogeneous catalysts and therefore they are of growing importance in academia and industry.[22-26] The most successful approach to obtain immobilized catalysts these days involves binding a homogeneous catalyst to a solid support with a linker. The linkers are typically bifunctional phosphines incorporating ethoxysilane groups for anchoring on oxide supports such as silica[27-30] or alumina[31]. The success of the immobilized catalysts is dependent on the linker type. Therefore, over the years mono- and bidentate chelate phosphine linkers have been explored for immobilized Ni,[32,33] Rh,[34-37] and Sonogashira Pd/Cu[38-40] catalyst systems. Most recently, new triphosphine linkers with short ($C_{1,2}$) and long (C_{4-11}) alkyl chains[9,41] and rigid scaffold linkers[37,42] have led to robust immobilized Ni acetylene cyclotrimerization and Rh olefin hydrogenation catalysts with unprecedented lifetimes. However, as a first step to test a new catalytic system, the classic and easily obtainable linker $(EtO)_3Si(CH_2)_3PPh_2$ (1) is still a good choice because of the ample already existing data base for comparison.[34-37]

Most of these data available refer to olefin hydrogenation,[9,34-37,43-49] which is of utmost importance for academia and industry. Additionally, only a few reactions in transition-metal catalysis have enjoyed a more detailed investigation than hydrogenation both in solution and on surfaces.[34-37,43-49] Therefore, in this contribution we will focus on the hydrogenation of 1-dodecene as the catalytic test reaction.

Especially for industrial applications where reactor sizes and prices prohibit large amounts of bulk, porous support materials are sought because they provide a large specific surface area and therefore a maximal number of binding sites for the catalysts and consequently high loading. The popular mesoporous silica with average pore diameters of 40 to 200 Å is also used most often in our work.[22,29-31,34-36] However, since the immobilized catalysts reside on the inner surface of the pores, the disadvantage of porous supports in general is that the necessary reaction time is prolonged because the substrates and products have to diffuse into and out of the pores. This effect is large and might increase reaction times substantially. For example, when silica with a pore diameter of 150 Å is used instead of the one with 40 Å, the hydrogenation of dodecene with an immobilized Rh catalyst takes only 30 hours instead of 120 hours under otherwise identical reaction conditions.[9] Therefore, an ideal support for bridging the gap between homogeneous and immobilized catalysts should provide a large external surface area which renders the tethered catalysts easily accessible to substrates without necessitating the diffusion into pores. Unfortunately, our experiments with non-porous silica (aerosil) with small particle sizes have been unsuccessful, as the material cannot be

handled in an inert gas stream and does not settle from suspensions. Other groups have attempted to use, for example, nanoalumina,[50] graphene oxide,[51] and layered phosphonate-modified materials[52,53] as supports. An interesting recent approach employed a zirconium phosphate/silica system.[54]

In the research presented in this chapter instead of porous oxides a layered zirconium phosphate (α-ZrP, in the following: ZrP) material that has been first described in 1964[1] has been used as the support for immobilized catalysts.[3] This material can be synthesized in a straightforward and reproducible manner.[2] The composition has been determined as $Zr(HPO_4)_2 \cdot H_2O$,[55-61] and the crystal structure has been elucidated as monoclinic space group $P2_1/n$.[2] The layered nature of ZrP is illustrated in Figure 3.[61]

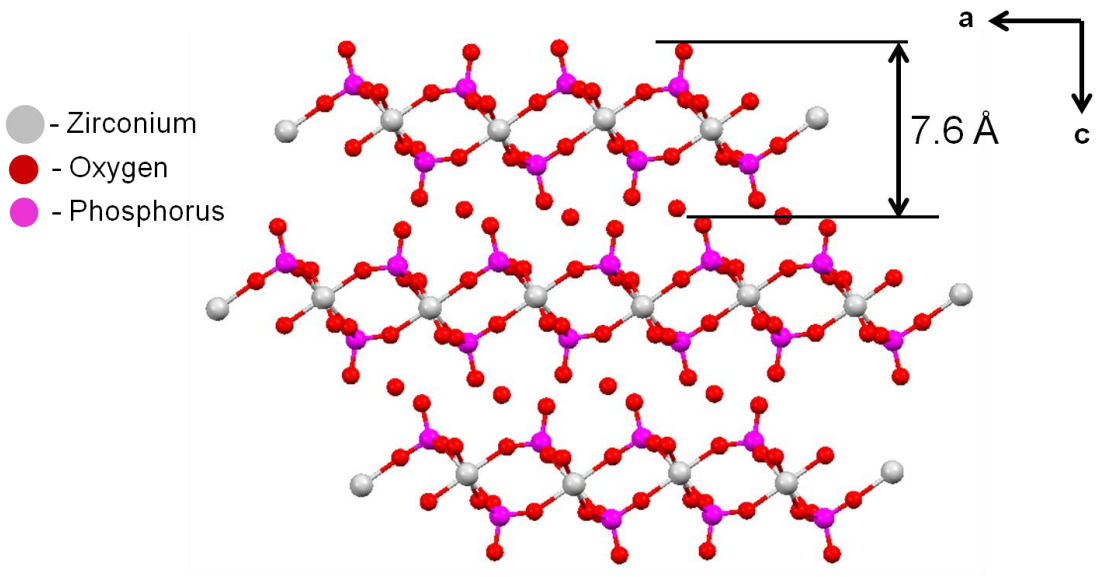

Figure 3: ZrP viewed down the b-axis showing the interlayer spacing and intercalated water molecules. Hydrogen atoms have been omitted for clarity.

Each Zr atom is bonded octahedrally to six different phosphate groups, while three of the O atoms of the phosphate groups are bonded to three different Zr atoms. The fourth O atom of each phosphate group is part of a surface OH group that extends into the interlayer region. The OH proton is acidic and can be used for surface modification, e.g. with chloro- or ethoxysilanes, epoxides, or isocyanates, or for ion exchange.[57-62]

Powder X-ray diffraction (PXRD) reveals that the interlayer spacing is 7.6 Å.[1,2]
In a first step, a Wilkinson-type Rh complex[34-37] is tethered to this ZrP support via the bifunctional phosphine $(EtO)_3Si(CH_2)_3PPh_2$ (1). The catalytic activity is then studied with respect to the hydrogenation of dodecene. In this way the missing link is filled into the gap between homogeneous and immobilized catalysts. All catalytically active centers should be fully exposed to the surrounding solution and thus easily accessible; therefore, fast reactions are expected and the results should not be blurred by pore diffusion.

Another incentive to radically change the nature of the support from silica to ZrP is that in the case of immobilized Rh catalysts on silica spherical Rh nanoparticles with very uniform and narrow size distribution form during hydrogenation.[9] Using a different and non-porous support material clarifies whether this nanoparticle formation is a universal feature when Rh catalysts are tethered by linkers with alkyl chains, or whether this only occurs on oxide supports. Another reason for testing a non-porous support is to investigate whether the size distribution and the regular shape of the nanoparticles in the case of silica were dominated by the pore structure as speculated in previous work.[9] In

this case, with ZrP as the support, the potential nanoparticles should have a higher tendency to agglomerate and they might exhibit more irregular structures. Overall, it is expected that, with ZrP as the support, highly active catalysts are obtained that mimic the performance of homogeneous catalysts, while they can easily be separated from the reaction mixture and recycled many times.

With every new type of support it is mandatory to make sure that the basic requirements for immobilization regarding the compatibility of linker, support, and transition metal complex are fulfilled. Most fundamentally, the ethoxysilane group of the linker should bind covalently and irreversibly to the support. Otherwise the catalyst will be in danger of leaching during catalysis. Importantly, especially with respect to ZrP as the support with traces of phosphoric acid potentially left in the material from its synthesis, it needs to be checked whether phosphonium salt formation occurs.[63,64] In this case the linker would no longer be able to coordinate to a transition metal center. Especially linkers with short alkyl chains might also decompose on the wrong type of support[65] or be prone to oxidation.[64,66]

With respect to the layered structure of the ZrP support it is also mandatory to check whether the linker is indeed only bound to the outside surface of the nanoplatelets, or whether it intercalates between the layers or even exfoliates them. In this unfavorable scenario diffusion of the substrate between the layers would again hinder the catalytic reaction or recovery of the material would be rendered problematic. Finally, one needs to

investigate whether transition metal complexes such as Wilkinson's catalyst with its medium sensitivity decompose on the reactive ZrP surface or retain their integrity. Furthermore, it has to be checked whether Wilkinson's catalyst can be bound to the surface even without a linker while retaining its catalytic activity and recyclability.

In summary, the aim of the work presented in this chapter is to follow the usual test protocol for new linker/support/catalyst systems, which incorporates the exploration of all points raised above using the bifunctional linker $(EtO)_3Si(CH_2)_3PPh_2$ (1) and Wilkinson's catalyst $ClRh(PPh_3)_3$. With this system it will ideally be possible to universally establish ZrP nanoplatelets as a practical non-porous alternative to the conventional mesoporous oxide supports. The olefin hydrogenation catalyst immobilized on the ZrP nanoplatelets with a bifunctional phosphine linker and without will be studied with respect to their activity and recyclability. Finally, the nature of the active species, whether they consist of immobilized homogeneous catalysts or nanoparticles, will be investigated.

2.3 Support Material

For the application as catalyst support material described in this chapter ZrP nanoplatelets in the size range of 150 to 400 nm have been prepared.[2,55,57-61,67] Figure 4 shows the SEM image of a representative sample with platelet sizes near 100 nm.

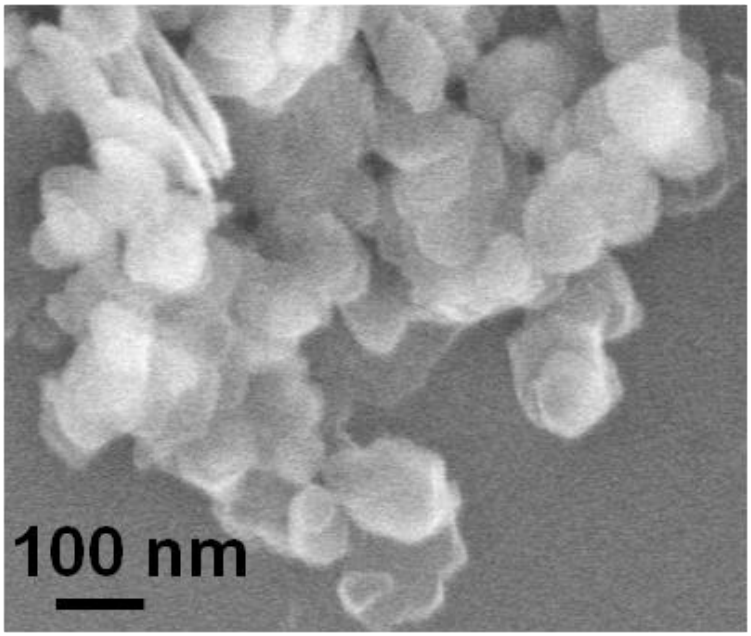

Figure 4: SEM image of zirconium phosphate (ZrP) nanoplatelets.

Unfortunately, the smaller platelets exhibit tendencies to agglomerate during the catalytic runs and thus the advantage of the easily accessible surface is lost. Other samples with small platelet sizes render their separation from the reaction mixture difficult by refusing to settle completely after the reaction, which is also obvious from the dark color of the supernatant after hydrogenation. Fortunately, the larger ZrP platelets with about 300 nm in size settle quickly after the catalytic reaction and only exhibit some agglomeration after extended periods of time. They also retain their specific surface area of 33.9 m^2/g.

2.4 Immobilization of the Linker

As presented in Figure 5, linker 1 has been immobilized on ZrP to form 1i using the standard procedure applied for immobilization on oxide supports.[29-40]. After heating a mixture of 1 and ZrP in toluene to 110 °C for 24 h, the resulting material 1i is separated from the reaction mixture by centrifugation and washed thoroughly with toluene. After drying, 1i is obtained as a white powder which is analyzed by TGA, PXRD, an electron microprobe, and solid-state NMR spectroscopy.[68,69]

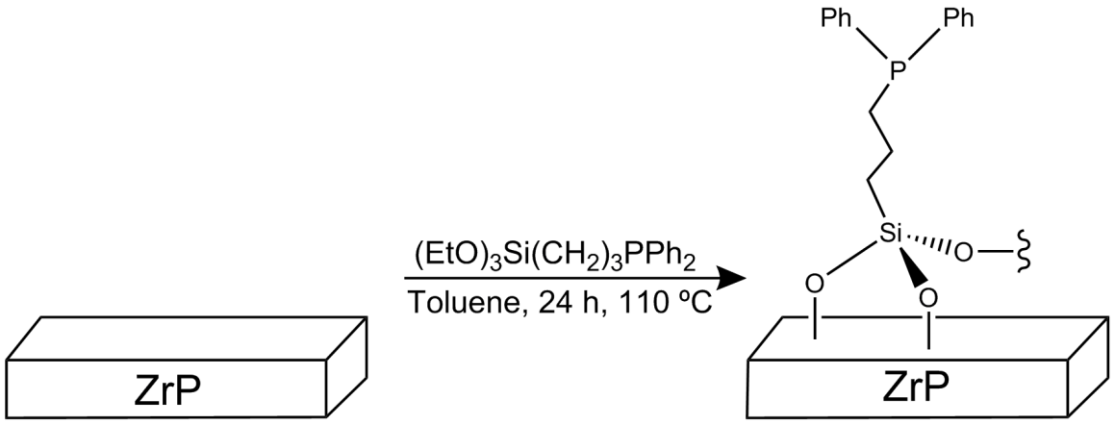

Figure 5: Surface modification of zirconium phosphate with the ethoxysilyl containing phosphine linker 1.

An overlay of the powder X-ray diffractogram of 1i with ZrP is shown in Figure 6. When comparing the powder diffraction pattern of pure ZrP with the pattern of 1i, it is obvious that the peaks are broadened substantially upon immobilization. This indicates that the surface modification lowers the crystallinity of the support. Most importantly, 1

does not intercalate between the ZrP layers during the immobilization step because the interlayer spacing of 7.6 Å remains unchanged. Therefore, we conclude that all linker molecules, as well as the Rh catalyst that will be coordinated to them later, are located on the outer surface of the nanoparticles. This will lead to a fast catalytic reaction since the substrate molecules do not have to diffuse in between the support layers.

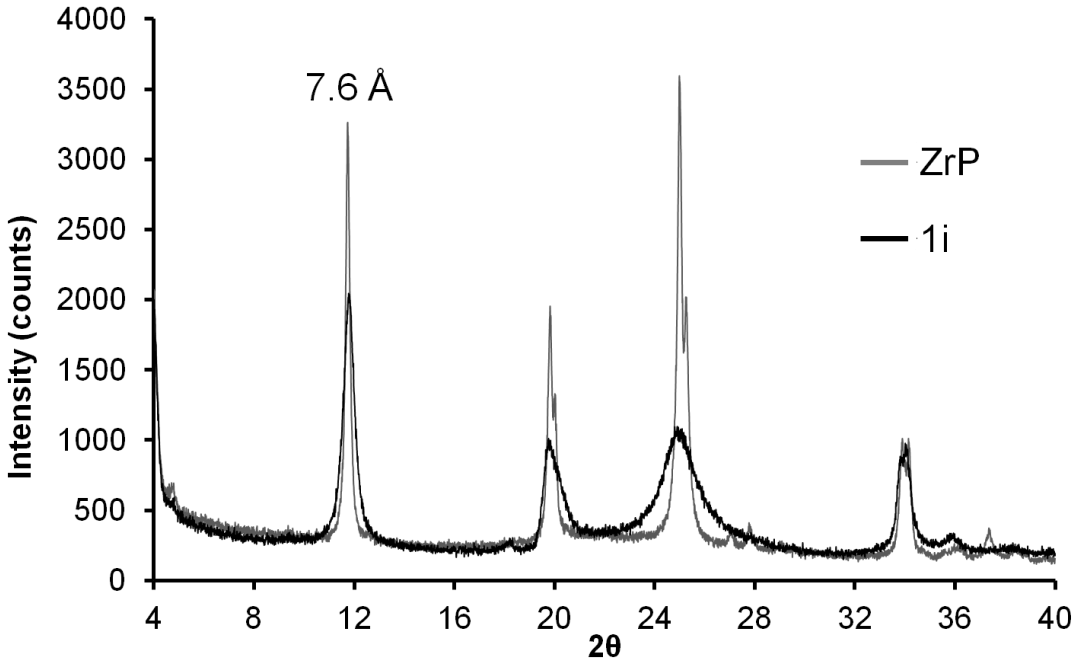

Figure 6: PXRD overlay of ZrP sample (grey) with 1i (black). Notice the broadness of the 1i peaks, indicating less crystalline ZrP particles.

Solid-state NMR spectroscopy is the most powerful method for characterizing linkers or catalysts immobilized on silica or alumina on the molecular level.[9,29-36,38-42,63-65] Since the majority of the linkers used in the community are bifunctional phosphines,

^{31}P CP/MAS NMR of the dry materials[29-36,38-42] or HRMAS NMR of slurries in solvents[9,31,38-40] are especially useful. Unfortunately, here the ^{31}P signal of the linker which is supposed to appear at ca. -18 ppm[31,63,64] is obscured by the huge signal of the ZrP support at about -19 ppm.[55,60,61] The signal shape and general appearance of the spectrum did not change when simple high-power decoupling was used instead of CP. However, in both cases the absence of a phosphine oxide signal which would have been expected at about 25 ppm[64,66] indicates that the immobilized linker is very robust and 1i can be handled in air when the material is dry. Furthermore, the absence of any phosphonium signal which would also be expected at about 25 ppm[63,64] proves that the phosphine is not quaternized by the acidic OH groups on the support surface. The ^{31}P CP/MAS measurement shows that careful washing of the latter is also sufficient to remove excess phosphoric acid which would result in a signal at 0 ppm.

Fortunately, the ^{29}Si CP/MAS spectrum of 1i (Figure 7) shows clearly one resonance even though the signal to noise ratio is not optimal because the overall content of linker on the platelets is low. Based on the chemical shift of about -69 ppm and in comparison with previous data[61] we conclude that, in contrast to the result after binding triethoxysilanes to well-dried silica,[29,30] there is no unreacted ethoxy group left at Si.

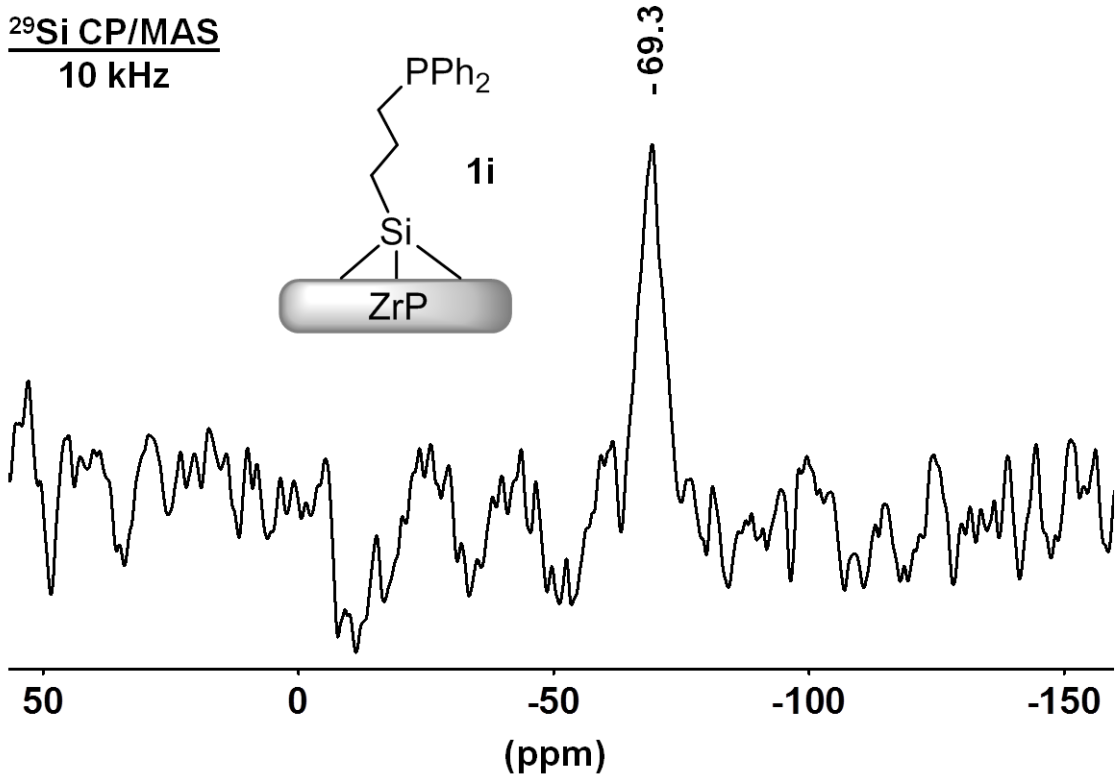

Figure 7: ^{29}Si CP/MAS NMR spectrum of 1i with ν_{rot} = 10 kHz.

The ^{13}C solid-state NMR spectrum corroborates this assumption. Therefore, besides the alkyl substituent at Si, there must be three oxygen atoms bound to either P or H. 1i can be bound to the ZrP support forming up to three covalent Si-O-P bridges, in analogy to forming three Si-O-Zn bridges when immobilizing ethoxysilanes on ZnO nanoparticles.[70] Although sterically not favored, this might be possible due to the nature of the surface which is not perfectly planar. Alternatively, one or two free or cross-linked silanol groups could be present in case of hydrolysis of the ethoxysilane groups during the immobilization step.

With respect to the robust anchoring of 1 on the surface which is proven by its resistance to leaching in spite of multiple washing cycles, there has to be at least one covalent Si-O-P connection. Cross-linking of the ethoxysilanes on the support surface cannot be excluded at this point, but any growth of a gel on the surface is unlikely due to the homogeneous distribution of the linker molecules on the smooth ZrP surface as seen by microprobe analysis (Figure 9). Furthermore, the presence of surface-detached, longer, and therefore mobile cross-linked arrays can be excluded by the absence of a ^{31}P HRMAS NMR signal of 1i.

The ^{13}C solid-state NMR spectrum of 1i (Figure 8) proves the covalent binding of the linker to the ZrP support because of the characteristic residual linewidths and chemical shift anisotropies (CSA)[69] of the signals. Although not resolved, the aryl carbon signal at about 127 ppm displays the typical large ^{13}C solid-state NMR CSA with the presence of rotational sidebands. Furthermore, in contrast to ethoxysilane-silica systems,[29-31] no ethoxy carbon signals are present, corroborating the above assumption regarding the binding mode. Up to three Si-O-P bonds are formed besides silanol groups due to hydrolysis. Again, the poor signal to noise ratio is a consequence of the comparatively low surface area and therefore linker contents. Nevertheless the carbon signals for the alkyl chain of 1i can be identified and assigned (Figure 8) in analogy to cases of similar immobilized linkers.[33]

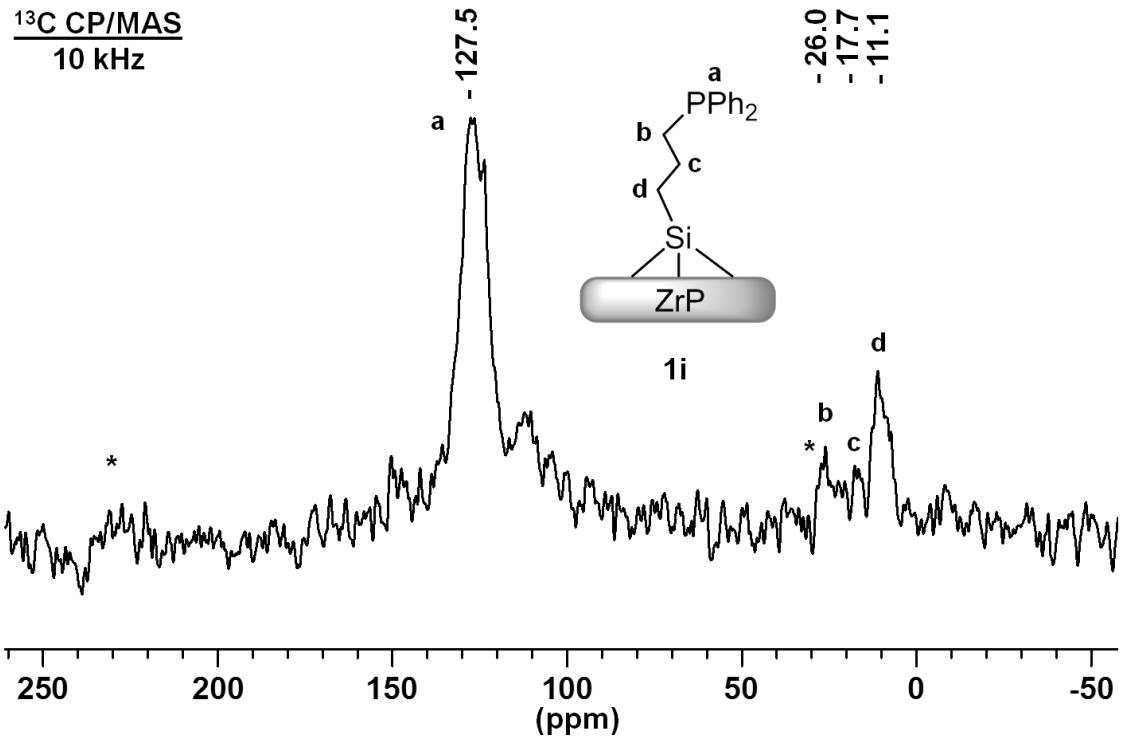

Figure 8: ^{13}C CP/MAS NMR spectrum of 1i with ν_{rot} = 10 kHz. Asterisks denote rotational sidebands of the aryl carbon signal.

The surface coverage of 1i with linker 1 has been obtained by determining the Si content of a sample with ICP-MS and it corresponds to 30 linker molecules (6.8 x 10^{-3} mmol of 1) per 100 nm^2 of surface area.

In order to determine whether the distribution of the supported linker is homogeneous on the surface of 1i, the material is subjected to microprobe analysis. The results are given in Table 1 and Figure 9. As the microprobe image shows (Figure 9), the linker distribution is even overall despite some far apart black spots from the loose powder on the pressed pellet.

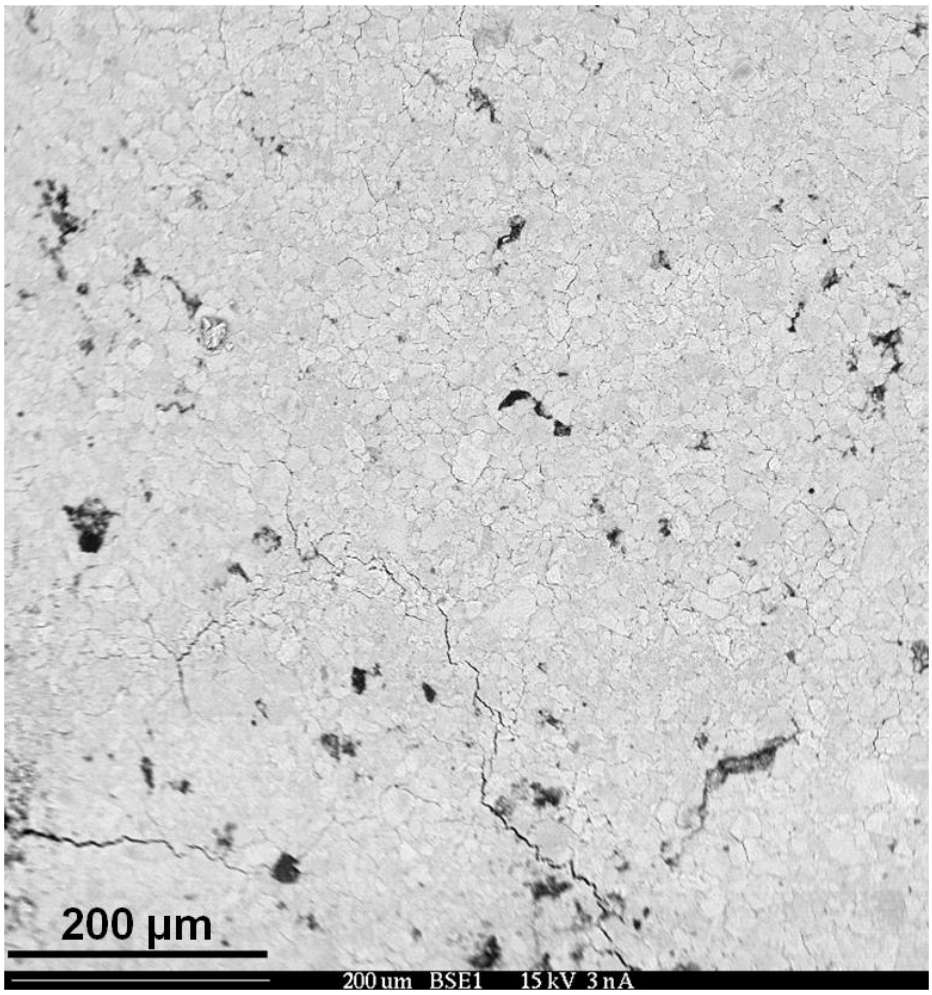

Figure 9: Microprobe image of the surface of a phosphine linker-modified ZrP nanoplatelet 1i.

Table 1: Microprobe atomic % data of 1i obtained from the sample with its image shown in Figure 9.

Sample	Atomic %			Zr : P	Zr : Si
	Si	Zr	P		
Bulk	0.4	6.7	13.8	1 : 1.9	17 : 1
Surface	0.4	0.7	1.4	1 : 2.2	2 : 1

The atomic ratios (Table 1) confirm that on the surface the number of Si atoms is in the same order of magnitude (0.4) as Zr (0.7), with the Zr : Si ratio being about 2 : 1. In the bulk, however, Zr is substantially more prevalent than Si, with a Zr : Si ratio of 17 : 1. This again corroborates the assumption that the silane linker 1 resides mostly on the surface of the support material, and practically does not intercalate. The microprobe analysis also indicates that the Zr : P ratio is higher in the bulk than on the surface of 1i (Table 1), which additionally corroborates the assumption that the phosphine linker resides on the surface of the ZrP nanoplatelets and does not intercalate.

2.5 Immobilization of the Catalyst

The immobilized Rh complex 1i-Rh has been obtained from 1i by ligand exchange with Wilkinson's catalyst $ClRh(PPh_3)_3$ at room temperature, as seen in Figure 10.

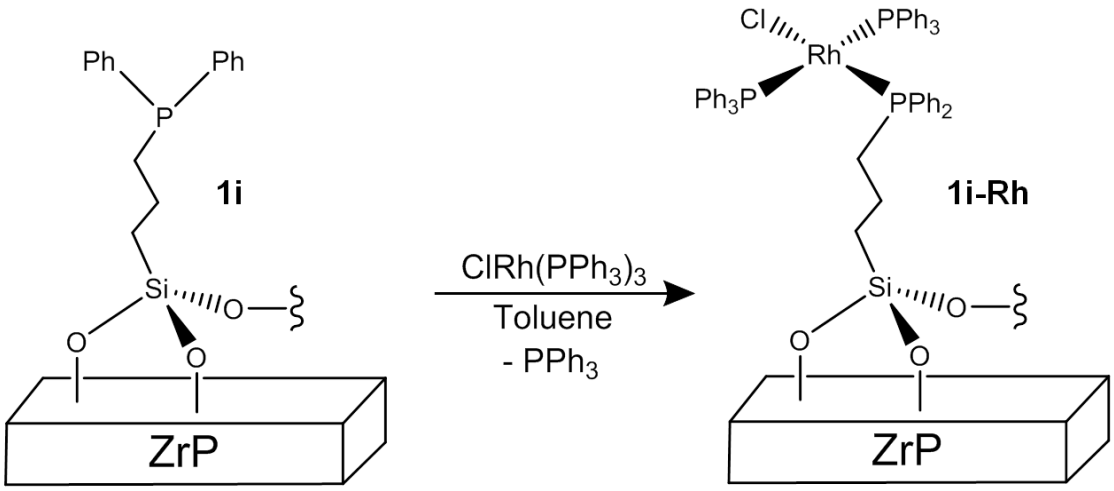

Figure 10: Formation of the immobilized Wilkinson-type catalyst 1i-Rh by ligand exchange with 1i.

^{31}P NMR shows that no free PPh_3 is found in the supernatant after washing the material with toluene. The presence and retention of the catalyst on the surface is indicated by the orange color of the support. With respect to the surface coverage of 1i with linkers only one PPh_3 ligand is replaced at the metal center. Based on earlier ligand exchange results[31,34-36] the phosphine trans to the Cl ligand is most likely the one replaced by the linker. Since $ClRh(PPh_3)_3$ can also be bound to the ZrP support directly without any linker, it is important to note that Wilkinson's catalyst does not intercalate between the ZrP layers. This is proven by the powder X-ray diffractogram of 1i-Rh which shows the peak corresponding to the layer distance of 7.6 Å in analogy to the display in Figure 6.

2.6 Catalysis

For testing the catalytic activity for olefin hydrogenation the procedure established previously was applied,[9,34-37,42] using dodecene as the substrate (Figure 11) and a hydrogenation apparatus described earlier[36] to monitor the hydrogen consumption.

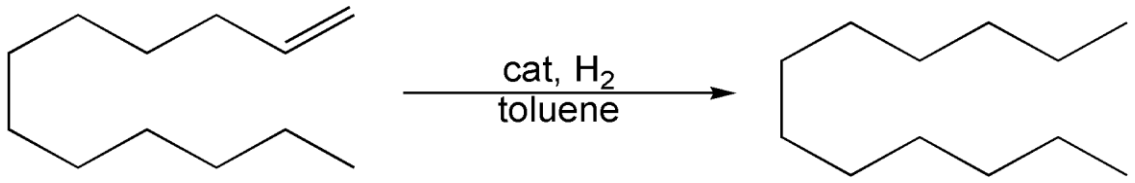

Figure 11: Catalytic hydrogenation of 1-dodecene (pressure 1.1 atm, substrate to catalyst ratio 100 to 1, 25°C, solvent toluene).

With this substrate an ample database is available[9,31,34-42] and the activity and longevity of the catalyst can be compared with the current state of the art characteristics of immobilized catalysts. As a first test it has been established that the unmodified ZrP support does not catalyze the catalytic reaction. As expected, no H_2 uptake takes place under the standard conditions with ZrP. On the other hand, Wilkinson's catalyst in solution exhibited the usual and characteristic activity pattern.[9] In contrast, Figure 12 shows the hydrogen uptake curves of 1i-Rh. There is no induction period, and during the first run the catalyst quantitatively hydrogenates the substrate within 23 hours. When the catalyst 1i-Rh is recycled in a batchwise manner, the activity increases somewhat and in the 15th cycle the hydrogenation is finished within 13 hours. It is noteworthy to mention

that the material darkens gradually and turns from beige in the first two cycles to olive green in the third cycle to black in all consecutive runs.

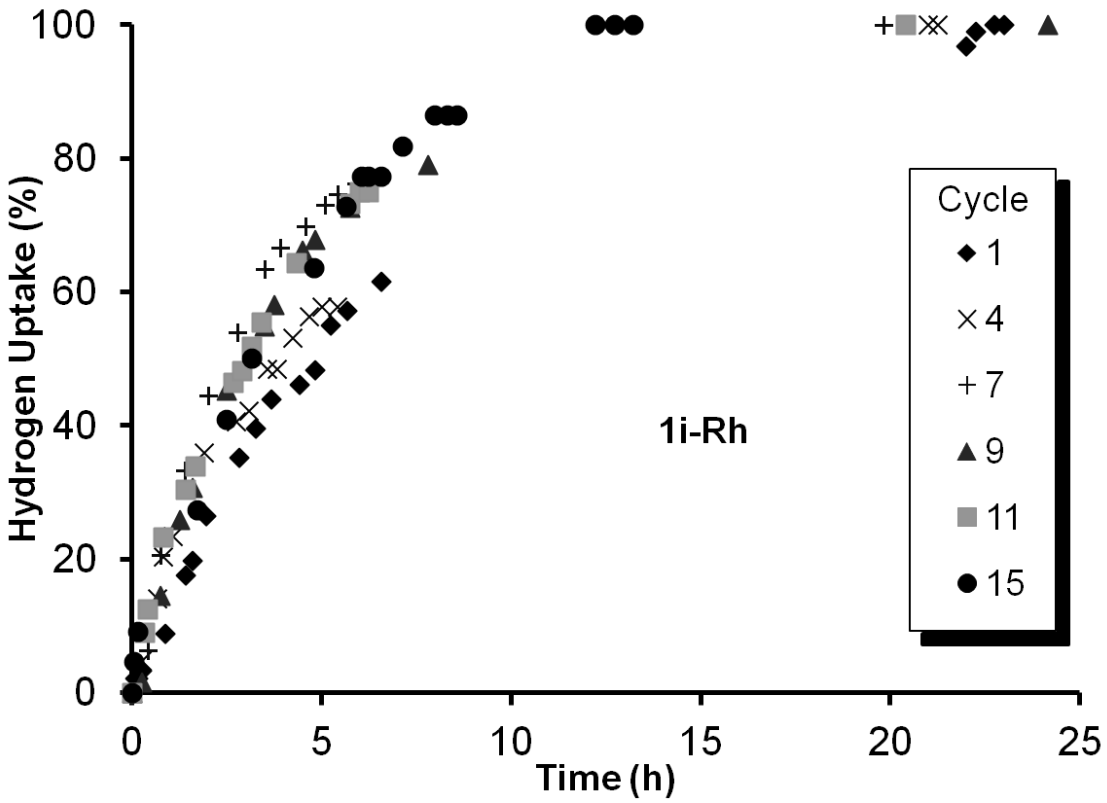

Figure 12: Catalytic activity and recycling characteristics of 1i-Rh for the hydrogenation of 1-dodecene.

Although this indicates the eventual formation of nanoparticles, as described earlier for a catalyst immobilized on silica,[9] the speed of the catalytic reaction is still unprecedented. Another advantage is that the material 1i-Rh settles within a few minutes after the catalytic runs, thus facilitating its separation from the reaction mixture and recycling. For comparison, Wilkinson-type Rh complexes tethered to silica with the same ligand 1,

for example, need 32 hours for this task[34] even in the first run. Chelate complexes of Rh, bound to silica, can be recycled about the same number of times, but the typical duration of one cycle with 100% substrate conversion is 35 hours and an elevated reaction temperature of 60 °C is needed.[34] Therefore, we can conclude that 1i-Rh is the fastest immobilized hydrogenation catalyst so far, when the standard conditions, as those described in Figure 11, are applied.

Next we further investigated the nature of the active species in the case of 1i-Rh. The fact that the material turns black within the first three runs indicates that Rh nanoparticles might have formed during catalysis. This is also indicated by the recycling characteristics of 1i-Rh, with its slow start, followed by high activity and finally consolidating at basically one catalytic activity curve for 13 more cycles. The analogous scenario has been found earlier with Rh catalysts immobilized by phosphine linkers with long alkyl chains.[9] In order to determine unequivocally whether nanoparticle formation takes place during catalysis with 1i-Rh, TEM images have been recorded. Figure 13 shows one representative image of 1i-Rh after a catalytic run.

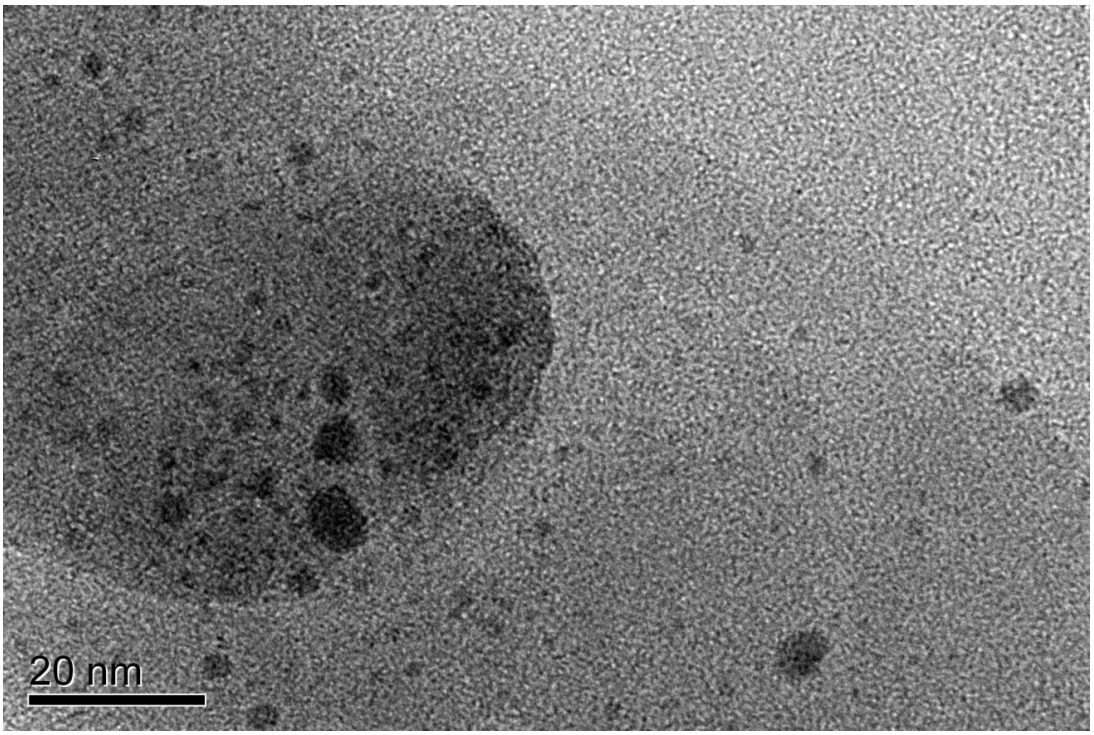

Figure 13: TEM image of catalyst 1i-Rh after one catalytic run.

Rh nanoparticles in a size range from about 1 to 8 nm are clearly visible, with those of 2 to 3 nm being most prevalent. Obviously, the smaller Rh nanoparticles lead to the fast catalytic reaction, as the larger particles with particle size distributions around 4 to 6 nm are characteristic for slower catalysts.[9] The wide variation in the nanoparticle size and the occurrence of very large irregular shaped ones indicates that the particles are not confined in pores or between the layers of the support and therefore they can grow to larger sizes. However, the great number of possible repetitive catalytic runs suggests that the nanoparticles cannot move as quickly and easily across the surface of the ZrP support to grow and thus become less active, as they can in the case of silica and in the presence of linkers with long alkyl chains.[9]

Finally, it has been tested whether binding $ClRh(PPh_3)_3$ directly to the ZrP support to form ZrP-Rh would yield an active and recyclable catalyst. Indeed, when combining a solution of Wilkinson's catalyst with a suspension of ZrP in toluene, the initially colorless support immediately turns bright orange. The picture in Figure 14 shows the mixture with the modified ZrP nanoplatelets in the process of settling.

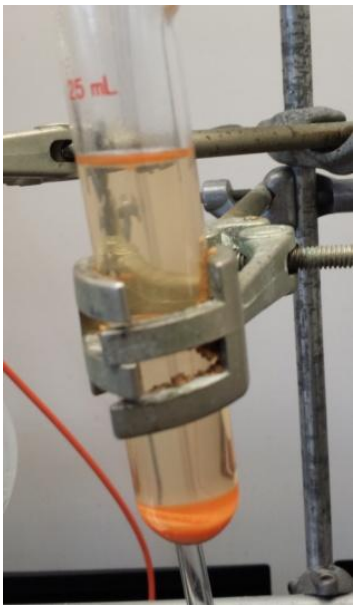

Figure 14: The nanoparticles of ZrP-Rh settle at the bottom of the Schlenk flask after combining ZrP nanoplatelets with $ClRh(PPh_3)_3$.

Next, the activity and recycling characteristics of ZrP-Rh have been studied and they are represented graphically in Figure 15. The color change of the liquid from the formation of Rh nanoparticles is documented in Figure 16. In contrast to the scenario encountered with 1i-Rh the catalyst displays an induction period of about two hours in the first cycle prior to assuming average activity. After a slower phase the hydrogenation is finally

complete within 45 hours. The time ZrP-Rh requires for the total substrate conversion is therefore nearly double the time needed by 1i-Rh. Interestingly, however, the consecutive runs with ZrP-Rh are faster before the activity is lost again, showing the same trend observed with 1i-Rh. In run 10 the time requirement already amounts to 90 hours. While ZrP-Rh is therefore much less active and recyclable than 1i-Rh, it still compared favorably with immobilized Wilkinson-type Rh complexes immobilized via chelate phosphine linkers, some of which required nearly 100 hours for full conversion in cycle 13.[34]

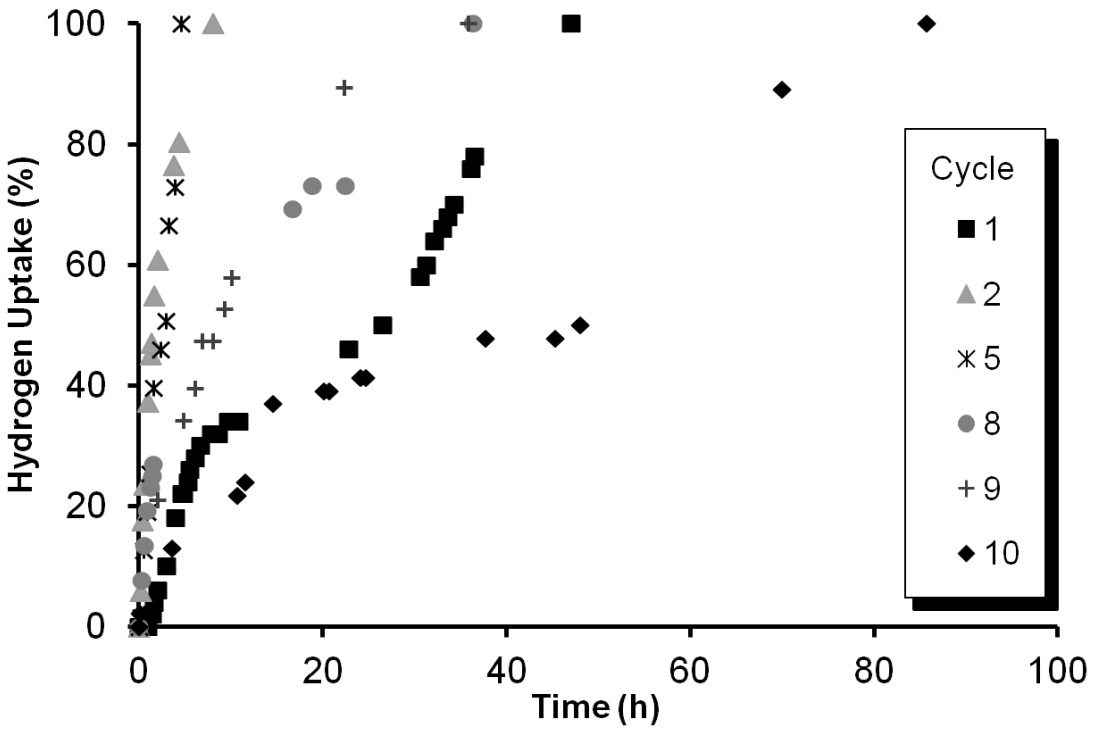

Figure 15: Catalytic activity and recycling characteristics of ZrP-Rh for the hydrogenation of 1-dodecene.

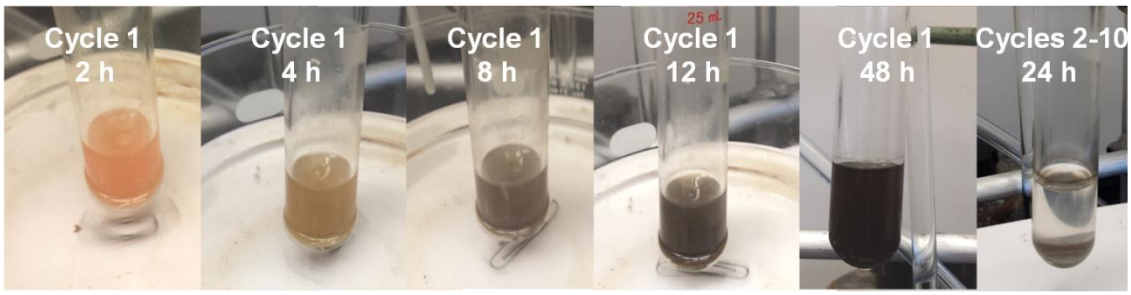

Figure 16: Color change of solid ZrP-Rh during the hydrogenation of 1-dodecene in the course of 10 cycles.

2.7 Conclusion

In summary, it has been demonstrated that a Wilkinson-type hydrogenation catalyst can be tethered irreversibly to zirconium phosphate nanoplatelets. It has been shown that the linker is evenly "distributed" on the outside of the nanoplatelets and therefore the catalyst is dispersed homogeneously on the surface. The ligand or catalyst do not intercalate into the layers of the zirconium phosphate support. The catalyst immobilized by the phosphine linker can be easily recycled by allowing it to settle after the catalytic reaction. The most favorably sized nanoplatelets of the support do not clump during the catalytic reaction but retain their high specific surface area. Therefore, most importantly, the obtained catalyst exhibits record speed in hydrogenating the standard substrate 1-dodecene and it can be recycled 15 times in a batchwise manner without major loss of catalytic activity. Following this successful first study, which yielded the most active and recyclable immobilized hydrogenation catalyst so far, in the future the application of chelate phosphine linkers[9,34-36,38-41,65] and rigid scaffold systems[37,42] is planned. Another

point of interest is that one is not restricted to ethoxysilanes as linkers because isocyanates, epoxides, phosphates and phosphonic acids also bond to the surface of α-ZrP.[61] Furthermore, the effect of varying the nanoplatelet sizes of the support material on the immobilized catalysts may be investigated.

2.8 Experimental Details

2.8.1 General Remarks

The ^{1}H, ^{13}C, and ^{31}P NMR spectra of liquids were recorded at 499.70, 125.66, and 202.28 MHz on a 500 MHz Varian spectrometer. ^{29}Si NMR spectra of liquids were recorded at 79.37 MHz on a 400 MHz Inova spectrometer. The ^{13}C, ^{29}Si, and ^{31}P spectra were recorded with ^{1}H decoupling if not stated otherwise. The solid-state NMR spectra were measured with a Bruker Avance 400 widebore NMR spectrometer equipped with a 4 mm MAS probehead. For the CP/MAS and MAS measurements ^{1}H high-power decoupling was applied. The recycle delays were 5 s for CP/MAS, and 10 s for MAS spectra. For more measurement details, see previous publications.[29,64] PXRD experiments were performed from 2° to 40° (2θ angle) using a Siemens D8 X-ray diffractometer system with a Cu anode source (Kα1, λ = 1.5406 Å) and a filtered flat LiF secondary beam monochromator. The divergence, receiver, and detector slitwidths were 2 mm, the scatter slit width was 0.6 mm. The interlayer distances were determined using Bragg's Law for the (0 0 2) diffraction plane of the diffraction pattern of α-ZrP.

Transmission electron micrographs (TEM) of the samples were acquired using a JEOL 2010 transmission electron microscope at an acceleration voltage of 200 kV. Samples were prepared by drop casting a ca. 0.01% (w/w) suspension of the nanoparticles on a formvar/carbon coated copper grid from Ted Pella. All reactions were carried out using standard Schlenk techniques and a purified N_2 atmosphere, if not stated otherwise. Reagents purchased from Sigma Aldrich or VWR were used without further purification. Solvents were dried by boiling them over Na, distilled, and stored under N_2. In addition, toluene is stored under nitrogen over 3Å molecular sieves. The ZrP nanoplatelets with sizes between 100 and 400 nm were synthesized as described[55,57-59,61,71] and dried thoroughly in vacuo at room temperature to remove water adsorbed on the surface. The linker was synthesized following the procedure and the data were in accordance with the reported ones.[64] Surface coverages were determined by ICP-MS using a Perkin-Elmer Optima 3000 dual-view ICP-MS instrument. For this purpose, 10 mg of 1i was immersed in 10 µL of HF and diluted with 15 mL of 2% HNO_3. The atoms Zr, Si, and P were measured to determine the surface coverage of 1 on ZrP. Quantitative compositional analyses were carried out on a four spectrometer Cameca SX50 electron microprobe at an accelerating voltage of 15 kV at a beam current of 20 nA. All quantitative work employed wavelength-dispersive spectrometers (WDS). Analyses were carried out after standardization using very well characterized compounds or pure elements. Pressed powder micro pellets were prepared by pressing a few milligrams of powder between the highly polished surfaces (0.25 µm) of hardened steel dies, and transferring the pellets onto double-sided conductive carbon tape. The pellets were

carbon coated before analysis to make them electrically conductive. The analyses of the pressed powder pellets were carried out with a 20 μm diameter beam while the stage was being moved 20 μm every 2 s, repeated over a ten spot traverse. This ensured representative sampling and minimized possible thermal damage to the samples. The hydrogenation reactions were monitored using the apparatus[36] by reading the consumption of hydrogen during the course of the reaction. The standard conditions listed in Figure 11 were applied.[34-37]

2.8.2 Immobilization of 1 on ZrP to give 1i

400 mg (1.33 mmol) of thoroughly dried α-ZrP is placed into a Schlenk flask and 200 mL of dry, degassed toluene is added. The white opaque liquid is stirred vigorously under an argon atmosphere and 105 mg (0.267 mmol) of 1 is added via syringe. Then the reaction mixture is heated to 95 °C for 12 h while stirring vigorously. The flask is cooled and stirred for 7 more hours. Then the contents are transferred to four 50 mL centrifuge tubes and centrifuged at 5000 rpm for 15 min. The supernatant is decanted and a white solid remains. 100 mL of toluene is added to the solid for washing, and the mixture is shaken thoroughly and centrifuged. The washing process is repeated three more times. Finally, all toluene is removed and the white solid is dried under vacuum at 70 °C for 12 h. The solid material 1i (0.3326 g, 83% with respect to ZrP) is then triturated with a mortar and pestle for 2 min and placed in a Schlenk flask for long-term storage.

2.8.3 Generation of 1i–Rh

10 mg (0.01 mmol) of Wilkinson's catalyst $ClRh(PPh_3)_3$ are placed in a Schlenk flask under nitrogen and dissolved in 10 mL of toluene. Then the dark red liquid is transferred via cannula to a second Schlenk flask containing 30 mg of 1i (corresponding to 0.077 mmol of 1) in 10 mL of toluene. During this process the reaction mixture turns orange-brown and is stirred for 24 h at room temperature. Then the stirring is stopped and the solid 1i–Rh settles to some degree. The supernatant appears orange/pink while the settled solid is orange/brown. The supernatant is removed via syringe and 5 mL of toluene is added. The sample is stirred again for 20 min and allowed to settle. The supernatant is removed and two more wash cycles are performed. After the third wash no more catalyst is removed from the support, as evidenced by the colorless supernatant and by ^{31}P NMR. 1i–Rh is then suspended in 5 mL of toluene and employed for catalyzing the hydrogenation of 1-dodecene.

2.8.4 Generation of ZrP–Rh

The material ZrP–Rh is prepared following the procedure described for 1i. Wilkinson's catalyst (10 mg, 0.01 mmol) is reacted with 25 mg of ZrP at 25 °C and washed thoroughly with toluene, as outlined under 1i above.

2.8.5 Hydrogenation with 1i–Rh and ZrP–Rh

Immobilized catalyst 1i–Rh (30 mg, containing 10 mg of Wilkinson's catalyst, corresponding to 0.010 mmol Rh) is suspended in 5 mL of toluene in a Schlenk flask. The mixture appears opaque and orange/pink in color. The flask is then attached to the hydrogenation apparatus described earlier[36] and 1 mmol of 1-dodecene dissolved in toluene (5 mL) is added to the suspension of 1i–Rh with a syringe through the stopcock. Subsequently the suspension was stirred vigorously and the hydrogen consumption was monitored. After complete substrate conversion the catalyst was allowed to settle, the supernatant was removed via syringe and the material was washed three times with 5 mL of toluene. To start the second and following cycles, fresh toluene was added and the described procedure was repeated. For the catalysis with ZrP–Rh (25 mg, containing 10 mg of Wilkinson's catalyst, corresponding to 0.010 mmol Rh) the same procedure as outlined here for 1i–Rh was applied.

CHAPTER III

ZIRCONIUM(IV) PHOSPHONATE–PHOSPHATES AS EFFICIENT ION EXCHANGE MATERIALS[*]

3.1 Overview

Layered metal phosphonate-phosphate hybrid materials are known to be ion exchange materials. Hybrids with zirconium metal centers were synthesized at varying phosphonate-phosphate ratios in order to explore the function and charge preference. The zirconium hybrid materials were found to have a range of applicable uses with preference for highly charged ions (3+) over lower charged ions (1+ and 2+). The addition of a large excess of phosphate altered the selectivity, and these materials were able to remove all ions from solution regardless of charge. In this thesis, we describe newly synthesized compounds that are simple to prepare, reproducible, stable, and offer a variety of separation schemes.

3.2 Introduction

Our laboratory has been involved with the synthesis and ion exchange behavior of metal(IV) phosphonate-phosphates. Our studies arose out of the pioneering work of

---

[*] Reproduced in part with permission from Silbernagel, R.; Martin, C. H.; Clearfield, A. *Inorg. Chem.* **2016**, *55*, 1651-1656. http://pubs.acs.org/doi/abs/10.1021/acs.inorgchem.5b02555

Dines et al.[72-74] and Alberti et al.[75-77] They prepared mixed derivatives of zirconium, 1,4-phenylenediphosophonic acid or phenylphosphonic acid, and phosphates, which are porous. Their intention was to obtain catalysts useful for hydrocarbon reactions. Subsequently, we prepared a series of these compounds directly, without the use of hydrofluoric acid, by mixing a $ZrOCl_2$ solution directly with the mixed phosphate-phosphonate compounds.[17,78-82] It was demonstrated that these compounds exhibited interesting ion exchange properties. For example, these compounds did not exchange significant amounts of Li^+, Na^+, or K^+ but did exchange increasing amounts of Rb^+ and Cs^+ as the amount of phosphate in the compound increased. Subsequently, it was shown that these exchangers preferred high charge ions, 3+ and later 4+, to those of lower charge.[13,17,83,84] This led to the development of a system for separating lanthanides from actinides by oxidizing the actinides to the actinyl state, AnO_2^+.[14,15] The composition of these ion exchangers may be represented by the general formula $M(O_3PC_6H_4PO_3)_{1-(x/2)}(O_3POA)_x \bullet nH_2O$, where M = Zr, A = H, and x may be equal to 0.5−1.6, as shown in Table 2.

Table 2: Measurements for hybrid synthesis.

x =	Amount of $C_6H_4(PO_3H_2)_2$ (g, mmol)	Amount of Phosphate (mmol)	Phosphonate : Phosphate Ratio
0.5	1.913, 8.038	5.359	1.5:1
0.8	1.530, 6.431	8.574	1:1.5
1.33	0.854, 3.590	14.254	1:4
1.6	0.510, 2.144	17.148	1:8

Similar compounds have been prepared with biphenyldiphosphonic acid as the ligand.[85] The problem arises from the fact that these materials are poorly crystalline, as shown in Figure 17.

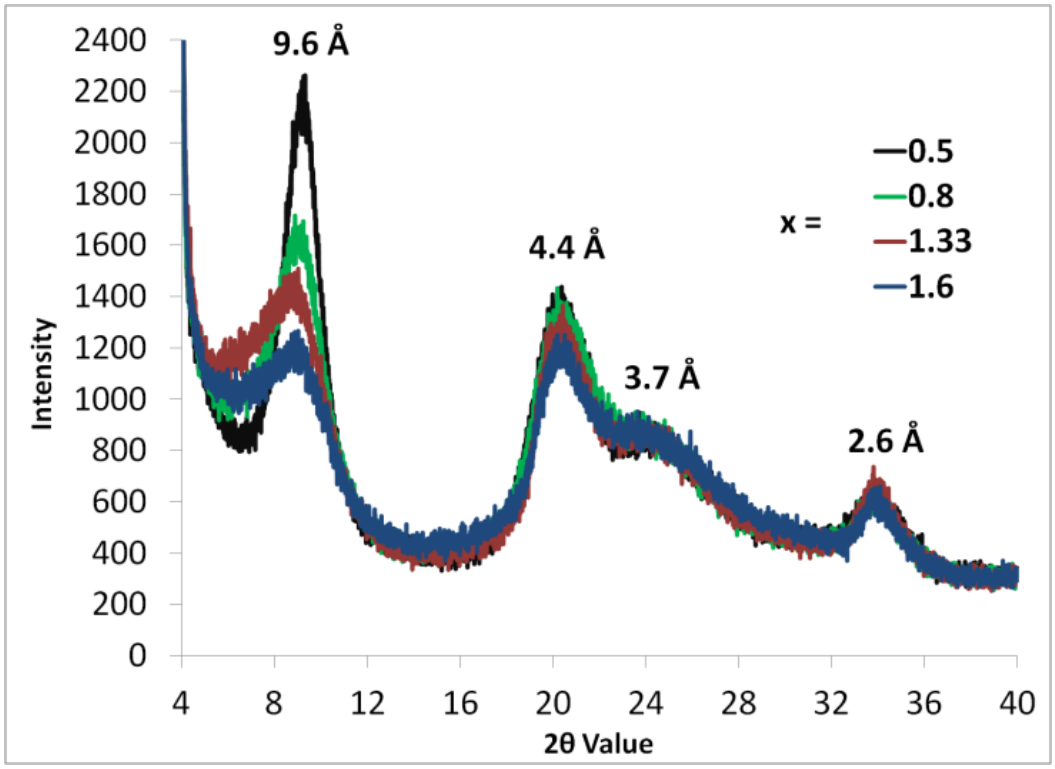

Figure 17: PXRD patterns of the H-Zr hybrids with the formula $Zr(O_3PC_6H_4PO_3)_{1-(x/2)}(O_3POH)_x \bullet nH_2O$, where x = 0.5, 0.8, 1.33, and 1.6. Numbers listed above the peaks are the d-spacing values.

With increasing phosphate, the crystallinity decreases. The first peak in the PXRD pattern for the monophenyl derivatives is 9.6 Å and that for the biphenyl derivatives 13.6 Å.[13,85-87] These values are indicative that the phosphonic acids cross-link the layers and are separated by the phosphate groups that are randomly distributed along the layers.

Based on previous data, a schematic drawing indicating the cross-linking nature and how micropores may be formed in this mixed derivative was determined, as seen in Figure 18.[13,85,86]

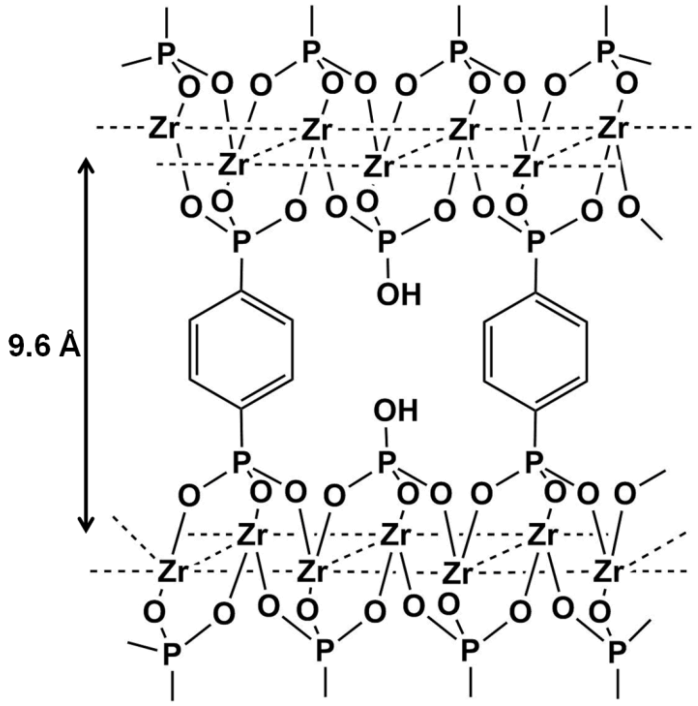

Figure 18: Suggested portion of Zr phosphonate-phosphate hybrid structure.

PXRD analysis shows the samples to be poorly crystalline with four broad peaks. As seen in Figure 17, the zirconium phosphonate-phosphate materials have a first peak at $2\theta = 9.2°$ and 9.6 Å corresponding to the distance between the layers, which is cross-linked by the phosphonate pillar. As phosphate is added to the compounds, the interlayer spacing remains constant but the peaks broaden, showing a reduction in the crystallinity as the phosphate in the hybrid materials increases.[13]

3.3 Analytical Determination of Materials

As seen in Figure 19, surface area analysis shows the N_2 sorption isotherms of the zirconium materials to be intermediates of type II and IV as previously reported,[13] indicating that, while micropores are present, the material also has mesoporous contributions stemming from the "house of cards" effect.[16] The pore size ranges from 14 to 250 Å. As the amount of phosphate increases, the pore sizes get larger. The percentage of pores that are larger than 50 Å increases from just 5% for x = 0.5 to over 35% for x = 1.6.

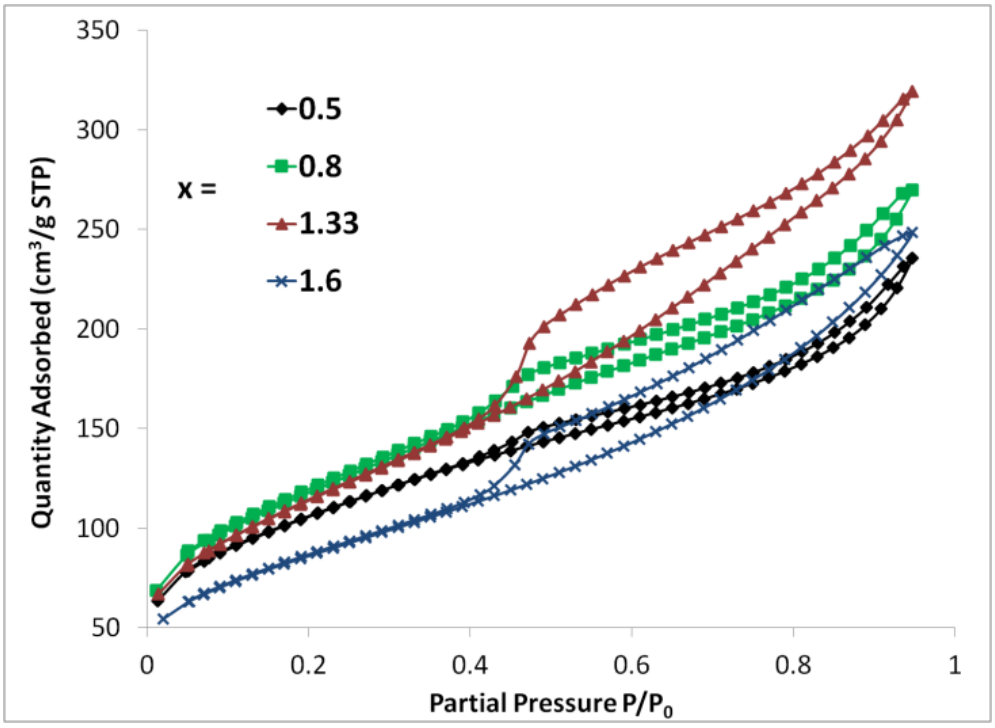

Figure 19: N_2 isotherms of zirconium phosphonate-phosphates with the formula $Zr(O_3PC_6H_4PO_3)_{1-(x/2)}(O_3POH)_x \bullet nH_2O$ where x = 0.5, 0.8, 1.33, 1.6.

The Brunauer−Emmett−Teller (BET) surface area values are shown in Table 3. For the zirconium-based hybrids, as the amount of phosphate added increases, the BET surface area increases, peaking at x = 0.8. We attribute a lower surface area for the x = 1.6 sample that is near the limit of phosphate that can be incorporated into the structure.

Table 3: Surface area of the protonated samples determined by BET method. Estimate of error <10%.

x for the H-Zr Sample	BET surface area (m^2/g)
0.5	381
0.8	428
1.33	418
1.6	314

SEM imaging shows that the particles are highly susceptible to agglomeration. Attempts to look at single particles showed that, as the amount of phosphate increases, so does the particle size with a value between 50 and 70 nm. The particle morphology for x = 0.5 and 0.8 is more circular. The other samples with additional phosphate (x = 1.33 and 1.6) indicate that the particles become thin platelets, much like zirconium phosphate.[67] The x = 1.33 sample shows the merging of two particle types, circular and thinner platelets. Figure 20 includes a comparison of the particle shape and size between the different samples.

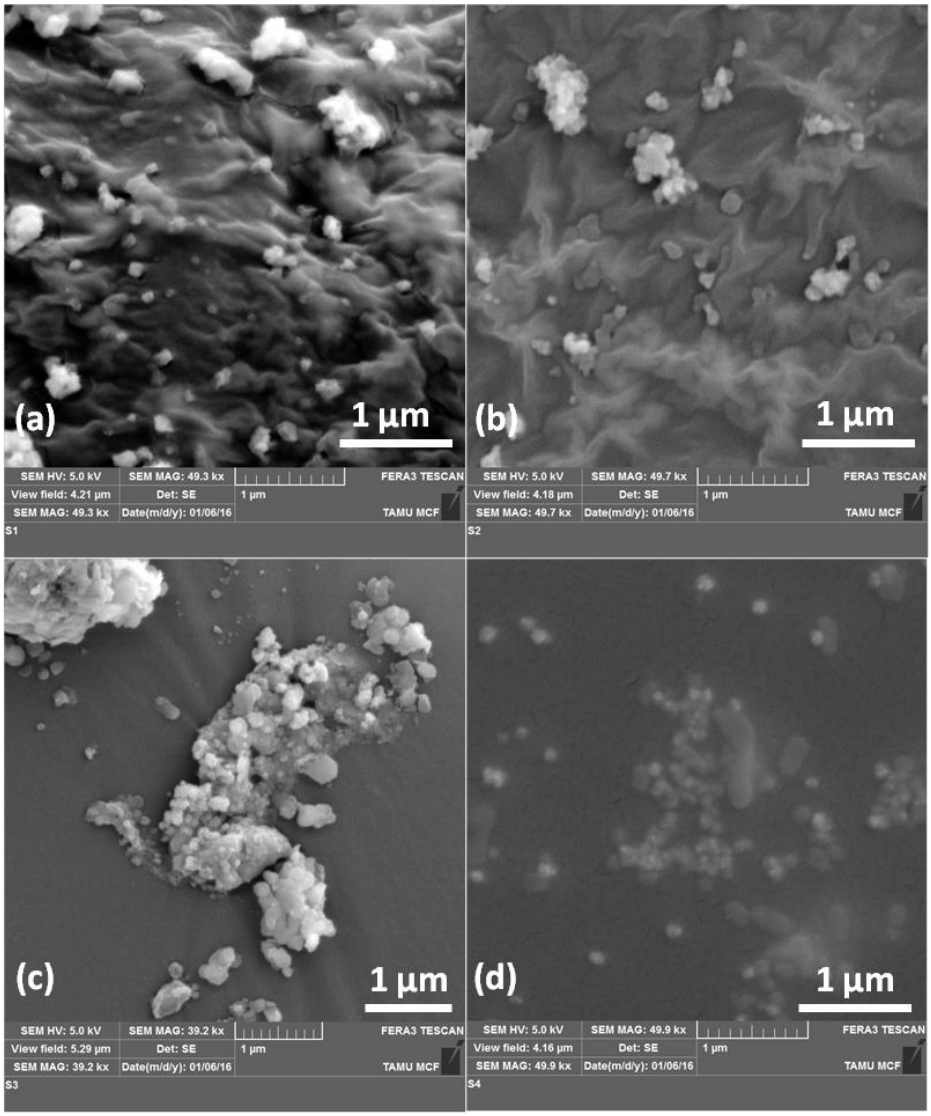

Figure 20: SEM images for $Zr(O_3PC_6H_4PO3)_{1-(x/2)}$ $(O_3POH)_x \bullet nH_2O$ where (a) x = 0.5, (b) x = 0.8, (c) x = 1.33, and (d) x = 1.6.

In addition to SEM, the solids were analyzed with IR spectroscopy and there are multiple characteristic bands in the region of 700-1600 cm^{-1}. There is a sharp, medium stretching of P-O-C symmetric and P-O asymmetric at 827 cm^{-1}.[88,89] A very large, broad set of peaks is seen at 1010 and 1040 cm^{-1}, which is the P-O-C symmetric and P-OH

stretching.[88,89] A weak broad peak is seen at 1150 cm^{-1} for the P-C stretching.[88] The peak is drastically reduced for the x = 1.33 and 1.6 samples, which have little phosphonate that contains the P-C bond. There is a sharp, weak resonance at 1390 cm^{-1} that is also present in the unreacted phosphonate ligand and is likely aromatic C=C-H stretching.[88] This signal is reduced in the x = 1.33 and 1.6 samples because they have less carbon. There is a broad, weak resonance in the region near 3400 cm^{-1} from the OH groups present in water. No evidence of P=O stretching, typically in the region of 1240 and 1350 cm^{-1},[88,90] was seen in the IR for the free phosphonate ligand or the H−Zr phosphonate−phosphate hybrids. The IR spectrum is shown in Figure 21.

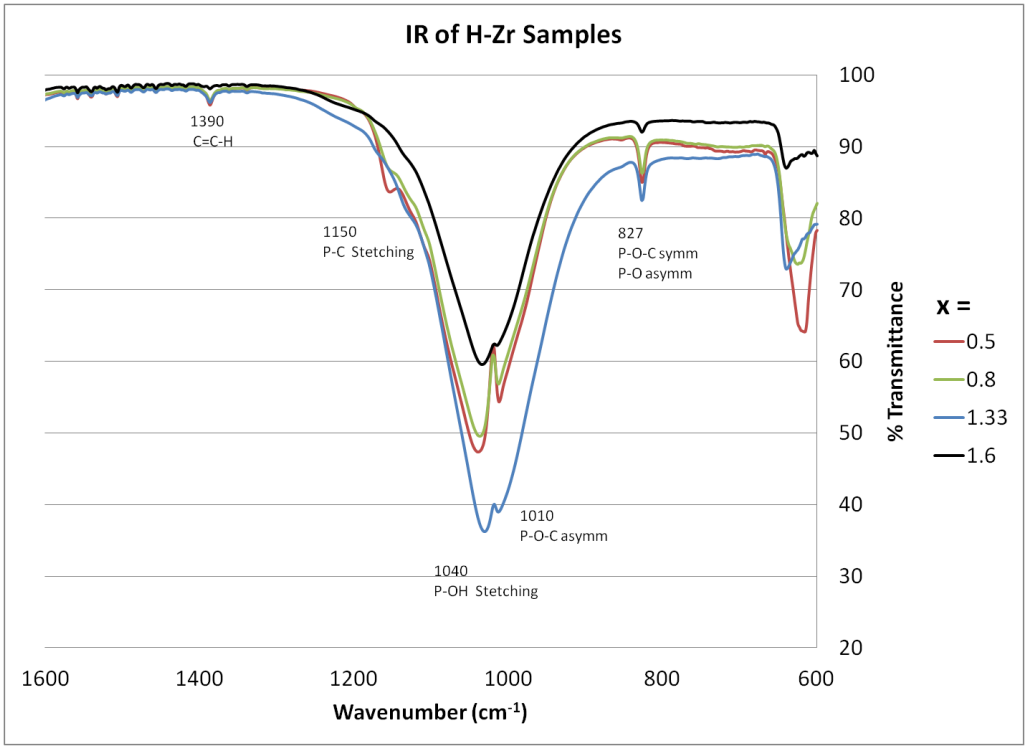

Figure 21: IR Spectrum of 600-1600 cm^{-1} region for $Zr(O_3PC_6H_4PO_3)_{1-(x/2)}(O_3POH)_x \bullet nH_2O$ where x = 0.5, 0.8, 1.33, 1.6.

Solid-state NMR analysis, as seen in Figure 22, which shows the different samples overlaid with multiple peaks present relating to the phosphonate and phosphate moieties. There are three peaks corresponding to three different binding modes of the phosphonate (+5.98, -0.76, and -7.49 ppm). The largest peak at -7.49 ppm is the most common binding mode of phosphonate,[78,86] and it is likely that all P-O are bonded to the zirconium layer, which supports the crosslinking of the phosphonate to create an interlayer spacing of 9.6 Å. The other less predominate peaks at +5.98 and -0.76 ppm are likely one or two P-O bonded to the zirconium layer with possible hydrogen bonding.[30,90] The phosphate also has three different binding modes to the zirconium layer. The peaks are shown at (-15.40, -23.56, and -28.96 ppm), with the predominate peak at -23 ppm likely being $(ZrO)_3POH$.[78,86]

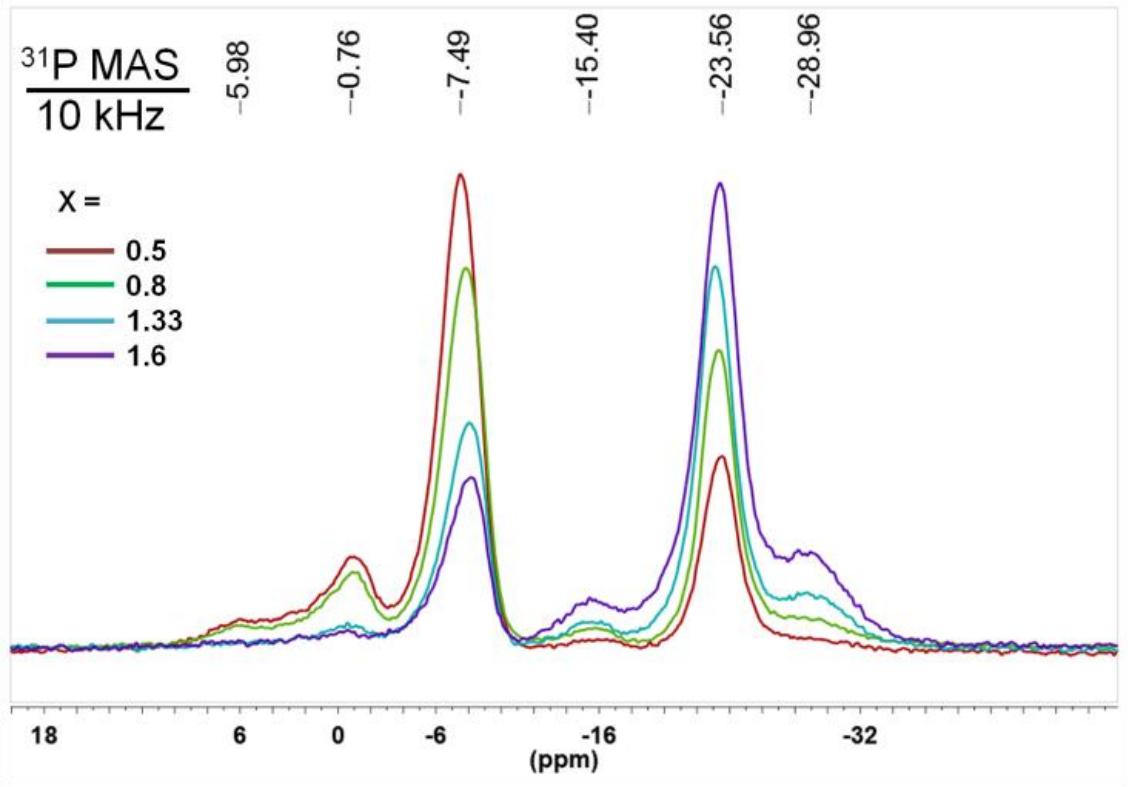

Figure 22: ^{31}P MAS NMR with ν_{rot} = 10 kHz of phosphonate and phosphate in H-Zr with a ratio of x = 0.5 to 1.6.

3.4 Composition of Zirconium Phosphonate-Phosphate Hybrids

Elemental analysis (EA), electro microprobe (MP), and TGA data were collected to determine the composition of the materials and are shown in Table 4. Table 4 shows some regularity of the data. The amount of zirconium increases as the phosphate ratio increases. The phosphorus content also increases, but the carbon content decreases drastically. The chlorine content of all samples was less than 0.3 wt %. It was first thought that the ratio of the phosphorus content had to be twice that of zirconium based

on the end product at 1000 °C, zirconium pyrophosphate, ZrP_2O_7, as determined by the PXRD pattern. The formulas were based upon the initial ratio of Zr-P provided in the synthesis;[78] however, it turns out that the actual ratio in the product is always less than 1:2. This must mean that small amounts of ZrO_2 are also formed because TGA was run with 90% air and an excess of oxygen present.

Table 4: Elemental analysis of zirconium phosphonate-phosphates with increasing phosphate content.

x =	EA		MP		TGA	
	C Wt%	H Wt%	Zr Wt%	P Wt%	Wt Loss % at 200 °C	Wt Loss % at 1000 °C
0.5	14.46	2.35	25.70	16.11	9.83	25.35
0.8	12.25	2.12	28.25	17.22	9.46	24.40
1.33	7.52	1.98	30.47	18.06	7.49	18.02
1.6	4.67	1.86	31.96	18.16	7.05	18.92

Utilizing the EA data from Table 4, and estimation from solid-state NMR we were able to determine the composition of the samples. The results are provided in Table 5.

Table 5: Molecular weight and formulas for zirconium phosphonate-phosphates. Estimate of error <4%.

x =	Mol Wt (g)	Compound Formulas
0.5	342.7	$Zr(O_3PC_6H_4PO_3)_{0.52}(HO_3PC_6H_4PO_3)_{0.13}(H_2O_3PC_6H_4PO_3)_{0.06}$ $(HPO_4)_{0.422}(OH)_{0.566}(H_2O)_{1.94}$
0.8	326.2	$Zr(O_3PC_6H_4PO_3)_{0.44}(HO_3PC_6H_4PO_3)_{0.11}$ $(HPO_4)_{0.698}(OH)_{0.514}(H_2O)_{1.69}$
1.33	306.2	$Zr(O_3PC_6H_4PO_3)_{0.27}(HO_3PC_6H_4PO_3)_{0.04}$ $(HPO_4)_{0.896}(H_2PO_4)_{0.214}(OH)_{0.794}(H_2O)_{1.23}$
1.6	296.0	$Zr(O_3PC_6H_4PO_3)_{0.185}(HPO_4)_{1.02}(H_2PO_4)_{0.285}(OH)_{0.935}(H_2O)_{1.11}$

These compositions were verified by EA, TGA, and Microprobe analyses. Understanding that the carbon content is only present in the phosphonate moiety (1,4-phenylene diphosphonic acid), and that only six carbons are possible from the phenyl ring helps to determine the actual amount of phosphonate present in the composition. To determine the different phosphonate orientations solid-state NMR was used for estimates on the most likely confirmation, as seen in the ^{31}P MAS region of (-8 to 6 ppm) of Figure 22. For charge balance and H content, some phosphonate must have some protons remaining resulting in the different forms of phosphonate: The fully deprotonated ($O_3PC_6H_4PO_3$) and the others being partially protonated ($HO_3PC_6H_4PO_3$ and $H_2O_3PC_6H_4PO_3$).

From there, the remaining P is from the phosphate and OH groups are determined for H from elemental analysis and charge balance. The water value is roughly estimated from the TGA weight loss at 200 ºC. The remaining phosphorus dictates the amount of phosphate present as (HPO_4 or H_2PO_4), with help from solid-state ^{31}P MAS NMR in the region from -28 to -15 ppm. To achieve charge balance, OH is added to achieve an overall charge of -4 to compensate for the +4 charge of Zr. Error for all calculated compositions is less than 4% from the actual EA data listed in Table 4.

3.5 Capacity Studies

Capacity studies were conducted with 25 mL of 1×10^{-3} M Tb^{3+} at pH ~ 3 and ~0.1 g of H−Zr hybrid and manually titrated with 0.0958 M NaOH. Before titration was attempted, the pH of the liquid before and after addition of the Zr phosphonate-phosphate ion exchange material was monitored for 1 h and specific values for each sample are shown in Table 6. For the initial pH change, no NaOH or acid was added; the pH drop is a result of ion exchange uptake of Tb and protons being released into the solution.

Table 6: Change of pH from addition of H-Zr samples in $1x10^{-3}$ M Tb^{3+} solution.

Before Titration, Monitoring pH	x =			
	0.5	0.8	1.33	1.6
Amount of Hybrid (g)	0.1005	0.1003	0.0998	0.1000
pH Before Addition of Solid	3.07	3.07	3.09	3.09
pH at 15 Seconds After Addition	2.82	2.80	2.74	2.78
pH at 1 Minute After Addition	2.76	2.72	2.65	2.67
pH at 60 Minutes After Addition	2.66	2.58	2.48	2.44

After stirring the solid in the Tb solution for 1 hour, the solution appeared opaque and milky white. With constant monitoring of pH, 0.0958 M NaOH was manually added into the Tb/Hybrid liquid stirring below. The typical scenario involved a sharp increase in the pH followed by a delayed increase of pH above 8. After the pH remained over 10, the titration was stopped. The graph of pH change versus addition of NaOH is shown in Figure 23 for each sample.

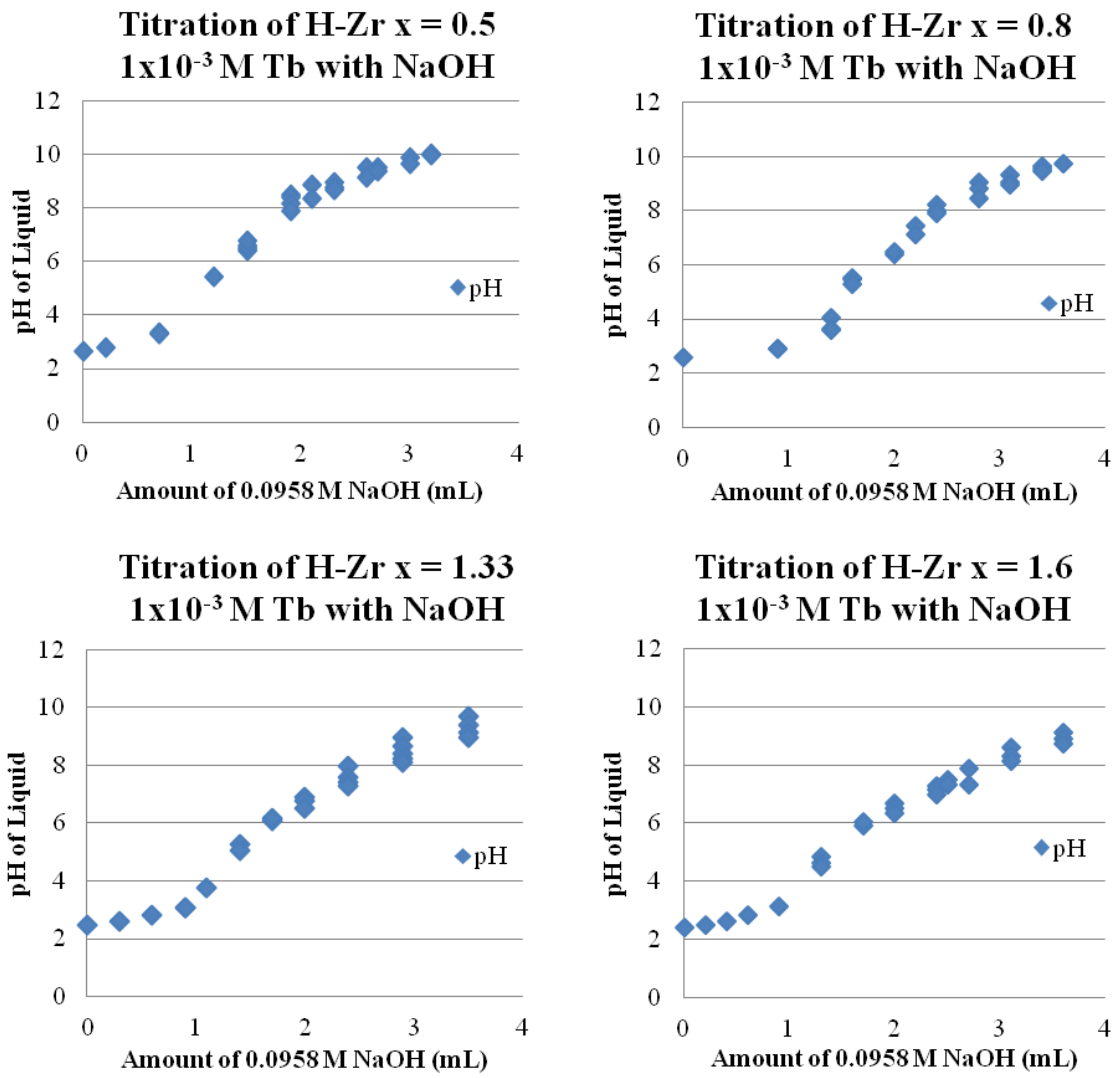

Figure 23: Titration curves for $1x10^{-3}$ M Tb and NaOH with H-Zr hybrids, where x = 0.5, 0.8, 1.33, and 1.60.

The amount of NaOH added to achieve a pH well above 10 was used to determine the mmol of H+ present. Dividing the H+ mmol capacity by the amount of hybrid used in grams resulted in the capacity value (mmol/g), as shown in Table 7.

Table 7: Capacity study of H-Zr hybrids with $1x10^{-3}$ M Tb^{3+} at pH = 3 and 0.0958 M NaOH.

x =	Amount of Sample (g)	Capacity Tb^{3+} (mmol/g)	Capacity H^{+} (mmol/g)
0.5	0.1005	1.14	3.42
0.8	0.1003	1.31	3.93
1.33	0.0998	1.60	4.80
1.6	0.1000	1.76	5.28

The capacity data illustrate that the samples with more phosphate have a higher capacity; which indicates that the phosphate does play a large role in ion exchange but as it will be revealed in Chapter IV, the phosphate is not the only possible site for ion exchange. Comparisons to other hybrid materials are shown in Appendix A.

3.6 Ion Exchange Properties

K_d values of phosphonate-phosphate hybrid materials have been determined previously for ions individually and used to calculate theoretical SFs that indicated the possibility of preferential pickup of highly charged cations (≥3+).[13,16] The K_d value is calculated by

$$K_d = [(C_i - C_{eq})/(C_{eq})](V/m)$$

where C_i is the concentration of the given ion in the solution with no sample material and C_{eq} is the equilibrium concentration of the given ion in the solution after mixing. V is the volume of liquid, and m is the mass of the ion exchanger used. The units are listed as mL/g in our case.

To determine if preferential pickup would occur in a competitive environment, solutions were prepared containing 2-5 ions, with each ion concentration at $1x10^{-4}$ M. ICP-MS was used to determine the ion count before and after interaction with the ion exchange material for 24 h. The percent removal for each ion was calculated by

$$\%R_{ion} = [(C_i - C_{eq})/(C_i)] \times 100$$

where C_i and C_{eq} are the same as those in the K_d definition. The amount of phosphate in the solid did not affect the uptake of M^{3+} ions, which remained at >98% for all materials. The increasing amount of phosphate significantly affected the uptake of 1+ ions. For all hybrid varieties, there is a useful selectivity preference that can provide facile separations of unwanted ions from solution. In this case, three ions were compared: Nd^{3+}, Sr^{2+}, and Cs^{+}. As more phosphate is added, the uptake of Sr^{2+} and Cs^{+} increases but the Nd^{3+} uptake remains unchanged; therefore, the SF decreases between neodymium/strontium and neodymium/cesium. The preferred hybrid for the separation of neodymium or lanthanides from lower charged ions would be the H-Zr x = 0.5 sample, as seen in Figure 24.

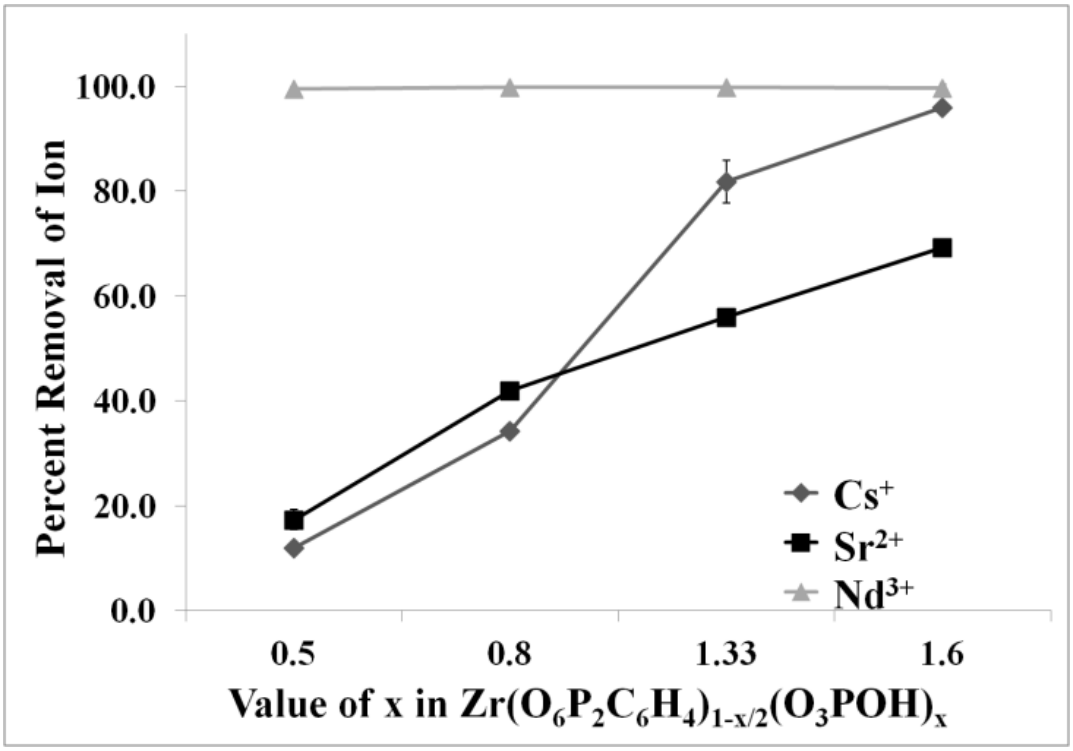

Figure 24: Ion exchange uptake for H-Zr hybrids for competitive ion studies with Nd, Sr, and Cs.

As seen in Figure 24, the uptake of Nd^{3+} remains above 99% for all samples; however, as the amount of phosphate increases, so does the uptake for Sr^{2+} and Cs^{+}. The x = 0.5 sample with a phosphonate-phosphate ratio of 1.5:1 has an uptake of Cs^{+} and Sr^{2+} below 20%, whereas the x = 1.6 sample with a phosphonate-phosphate ratio of 1:8 has nearly 98% uptake of Cs^{+} and 70% uptake of Sr^{2+}. Therefore, similar materials can offer a wide variety of separation options. The K_d values for the various H−Zr hybrids are listed in Table 8 and the separation factors are in Table 9.

Table 8: K_d values (mL/g) of test 1: Nd^{3+} and Sr^{2+} & test 2: Nd^{3+} and Cs^{+} uptake.

x =	Test 1		Test 2	
	K_d Nd	K_d Sr	K_d Nd	K_d Cs
0.5	38,000 ± 4,000	50 ± 10	58,000 ± 8,000	30 ± 10
0.8	100,000 ± 17,000	180 ± 10	139,000 ± 42,000	130 ± 10
1.33	136,000 ± 35,000	320 ± 10	199,000 ± 65,000	1,200 ± 300
1.6	75,000 ± 39,000	560 ± 20	125,000 ± 22,000	6,000 ± 800

Table 9: Separation factors (SF) obtained in 2-ion competitive uptake of Nd^{3+} and Sr^{2+} and Nd^{3+} and Cs^{+}.

x =	Separation Factors (SF)	
	Nd^{3+} / Sr^{2+}	Nd^{3+} / Cs^{+}
0.5	760 ± 290	1,900 ± 1,400
0.8	560 ± 130	1,100 ± 440
1.33	430 ± 130	170 ± 130
1.6	130 ± 80	20 ± 7

The results in Tables 8, 9 and previous work[13-17] show a clear preference for Nd over Sr and Cs. With excess phosphate addition, the preference for Sr and Cs increases, while the uptake of Nd remains near 99%+.

The dependence of ion uptake versus pH was also determined. A solution of 1×10^{-4} M Tb^{3+} was prepared at pH 1, 2, and 3. The uptake of Tb was determined by a comparison of the control samples without ion exchange material at the different pH values. The uptake of Tb^{3+} was monitored with varying pH values from 1 to 3, as shown in Figure 25.

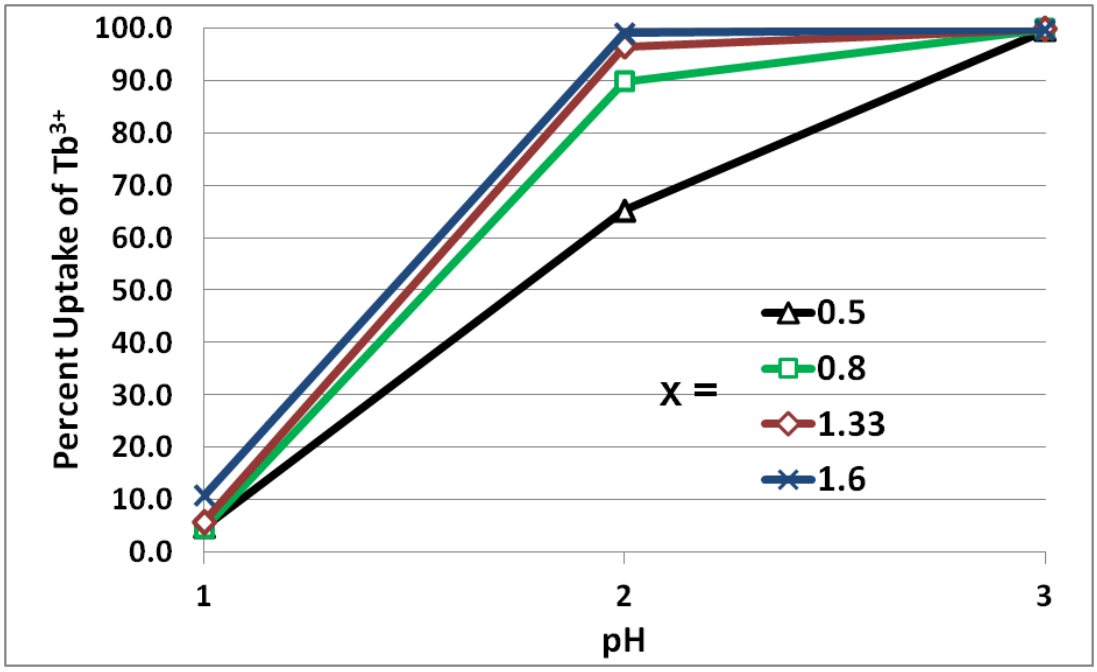

Figure 25: Ion exchange comparison of Tb^{3+} uptake versus pH for the H-Zr hybrids. High uptake of Tb at pH = 3, and low uptake of Tb at pH = 1.

Tb pickup is low at pH 1 and improves with increasing pH. The lowest achievable pH for the incorporation of Tb^{3+} and other lanthanides[13] is exhibited at pH = 2. The uptake increases with additional phosphate at each pH value. A Tb uptake greater than 98% is achieved at pH = 3 for all samples.

The speed of ion exchange was also determined. The uptake of 1×10^{-4} M Tb^{3+} at pH = 3 was monitored with the H−Zr hybrids at various times: 10, 60, and 1440 minutes (24 h), as shown in Figure 26.

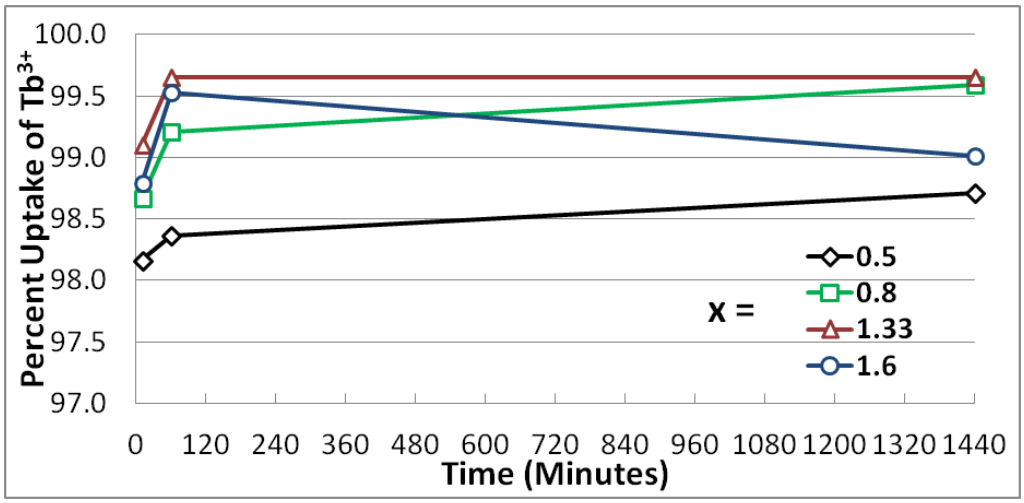

Figure 26: Kinetic study of $1x10^{-4}$ M Tb^{3+} uptake at pH = 3 with time points at 10 min, 60 min, and 1440 min. Greater than 98% uptake of Tb^{3+} is achieved within 10 minutes. Estimate of error 0.5%.

The uptake of Tb is very fast; with greater than 98% removed from the solution in the first 10 min. Equilibrium is reached after 60 min. For all three hybrid varieties, there is a useful selectivity preference that can provide facile separation of unwanted ions from solution. In the case of trying to recover lanthanides from wastewater, H−Zr (x = 0.5 and 0.8) hybrids are good choices. If the removal of unwanted ions with less reliance on charge was desired, then the best option is the H−Zr (x = 1.6) hybrid. These hybrid ion exchangers offer many options of selectivity for the separation of unwanted ions.

3.7 Conclusions

Herein, we have presented several varieties of zirconium phosphonate-phosphate hybrids that have offered multiple modes of selectivity. The unusual selectivity preferences seen

for the H−Zr (x = 0.5 and 1.6) hybrid shows the depth and range that these materials can achieve. Separation of ions from one another can be done based on charge. Complete removal of all ions from solution is also achievable.

3.8 Experimental Details

3.8.1 Materials and Methods

All chemicals were used as received without further purification. Zirconyl chloride octahydrate ($ZrOCl_2 \cdot 8H_2O$) was purchased from Aldrich. Inductively coupled plasma mass spectrometry (ICP-MS) metal-grade nitric acid was purchased from Fisher. Phosphoric acid (85%) was purchased from EMD. 1,4-Phenylenediphosophonic acid [$C_6H_4(PO_3H_2)_2$] was prepared by a modified Hirao palladium cross-coupling reaction.[91] The 120 mL Teflon digestion vessels used in the hydrothermal experiments were purchased from Savillex. Neodymium nitrate hexahydrate [$Nd(NO_3)_3 \cdot 6H_2O$, 99.9%], cesium nitrate [$Cs(NO_3)$, 99.9%], and terbium chloride hexahydrate ($TbCl_3 \cdot 6H_2O$, 99.9%) were purchased from Strem Chemicals. Strontium nitrate [$Sr(NO_3)_2$, 99.0%] was purchased from Fisher Scientific. All salts were used without further purification. ICP-MS standards of all ions investigated were purchased from Inorganic Ventures. Powder X-ray diffraction (PXRD) patterns were obtained with a Bruker D8 X-ray diffractometer using Cu Kα radiation (λ = 1.542 Å) at room temperature operated at 40 mA and 40 kV by the step-scan method (step 0.009°; time 0.1 s). Thermogravimetric analysis (TGA)

spectra were obtained using a TA Instrument Q500 analyzer at a heating rate of 10 °C/min to 1000 °C under 10% nitrogen/90% air. Microprobe (MP) Analysis contained quantitative compositional analyses that were carried out on a four-spectrometer Cameca SX50 electron microprobe at an accelerating voltage of 15 kV at a beam current of 20 nA. All quantitative work employed wavelength-dispersive spectrometers. Analyses were carried out after standardization using very well characterized compounds or pure elements. Analyses of the pressed powder pellets were carried out with a 20-μm-diameter beam, while the stage was being moved 20 μm every 2 s, repeated over a 10 spot traverse. This ensured representative sampling and minimized thermal damage to the samples. Scanning Electron Microscopy (SEM) images were taken with Tescan FERA-3 model GMH focused-dual-beam microscope. Samples were prepared using copper grids from Ted Pella and coated with 5 nm platinum/palladium mixture. For the solid-state NMR analysis, the ^{13}C, ^{29}Si, and ^{31}P NMR spectra were recorded with ^{1}H decoupling if not stated otherwise. The solid-state NMR spectra were measured with a Bruker Avance 400 wide-bore NMR spectrometer equipped with a 4 mm magic-angle-spinning (MAS) probehead. For the MAS measurements, ^{1}H high-power decoupling was applied. The recycle delays were 10 s for MAS spectra. The spinning speed was 10 kHz. N_2 adsorption−desorption isotherms were obtained at 77 K on Micrometritics ASAP 2020 system. Samples were preconditioned by heating at 120 °C for 12 h. IR spectroscopy data of the powders were recorded on a Shimadzu IRAffinity-1 FTIR instrument with a Pike Technologies MIRacle ATR plate. For the titrimetry data, the

NaOH concentration for the capacity studies was determined by a Mettler Toledo EasyPlus automatic titrator with a KHP standard from Fisher Scientific.

3.8.2 Synthesis

The materials having the general formula $Zr(O_3PC_6H_4PO_3)_{1-(x/2)}(O_3POH)_x \bullet nH_2O$, where x = 0.5, 0.8, 1.33, and 1.6, were synthesized hydrothermally by a modification of the method reported by Burns et al. (x = 1.0).[13] Samples were prepared by dissolving an amount of $[C_6H_4(PO_3H_2)_2]$ in 15.70 mL of H_2O, followed by the corresponding phosphate, as summarized in Table 2. Finally, an aliquot of a 0.5 M solution of $ZrOCl_2 \bullet 8H_2O$ (21.44 mL, 10.7175 mmol) was added dropwise to the solution. Upon addition of the metal solution, precipitation occurred. The sample was heated hydrothermally in a Teflon pressure vessel at 120 °C for 4 days. After cooling, the white solid was thoroughly washed with H_2O over vacuum filtration and dried in air at 60 °C overnight. The resulting solid was ground into a fine, white powder.

3.8.3 Ion Uptake Determination for Competitive Study

Solutions were prepared containing 5 mL of 1×10^{-4} M $Cs(NO_3)$, $Sr(NO_3)_2$, and $Nd(NO_3)_3$ at pH = 3.00. An aliquot of solution was added to a measured amount of each sample and mixed thoroughly for 24 h. The solution was separated from the solid by centrifugation and analyzed before and after interaction with an ion exchanger using a

PerkinElmer NexION D inductively coupled plasma mass spectrometer (ICP-MS) to determine the ion concentration. The solution distribution coefficients (K_d) and separation factors (SF) between ions were calculated from the ICP-MS data.

CHAPTER IV

H-ZR AND H-SN PHOSPHONATES AS RADIOLYTICALLY STABLE SORBENT MATERIALS FOR RADIOCHEMICAL SEPARATIONS AND CR(VI) UPTAKE*

4.1 Overview

Zirconium and tin phosphonates were synthesized to determine ion preference and radiolytic stability. The Sn and Zr phosphonate compounds were found to have preference for highly charged positive ions (3+) over lower charged (1+, 2+). The materials were also exposed to 3.18 million gray from Co-60 and were shown to retain their structure and performance. Uptake of radioactive Am-241 with varying pH is also explored. In this chapter, we describe these unusual materials that are simple to prepare, reproducible, and do not require phosphate addition. An unexpected preference for Cr(VI) was discovered for the Zr phosphonate and early work will be discussed herein.

4.2 Introduction

We have been interested in the properties of Zr/Sn phosphonate-phosphates over many years[17,78,79,81,85] based on the fundamental work of Dines et al.[72-74] and Alberti et al.[76,77,92] These materials have been utilized to complete separations of lanthanides from actinides

---

* Reproduced in part with permission from Silbernagel, R.; Shehee, T. C.; Martin, C. H.; Hobbs, D. T.; Clearfield, A. *Chem.Mater*. **2016**, *Accepted.*
http://pubs.acs.org/doi/abs/10.1021%2Facs.chemmater.6b00199 © 2016 American Chemical Society.

in spent nuclear fuel.[13-17] The typical composition is $M(O_6P_2C_6H_4)_{1-x/2}(O_3POH)_x \bullet nH_2O$ where M = Zr or Sn, and x = (0.5, 0.8, 1.33, 1.6), as discussed in Chapter III.[18] These layered compounds exhibit selectivity preferences for ions of higher charge (3+, 4+) and less affinity for ions of lower charge (1+, 2+). For this work, we have prepared materials without the addition of phosphate (O_3POH), or in the formula above x = 0. These materials were prepared as control samples and yet, without phosphate, they achieve uptake of M^{3+} ions with high performance. Surprisingly, Cr(VI), which exists as an anionic complex, was also removed from solution by this Zr phosphonate material. This discovery yielded new information about the Zr phosphonate compound, which has ion preferences different from all other materials, including the Sn phosphonate. Especially important is the robustness of these materials to radiation. Similar compounds have been subjected to Co-60 gamma radiation.[93] The radiolytic stability of these samples was measured with 3.18×10^6 gray gamma from a Co-60 source.

In our previous work with hybrid materials including both phosphonate and phosphate, we believed that the phosphate was the primary means for ion uptake. Now we have shown with the samples without phosphate, that there must be available phosphonic acid moieties and free OH groups to participate in the removal of 3+ ions. The fact that there is a preference for ions of higher charge over those of lower charge is still being determined. Herein, we describe the synthesis, characteristics, ion exchange preferences and performance of these unusual materials. The benefit of these Zr/Sn layered

phosphonates is that they offer simplicity of preparation, robustness, reproducibility, all without addition of phosphate.

4.3 Physical Properties of Zr and Sn Phosphonates

PXRD analysis shows the samples to be poorly crystalline with four broad peaks. As seen in Figure 27, both the tin phosphonate and zirconium phosphonate materials have a first peak at (9.2°, 9.6 Å) corresponding to the distance between the layers which is crosslinked by the phosphonate pillar. The subsequent peaks of the tin phosphonate occur at a higher 2θ angle as a result of the smaller size of the Sn^{4+} ion compared to Zr^{4+}.

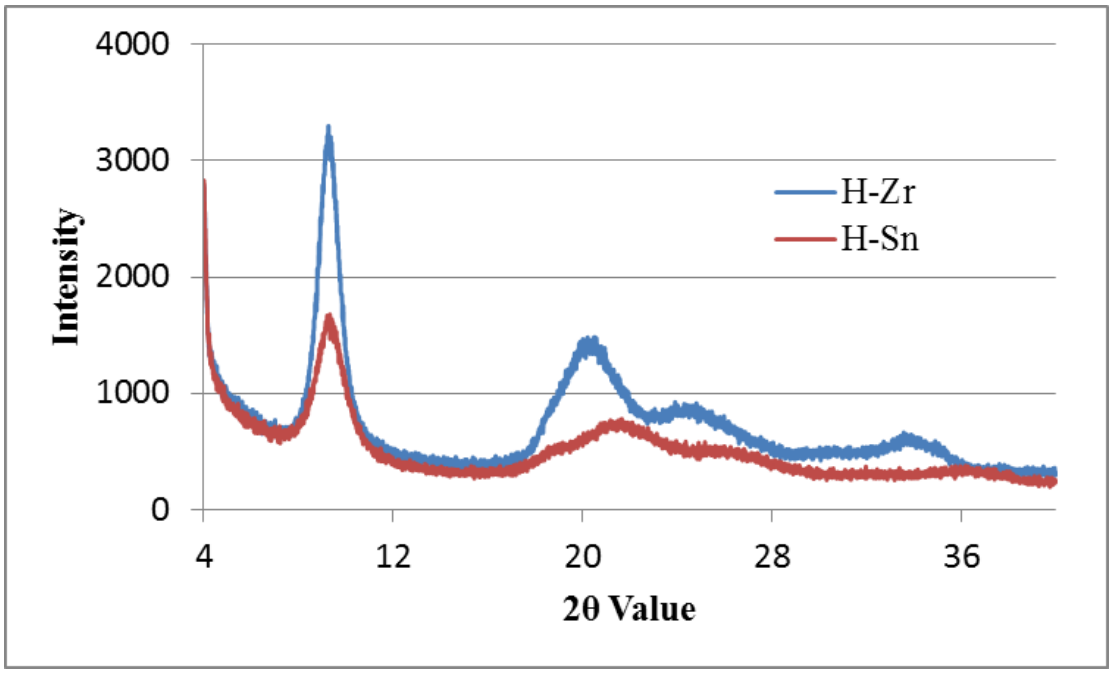

Figure 27: PXRD spectra of zirconium and tin phosphonates, x = 0.

Surface area analysis in Figure 28 shows the N_2 sorption isotherms of the zirconium materials to be an intermediate between Type II and IV while the isotherms of the tin materials are Type I, as previously reported.[18]

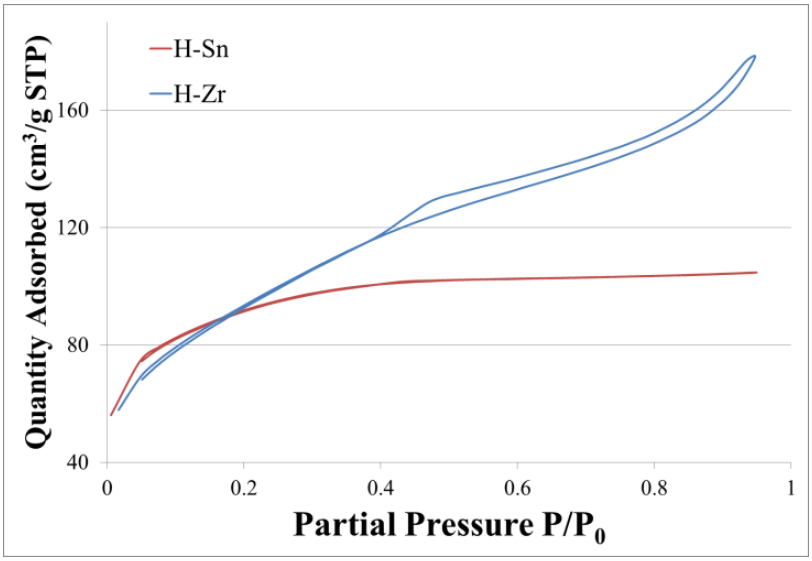

Figure 28: N_2 isotherms of tin and zirconium phosphonates, x = 0.

The isotherms for the phosphonate materials show no hysteresis loop for the tin phosphonate, and a small H4 loop for the zirconium phosphonate, indicating that while micropores are present in both materials, the zirconium material also has mesoporous contributions.[16] The BET surface area values are shown in Table 10.

Table 10: Surface area of the H-Zr/H-Sn x = 0 samples determined by BET method. Estimate of error <10%.

Sample	BET Surface Area (m^2/g)
H-Sn, x = 0	313
H-Zr, x = 0	336

TGA analysis for the tin phosphonate and zirconium phosphonate compounds (x = 0) respectively show water loss of 10.73% and 8.93% of initial weight by 200 °C and subsequent stability until 420 °C where decomposition resulted in a total weight loss of 28.72% and 24.45%, respectively. The weight loss is shown in Figure 29. PXRD verified that the decomposition product is ZrP_2O_7 or SnP_2O_7 and likely includes various Zr/Sn oxides.

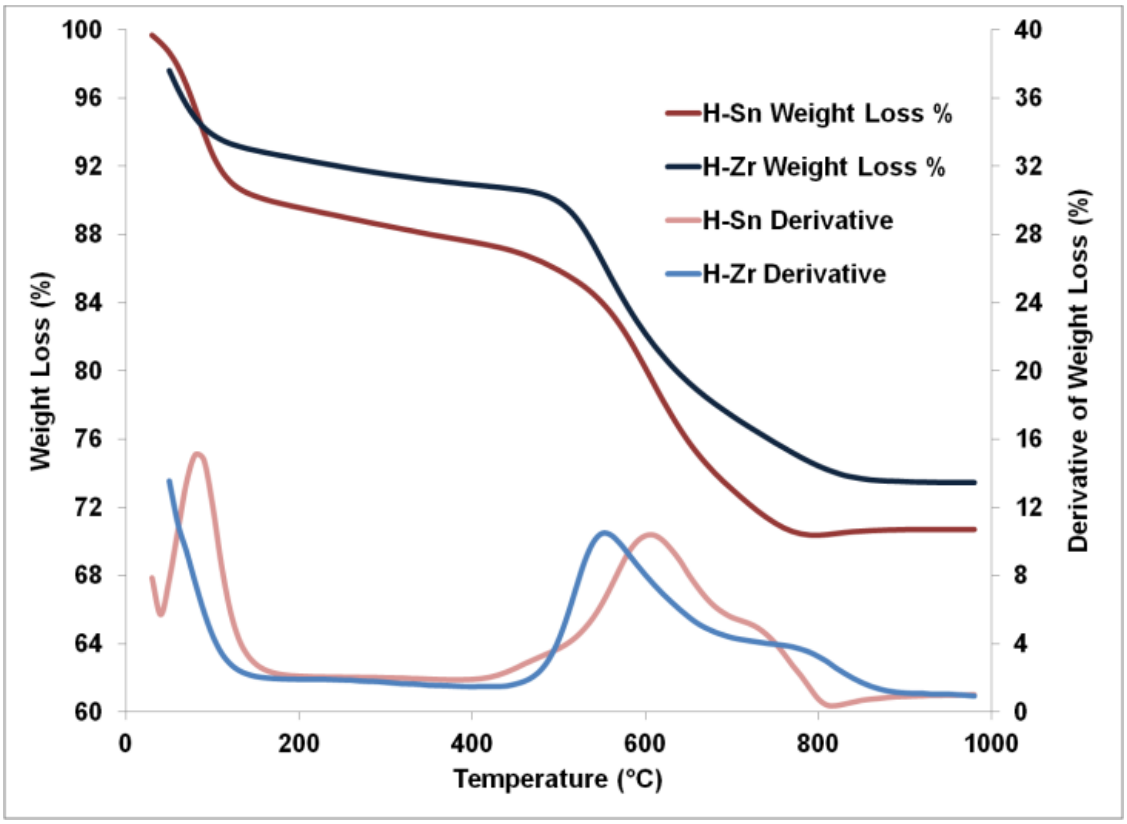

Figure 29: TGA Patterns for the H-Zr and H-Sn x = 0 weight loss percentage and derivative of weight loss. Powders are stable up to 420 °C.

The IR spectra of H-Zr and H-Sn x = 0 are shown in Figure 30. For both samples, there are symmetric and asymmetric P-O-C stretching modes of the phosphonate groups at 827 and 1010 cm^{-1}.[94] P-OH stretching is seen at 1040 cm^{-1} and the P-C stretching region is located at 1150 cm^{-1}.[89] The peak at 1390 cm^{-1} is most likely C=C-H stretching.[88] There is broad O-H stretching in the region near 3500 cm^{-1}. The IR does not show evidence that the P=O is retained in the phosphonate, which would typically be observed between 1240-1350 cm^{-1}.[88,94]

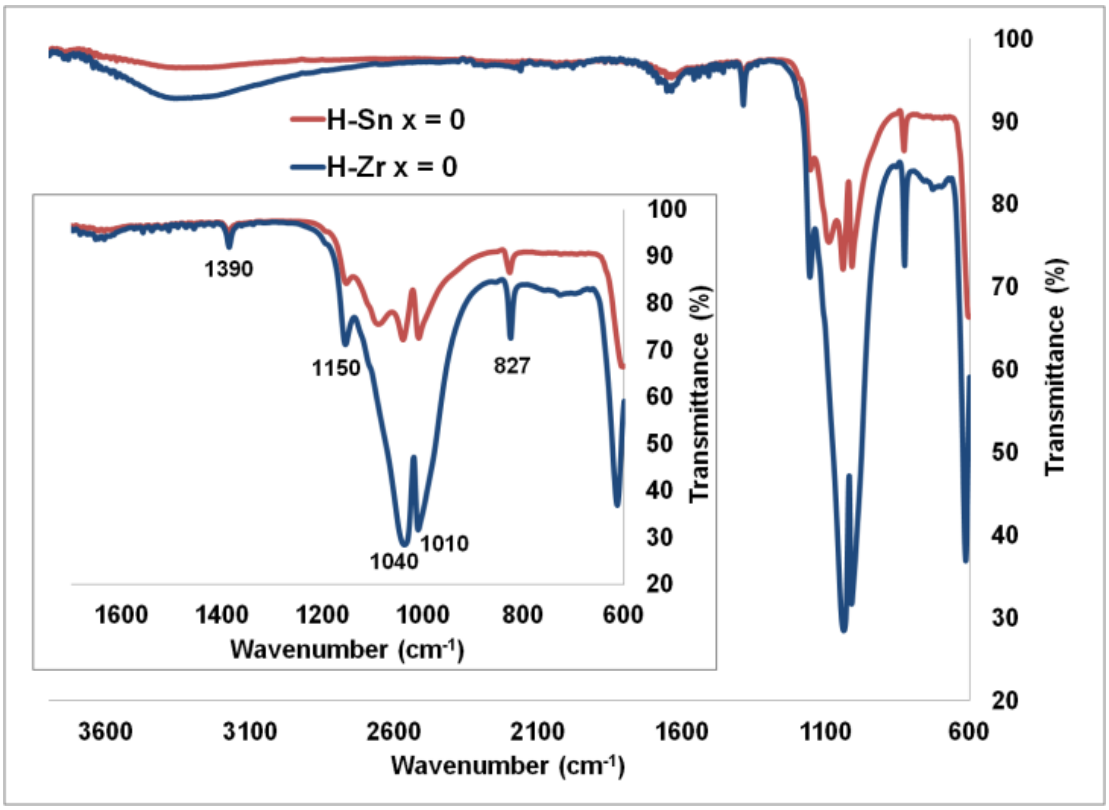

Figure 30: IR of H-Sn and H-Zr x = 0 compounds. Inset photo is zoomed in region of 600-1600 cm^{-1}.

Scanning electron microscopy reveals the particle size and shape. As seen in Figure 31, the particles look different when comparing the H-Sn and H-Zr x = 0. The Zr has round particles; whereas, the Sn particles are oddly shaped and thin. We employed a wide variety of solvents and sonication but there was agglomeration in all cases. Single particles ranged in size from 50-70 nm in size.

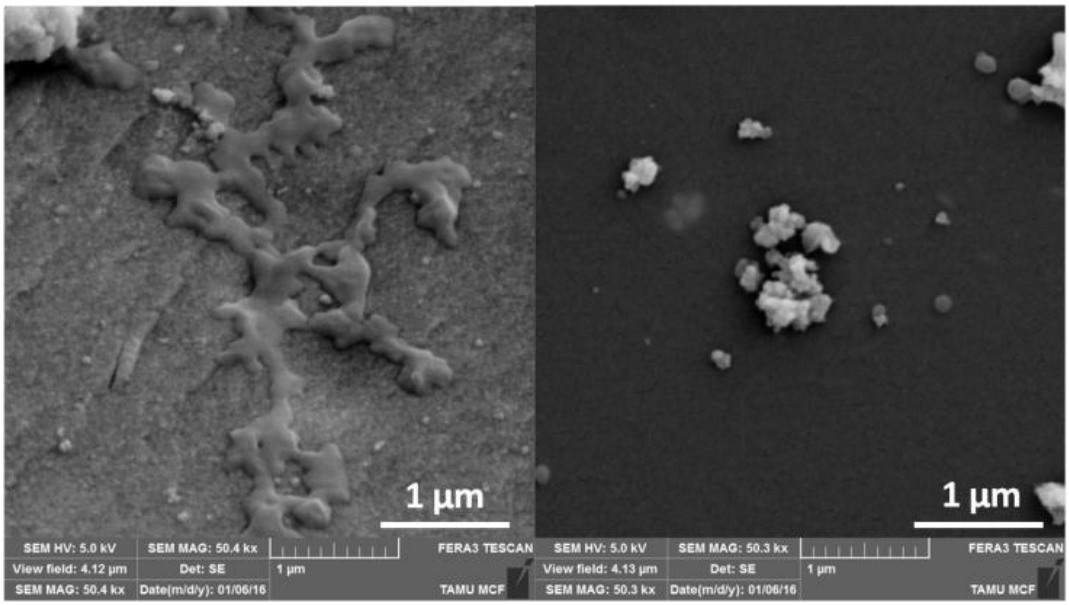

Figure 31: SEM images of H-Sn (left) and H-Zr (right) x = 0.

Solid-State NMR analysis, as seen in Figures 32 and 33, show a peak at approximately 3 ppm in the tin phosphonate compound, corresponding to the phosphonate pillar, whereas, the second peak at -16 ppm which represents the phosphate, is not present.[95] The same trend is observed for zirconium compounds in Figure 33, with peaks at -7.38 ppm, -1.16 ppm, and 5.37 ppm that relate to the different binding modes of the phosphonate. The largest peak at -7.38 ppm is most likely the phosphonate triply bonded

to the Zr or $(POZr)_3$, which allows for crosslinking of the layers and the 9.6 Å interlayer distance. The phosphate peak is absent and would be located at -23 ppm.[78]

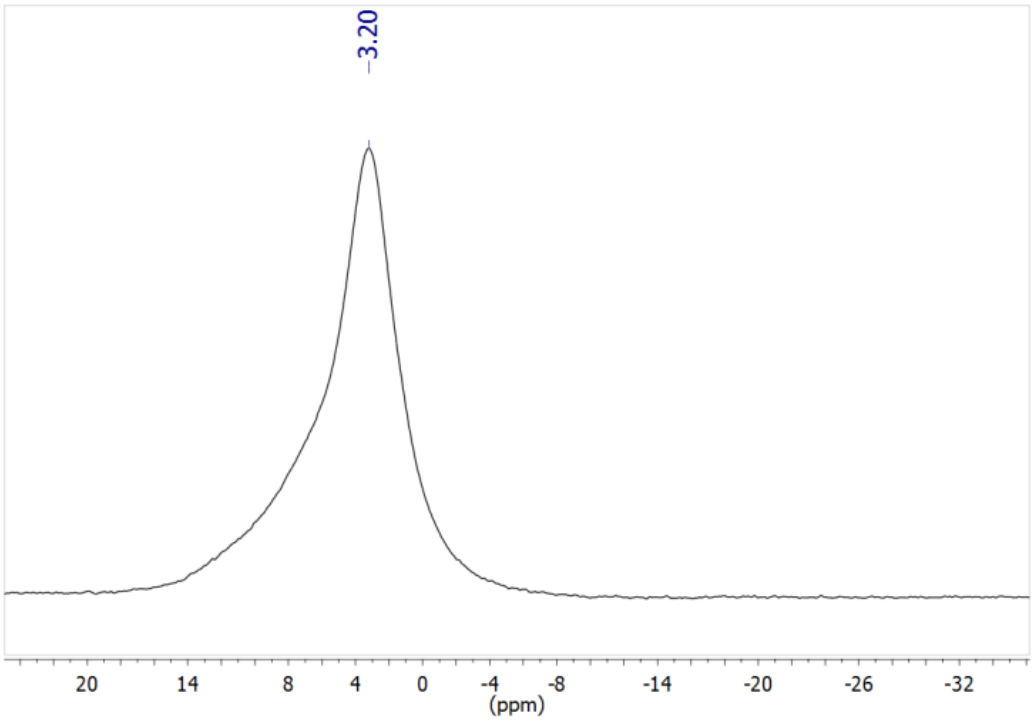

Figure 32: ^{31}P MAS NMR with ν_{rot} = 10 kHz of H-Sn x = 0 sample with no phosphate, which would be a peak present at -16 ppm.

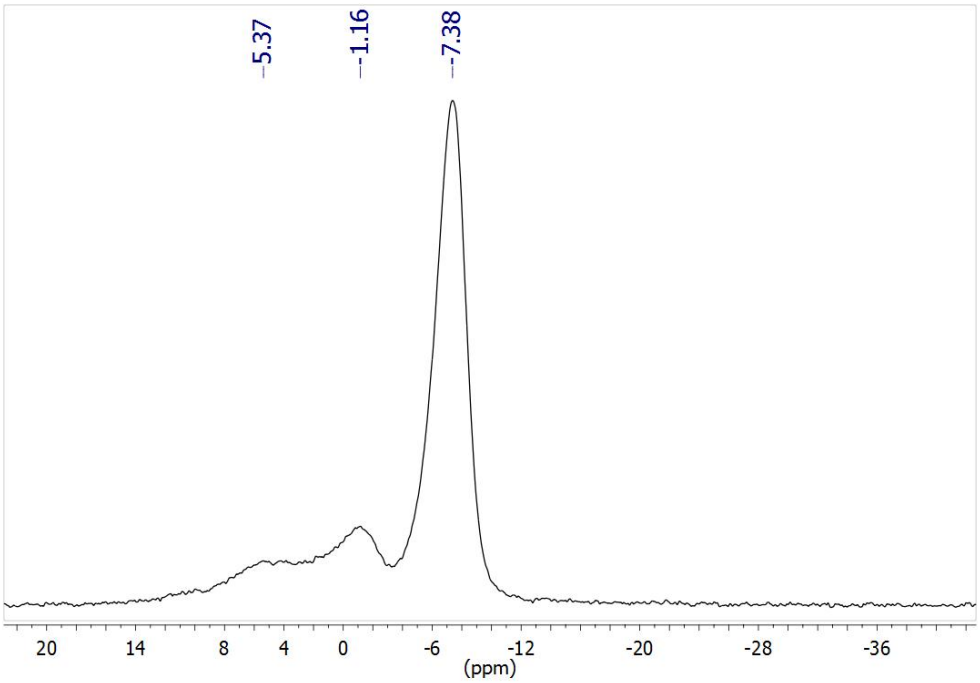

Figure 33: ^{31}P MAS NMR with ν_{rot} = 10 kHz of phosphonate in H-Zr with a ratio of x = 0. No phosphate peak is seen at -23 ppm, thus confirming the absence of phosphate.

Capacity studies were carried out with addition of ~0.1 g of sample being added into 20 mL solution of $1x10^{-3}$ M Eu^{3+} at pH = 3. After stirring for one hour, titration was completed manually with 0.0958 M NaOH. Upon addition of NaOH, the pH was recorded. Once a pH of 10 was achieved, the titration was suspended. The capacity was determined from the concentration of NaOH (mmol) required, once the pH = 10. This value was then divided by the amount of ion exchanger (g) to achieve a value of (mmol/g), as shown in Table 11.

Table 11: Capacity study of H-Zr/H-Sn x = 0 with $1x10^{-3}$ M Eu^{3+} at pH = 3 and 0.0958 M NaOH.

Sample	Amount of Sample (g)	Capacity Eu^{3+} (mmol/g)	Capacity H^{+} (mmol/g)
H-Zr, x = 0	0.1001	0.64	1.91
H-Sn, x= 0	0.0999	1.02	3.07

The H-Zr x = 0 sample has a much lower capacity than other Zr hybrids with phosphate.[18] From preliminary data, it appears that the Sn varieties with and without phosphate have a higher capacity than their Zr counterparts.

Electron microprobe and elemental analysis were completed and are shown in Table 12. Electron microprobe shows the Sn and Zr materials to be homogeneous. In the case of the H-Zr x = 0 material, the formula is not straightforward. Since IR does not show evidence of P=O retention (Figure 30), and Solid-State NMR (Figure 33) shows three different binding modes of the Zr phosphonate, the structure determination is quite difficult as there may be multiple modes of binding in the structure that are not exhibited with the H-Sn x = 0 sample due to the broadness of the peak at 3 ppm. The complications of the H-Zr x = 0 sample have led to a suggested composition that deviates drastically from the calculated proton content.

Table 12: Data on H-Zr/H-Sn x = 0 samples from microprobe and elemental analysis. C and H were analyzed by EA and Sn/Zr, P, and Cl were analyzed by electron microprobe.

Weight %	H-Sn x = 0	H-Zr x = 0
C%	16.93	17.71
H%	2.51	2.23
Sn/Zr%	30.58	22.91
P%	14.96	14.57
Cl%	1.54	0.25

4.4 Ion Uptake and Preference

K_d values of phosphonate materials have been determined previously for ions individually and used to calculate theoretical separation factors that indicated the possibility of preferential pickup of highly charged cations (≥ 3+). For single ion data see previous publications.[13,16,18] In an attempt to understand how the phosphate affects ion uptake, competitive measurements with samples that contained no phosphate were carried out. To determine the selectivity preference of the materials without phosphate, a competitive experiment with Nd^{3+}, Eu^{3+}, Ce^{3+}, Sr^{2+}, and Cs^{+} at a concentration of $1x10^{-4}$ M was executed. For each solution, ICP-MS was used to determine the concentration initially and after each sample material had been mixed in solution for 24 hours. The uptake, K_d and SF were all described previously in Chapter III. The separation factors (SF) are shown in Table 13.

Table 13: Separation factors (SF) for competitive ion exchange study with $1x10^{-4}$ M of Nd^{3+}, Eu^{3+}, Ce^{3+}, Sr^{2+}, Cs^{+} at pH = 3 and 50 mg of H-Sn/H-Zr x = 0.

SF	H-Sn x = 0	H-Zr x = 0
Nd^{3+}/Sr^{2+}	16 ± 1	2,500 ± 100
Ce^{3+}/Sr^{2+}	16 ± 1	2,100 ± 50
Eu^{3+}/Sr^{2+}	15 ± 2	3,500 ± 200
Nd^{3+}/Cs^{+}	49,000 ± 11,000	25,000 ± 6,000
Ce^{3+}/Cs^{+}	50,000 ± 13,000	208,000 ± 8,000
Eu^{3+}/Cs^{+}	46,000 ± 6,000	355,000 ± 40,000

The H-Zr x = 0, has a clear preference for ions of 3+ charge. There was absolutely no affinity for Sr^{2+} and Cs^{+} and 99% uptake of Nd^{3+}, Ce^{3+} and Eu^{3+}. H-Sn x = 0, prefers 3+ ions but has a slight affinity for Sr^{2+} as well. The H-Zr and H-Sn x = 0 show affinity for 3+ ions similar to samples that also contain phosphate.[13,18]

Next, how pH may affect the performance of ion uptake was analyzed. In this case, we prepared a solution of Tb^{3+} at $1x10^{-4}$ M with a pH of 1, 2, and 3. Tb uptake was monitored with varying pH, as seen in Figure 34. Incorporation of Tb was 55% at pH = 1 for H-Zr and near 70% for H-Sn. At pH ≥ 2, the Tb uptake becomes greater than 97%.[13,18]

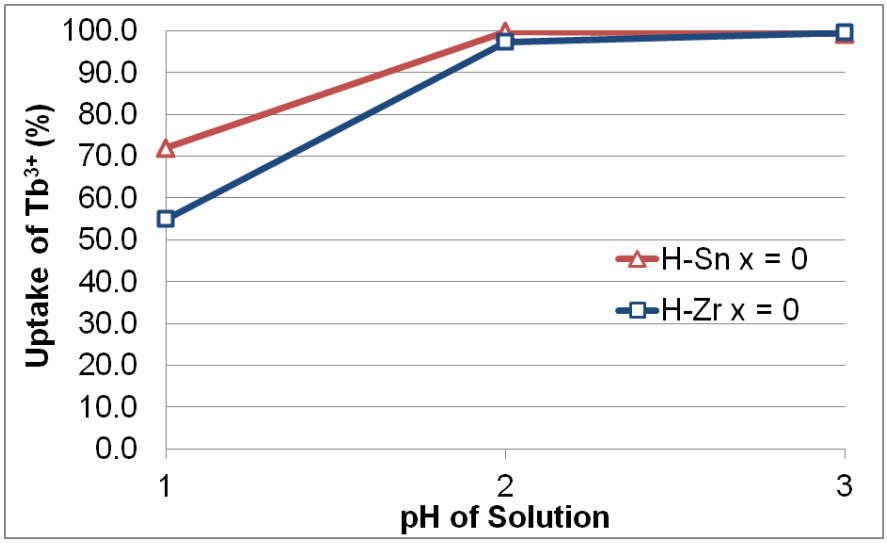

Figure 34: Comparison of Tb^{3+} uptake versus pH for the H-Zr/H-Sn x = 0 samples.

4.5 Uptake of Radioactive Material

As part of our collaboration with SRNL, we have been studying ion exchange to complete separations of spent nuclear fuel. Work from our collaborators has focused on oxidation of Am^{3+} to AmO_2^+ to complete separations from Ln^{3+}.[13-16] The traditional Zr/Sn phosphonate-phosphates have affected separations of An^{3+} from Ln^{3+} through means of oxidation of Am^{3+} to AmO_2^+.[13,14] A separation of AmO_2^+ and Cm^{3+} was successful with a SF of 20.[15]

In order to determine the performance of the Zr/Sn phosphonate without phosphate, uptake was tested with ^{241}Am(III) from SRNL, with a concentration ^{241}Am: 1005 ppb (4.17×10^{-6} M), at pH = 3 as shown in Table 14.

Table 14: K_d and uptake of Am-241 with 10 mg of H-Sn/H-Zr x = 0 ion exchange materials at pH = 3.

Sample Type	Am-241 ppb	Uptake of Am-241 (%)	K_d $^{241}Am^{3+}$ (mL/g)
H-Sn x = 0	6.6 ± 1.9	99.3	30,000 ± 12,000
H-Zr x = 0	2.5 ± 0.5	99.7	78,000 ± 20,000

Uptake of $^{241}Am^{3+}$ was greater than 99% for both samples at pH = 3, which is similar to results previously achieved with samples that contained phosphate.[13]

To determine the effect of pH with uptake we investigated Am-241 uptake with varying pH. 1.25 mL of ^{241}Am: 262 ppb ($1.09x10^{-6}$ M) was mixed with 10 mg of ion exchanger. K_d and uptake of Am-241 was determined by ICP-MS of ion concentration in solution before and after ion exchange as shown in Table 15. To ensure mass balance and that the ion exchange material was actually removing the ion from solution, microprobe analysis of the solid was completed afterward and verified presence of the ion within 3% of the ICP-MS results. Actual pH measurements were 1.17, 2.19, and 3.13.

Table 15: K_d and percent removal of Am-241 from solution through use of Zr or Sn phosphonates.

Sample Type	H-Sn x = 0	H-Zr x = 0
K_d Am-241 pH~1	1,000	900
Removal of Am-241 pH~1	89.7%	89.2%
K_d Am-241 pH~2	29,000	18,000
Removal of Am-241 pH~2	99.6%	99.4%
K_d Am-241 pH~3	232,000	149,000
Removal of Am-241 pH~3	99.9%	99.9%

Ion exchange of Am^{3+} at pH 2 and 3 is large, with greater than 99% uptake of Am-241. As the pH decreases, so does the uptake, which is a trend also seen for lanthanides and actinides with phosphate-containing ion exchangers.[13,14,18] Interestingly, the uptake of Am^{3+} at pH = 1.17 at 89% is the largest exhibited at a pH below 2. This is the first occurrence of Am^{3+} uptake with a Zr/Sn based ion exchanger at a pH near 1. This was not achievable with phosphonate-phosphate based ion exchangers as the pKa of the phosphate moiety is higher than the phosphonate. These new H-Zr/H-Sn x = 0 materials without phosphate offer a new method for conducting separations at pH < 2, that was not previously attainable.

4.6 Radiolytic Stability of Materials

The H-Sn and H-Zr x = 0 samples were irradiated dry with a Co-60 gamma source with a total dose of 3.18 million gray ($3.18x10^8$ rad) with a dose rate of $1.617x10^5$ rad/hr, in a manner similar to Zr Phenyl Phosphonate.[93] After irradiation, the powdered samples were analyzed via PXRD to determine if the structure had been altered. Upon removal from the irradiator, the solids had changed from white to off-white in color. Analysis of PXRD before and after irradiation indicates the structure remains unchanged, with similar interlayer spacing values (9.6 Å), as shown in Figure 35.

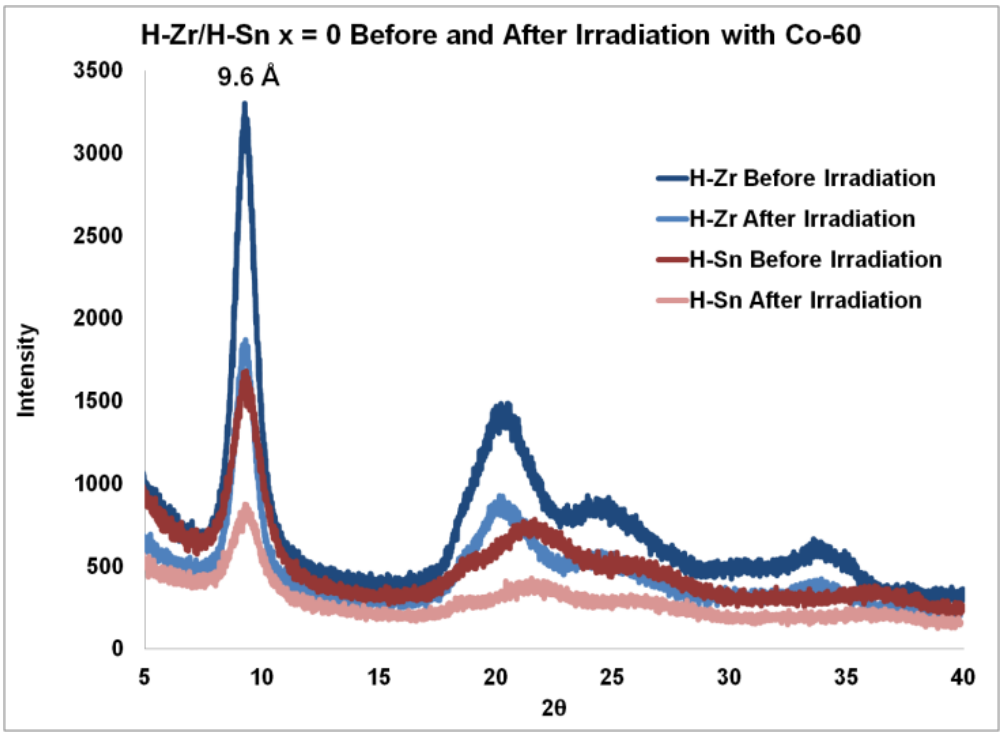

Figure 35: PXRD of H-Sn and H-Zr with a ratio of x = 0 before and after irradiation with Co-60. Very little change in structure is observed after irradiation.

Performance of the ion exchangers after irradiation was measured by conducting a competitive test with uptake of Nd^{3+} and Cs^{+}. The K_d results from the competitive uptake are listed in Table 16.

Table 16: Competitive uptake of Nd^{3+} and Cs^{+} with solids irradiated with Co-60 that received a dose of $3.18x10^6$ gray gamma.

Sample	K_d Nd^{3+}	K_d Cs^{+}	SF Nd^{3+}/Cs^{+}
H-Zr x = 0	240,000 ± 90,000	30 ± 10	8,000 ± 6,000
H-Sn x = 0	110,000 ± 28,000	10 ± 3	11,000 ± 8,000

After irradiation, the preference of 3+ ions remains, with 99.9% removal of Nd and only 9.0% removal of Cs, after the solids were subjected to gamma radiation as high as $3.18x10^6$ gray. Based on the structural and selectivity performance after irradiation and stability towards Am-241 during ion uptake we believe these materials can contribute towards separations in the nuclear fuel cycle.

4.7 Unexpected Uptake of Cr(VI) with Zr Phosphonate Material

Cr(VI) is a highly carcinogenic compound that is found in the industries of plating and electroplating, leather tanneries, textile manufacturing, steel production, etc.[96] Cr(VI) is of particular environmental concern due to its toxicity and mobility and is challenging to remove from industrial wastewater. It is a strong oxidizing agent that is carcinogenic and mutagenic and diffuses quickly through soil and aquatic environments. It does not form insoluble compounds in aqueous solutions, so separation by precipitation is not feasible.[20]

Cr(VI) removal technologies have advanced in recent years, including adsorption,[97,98] chemical reduction,[99] biological methods,[100,101] membrane filtration,[102] and ion exchange.[103] Nevertheless, many of these technologies are marginally cost-effective or difficult to implement in developing countries. The main advantages of ion exchange are the recovery and reuse of Cr(VI), simple operation, less sludge production and the reducing of Cr(VI) concentrations to near-zero levels.[104,105]

Removal of Cr(VI) was attempted at pH ~ 3 with our phosphonate-phosphate hybrids. The chemical form of Cr(VI) at pH = 3 likely exists as 20% $Cr_2O_7^{2-}$ and 80% $HCrO_4^-$, as seen in Figure 36.[20,96]

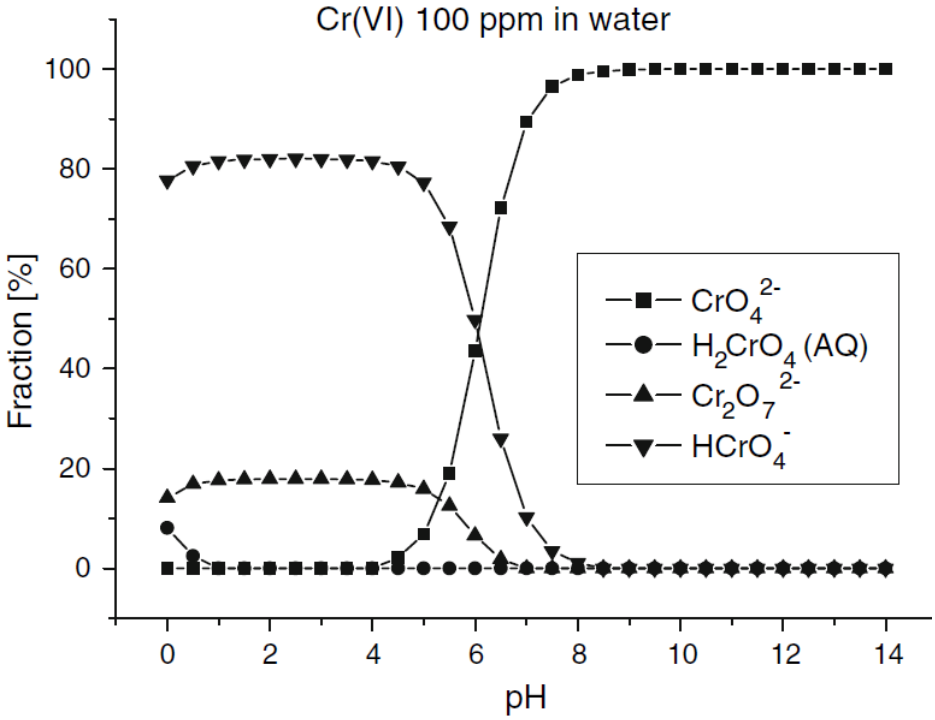

Figure 36: Cr(VI) complexes at varying pH values.

We have synthesized Zr/Sn phosphonate materials that prefer ions of 3+/4+ charge over those of lower charge. The typical composition is $M(O_6P_2C_6H_4)_{1-x/2}(O_3POH)_x \bullet nH_2O$ where M = Zr or Sn, and x = (0, 0.5, 0.8, 1.0, 1.33, 1.6). Attempts to determine anion uptake were not completed previously; therefore, Cr(VI) was selected. The K_d value is calculated by the equation, $K_d = (C_i-C_{eq})/(C_{eq}) * (V/m)$, where C_i is the initial

concentration of the Cr(VI) solution at pH 3.06, which was $4.02x10^{-4}$ M. The C_{eq} was the equilibrium concentration for each of the samples, as deteremined by ICP-MS. V is the volume of liquid used and m is the mass of the solid, which were 5 mL and 200 mg, respectively. The uptake and K_d values are shown in Table 17.

Table 17: K_d and percent uptake values obtained for Cr(VI) at pH=3.06. Estimate of error < 5%.

Hybrid	Source	K_d value (mL/g)	Uptake of Cr from Solution
RMS H-Sn Hybrid x = 1	RMS-II-65	<10	13%
RMS Na-Sn Hybrid x = 1	RMS-II-74	<10	11%
CHM H-Sn Hybrid x = 0	CHM-I-2-A	20	48%
RMS H-Zr Hybrid x = 1	RMS-II-54	90	79%
RMS Na-Zr Hybrid x = 1	RMS-II-84	0	0%
CHM H-Zr Hybrid x = 0	CHM-I-15-A	19,000	99.9%

RMS samples were prepared by the author and CHM samples were prepared by Caroline Martin, the undergraduate technician. Most samples did poorly but the H-Zr phosphonate x = 0 performed well with a K_d near 19,000 and 99.9% Cr uptake. Surprisingly, a similar H-Zr x = 1 sample with phosphate was drastically different in performance, with only 13% uptake of Cr. It was then decided to focus on the H-Zr x = 0 phosphonate, which performed well during the first trial. This time less than 200 mg of H-Zr x = 0 material was used to increase our efficiency, all while using the same amount of liquid (5 mL), as seen in Table 18.

Table 18: K_d and percent uptake values obtained for Cr(VI) at pH=3.06 with varying amounts of solid. Estimate of error < 5%.

Sample	Source	Amount of Solid (mg)	K_d value (mL/g)	Uptake of Cr(VI) from Solution
ACS H-Zr x = 0	ACS-I-2-B	20	6,000	96.2%
ACS H-Zr x = 0	ACS-I-2-B	50	18,000	99.4%
ACS H-Zr x = 0	ACS-I-2-B	100	24,000	99.8%
ACS H-Zr x = 0	ACS-I-2-B	200	40,000	99.9%
ACS H-Zr x = 1	ACS-I-2-C	100	<10	6.0%
ACS H-Zr x = 1	ACS-I-2-C	200	<10	1.8%

The use of H-Zr x= 0, which was synthesized by two technicians (ACS & CHM), months apart, results in Cr(VI) removal from solution. Addition of phosphate (H-Zr x = 1); however, has no affinity for Cr(VI). The H-Zr x = 0 performed well at all amounts of solid and 5 mL of solution but with 100 mg a K_d near 24,000 and 99.8% Cr(VI) uptake was achieved. 20 mg resulted in a K_d near 6,000 and 96.2% Cr(VI) uptake.

The expected mechanism would be that the Cr(VI) is reduced to Cr(III) but no evidence of this change was observed. First off, Cr(VI) is yellow and Cr(III) is blue-green.[106] When uptake of Cr(VI) is achieved by the H-Zr x = 0 sample, the material appears yellow, as seen in Figure 37. Also, if Cr(III) were present, all the ion exchangers should be able to remove Cr(III) as we have done previous work that shows no problem with 99% uptake of Cr(III) but the only compound to complete Cr(VI) removal is H-Zr x = 0.

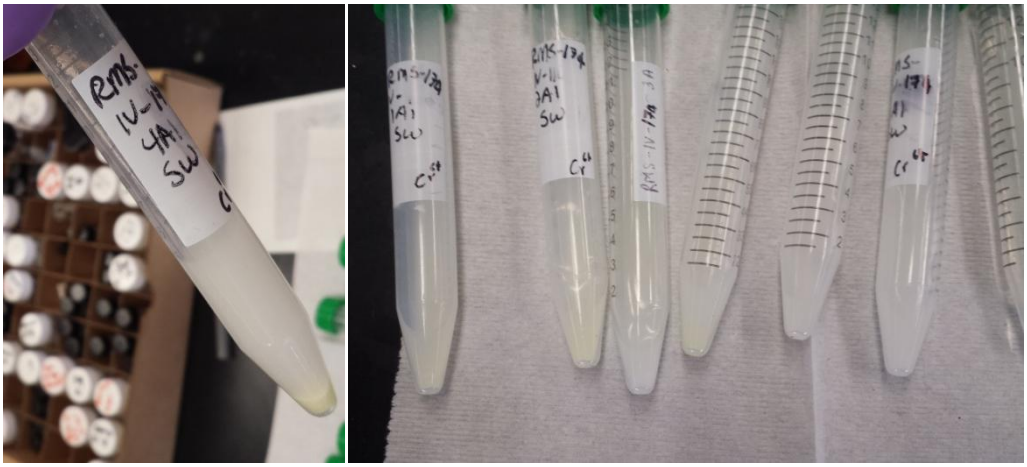

Figure 37: Cr(VI) uptake with H-Zr x = 0, showing a yellow tint on the samples that achieved uptake of 99%.

4.8 Conclusion

Herein, we have presented the capabilities of Zr/Sn x = 0 materials that do not contain phosphate. There is a clear selectivity preference for 3+ ions over those of lower charge (1+, 2+). Amazingly, these materials are comparable to their phosphonate-phosphate counterparts in performance and radiolytic stability, all without the additional phosphate in the synthesis. Furthermore, uptake of Am-241 at pH = 1.17 at 89% is the highest documented for these materials at a pH < 2. These robust materials have documented stability towards gamma radiation. Surprisingly, the H-Zr x = 0 sample was able to remove 99% of Cr(VI) from solution, which is the first time uptake of an anion was achieved with any Zr/Sn phosphonate-phosphate material. More work will be completed to determine the mechanism of this uptake and applications towards environmental remediation.

4.9 Experimental Materials and Methods

4.9.1 Materials

All chemicals were used as received without further purification. Stannic chloride pentahydrate ($SnCl_4 \cdot 5H_2O$), Zirconyl chloride octahydrate ($ZrOCl_2 \cdot 8H_2O$), and ICP-MS Trace Metals Grade HNO_3 were from Fisher Scientific. 1,4-phenylenebis(phosphonic acid ($C_6H_4(PO_3H_2)_2$) was prepared by a modified Hirao Pd cross-coupling reaction.[91] The 120 mL Teflon® digestion vessels used in the hydrothermal experiments were purchased from Savillex. Neodymium nitrate hexahydrate ($Nd(NO_3)_3 \cdot 6H_2O$, 99.9%), cesium nitrate ($Cs(NO_3)$, 99.9%), europium nitrate hexahydrate ($Eu(NO_3)_3 \cdot 6H_2O$, 99.9%), and cerium nitrate hexahydrate ($Ce(NO_3)_3 \cdot 6H_2O$, 99.9%), and terbium chloride hexahydrate ($TbCl_3 \cdot 6H_2O$, 99.9%) were purchased from Strem Chemicals. Strontium nitrate ($Sr(NO_3)_2$, 99.0%) was purchased from Fisher. All lanthanide salts were used without any further purification.

The Am-241 stock solution was recovered from fuel reprocessing at the Savannah River Site. The Am was purified by passing it through an Eichrom DGA-branched column in ~1 M HNO_3 and then eluted off the column with 0.01 M HNO_3. The Am-241 purity was determined by spectroscopic techniques (Avantes AvaSpec-2048TEC Thermo-electric cooled Fiber Optic Spectrometer coupled with a 100 cm World Precision Instruments LWCC liquid waveguide capillary cell with an Ocean Optics LS-1 tungsten halogen

lamp). The data were collected and compiled in the AvaSpec-USB2 7.2 software in absorbance mode. ICP-MS Standards of all lanthanide ions investigated were purchased from Inorganic Ventures. All work with Am-241 was carried out by the analytical laboratory at the SRNL. Sodium bichromate dihydrate ($Na_2Cr_2O_7$•$2H_2O$, 99.5%) was purchased from Sigma Aldrich and was used without purification. The Cr(VI) reference standard for ICP-MS was purchased by Inorganic Ventures.

4.9.2 Synthesis

The materials were synthesized hydrothermally by a modification of the method reported by Burns et al.[13-16] Samples were prepared by dissolving an amount of $C_6H_4(PO_3H_2)_2$ (1,4-phenylenebis(phosphonic acid)) in 15.70 mL of H_2O, followed by dropwise addition of 0.5 M solution of $SnCl_4$•$5H_2O$ or $ZrOCl_2$•$8H_2O$ (21.44 mL, 10.7175 mmol). Upon contact with the metal solution and the phosphonate, there was immediate precipitation, which looked like a thin, white gel. The sample was heated hydrothermally in a Teflon® pressure vessel at 120 °C for 4 days. After cooling, the white solid was washed with water and air-dried at 60 °C overnight. The resulting solid was ground into a fine, white powder.

4.9.3 Instruments and Procedure

Powder X-ray diffraction patterns (PXRD) were obtained using a Bruker D8 X-ray Diffractometer using Cu-Kα radiation (λ=1.542 Å) at room temperature operated at 40 mA and 40 kV by the step-scan method (step 0.009, time 0.1 s). Analysis of water and total weight loss was determined by thermogravimetric analysis (TGA) obtained using a TA Instrument Q500 at a heating rate of 10 °C min^{-1} to 1000 °C under 10% N_2 and 90% air. Quantitative compositional analyses of Zr and P were carried out on a four spectrometer Cameca SX50 electron microprobe at an accelerating voltage of 15 kV at a beam current of 20 nA. All quantitative work employed wavelength-dispersive spectrometers (WDS). Analyses were carried out after standardization using very well characterized compounds or pure elements. The analyses of the pressed powder pellets were carried out with a 20 μm diameter beam while the stage was being moved to ensure representative sampling and minimized possible thermal damage to the samples.

The ^{31}P MAS spectra were recorded with ^{1}H decoupling if not stated otherwise. The solid-state NMR spectra were measured with a Bruker Avance 400 widebore NMR spectrometer equipped with a 4 mm MAS probehead. The recycle delays were 10 s and 10 kHz was the spinning speed. N_2 adsorption-desorption isotherms were obtained at 77 K on Micrometritics ASAP 2020 system. Samples were preconditioned by heating at 120 °C for 12 h. SEM Images were taken with Tescan FERA-3 Model GMH Focused

Dual Beam Microscope. Samples were prepared using copper grids from Ted Pella and were coated with a 5 nm Pt/Pd mixture.

4.9.4 Ion Uptake Determination

Solutions were prepared containing between 2 and 5 mL of $1x10^{-4}$ M $Cs(NO_3)$, $Sr(NO_3)_2$, $Nd(NO_3)_3$, $Eu(NO_3)_3$, $Ce(NO_3)_3$, and $Sm(NO_3)_3$ at pH = 3. An aliquot of solution was added to a measured amount of each sample and mixed thoroughly for 24 hours. The solution was separated from the solid by centrifugation and analyzed before and after interaction with the ion exchanger using a Perkin Elmer NexION D Inductively-coupled Plasma Mass spectrometer (ICP-MS) to determine ion concentration. The distribution coefficients (K_d) and separation factors (SF) were calculated from the ICP-MS data.

CHAPTER V

NA-ZR HYBRID ION EXCHANGE FOR RARE EARTH RECOVERY FROM COMPACT FLUORESCENT LAMPS (CFLS)

5.1 Introduction

Rare Earth Elements (REE) are comprised of Y, Sc and lanthanides (La-Lu), and are named so due to their limited abundance compared to common Earth elements (Ca, Mg). REE are utilized in a wide variety of green technologies such as; photovoltaic film coatings, wind-turbine and vehicle batteries, magnets, catalysis, and lighting.[21,107,108] Compact Fluorescent Lamp (CFL) phosphor powder accounts for 12% of the rare earth market[21] and contains large quantities of Y and Eu. In 2011, due to trade barriers placed by China, the price of REE increased dramatically. Between 2001 and 2011, the price increase was 400% for yttrium and 600% for europium.[21] The price has stabilized to some degree after 2012 but supply concerns remain evident. Figure 38 illustrates the elements that are projected to be in critical supply from 2015-2025 by the Department of Energy.[21]

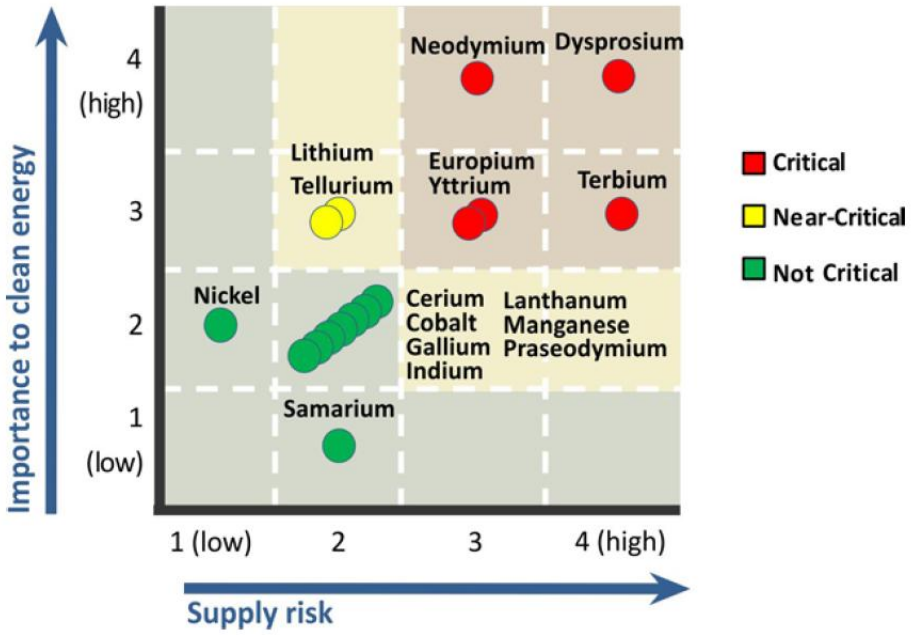

Figure 38: Criticality matrix estimated by DOE from 2015-2025.

The elements with critical supply projected from 2015-2025 are Dy, Tb, Nd, Eu, and Y. With the price spike and critical supply concerns, recycling of REE was proposed as a mechanism to reduce the supply concerns of Y and Eu. Presently; disposal of CFLs is illegal because they contain a small portion of mercury. Due to the limited economic impact of recycling CFLs, it is estimated that 24% of all CFLs are collected and treated for mercury removal.[109] It is believed that collection of CFLs would increase if there was an economic impact with the CFL waste and that would be contributed to recycling of CFLs to reclaim REE. Solvay corporation has already initiated plans implementing recycling of REE.[110] The plan would be to remove the mercury from the waste stream, use previous technologies to place the REE in solution phase, and then conduct a means

to complete a separation of REE from the waste bulk. We propose using ion exchange materials to separate the rare earths from the waste bulk.

5.2 REE Composition of CFLs

Three compact fluorescent lamps of different heat and light color, labeled as (soft white, neutral, and cool white) were purchased and analyzed for Y, Al, Tb, Ce, Eu, Hg, Mn content. We therefore extracted the white powder by mechanical scraping with a wooden spatula from fluorescent lamps as shown in Figure 39.

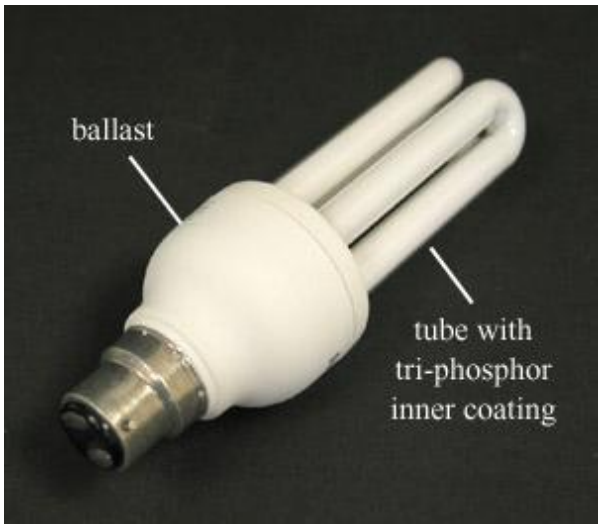

Figure 39: A compact fluorescent lamp (CFL) with a white tri-phosphor coating.

The extracted soft white CFL phosphor powder was analyzed by Electron Microprobe to determine the elemental content. As seen from Figure 40, the microprobe analysis of the

soft white CFL powder illustrates that the components of this powder are predominately Al and Y, with a small amount of Eu, Tb, and Ce.

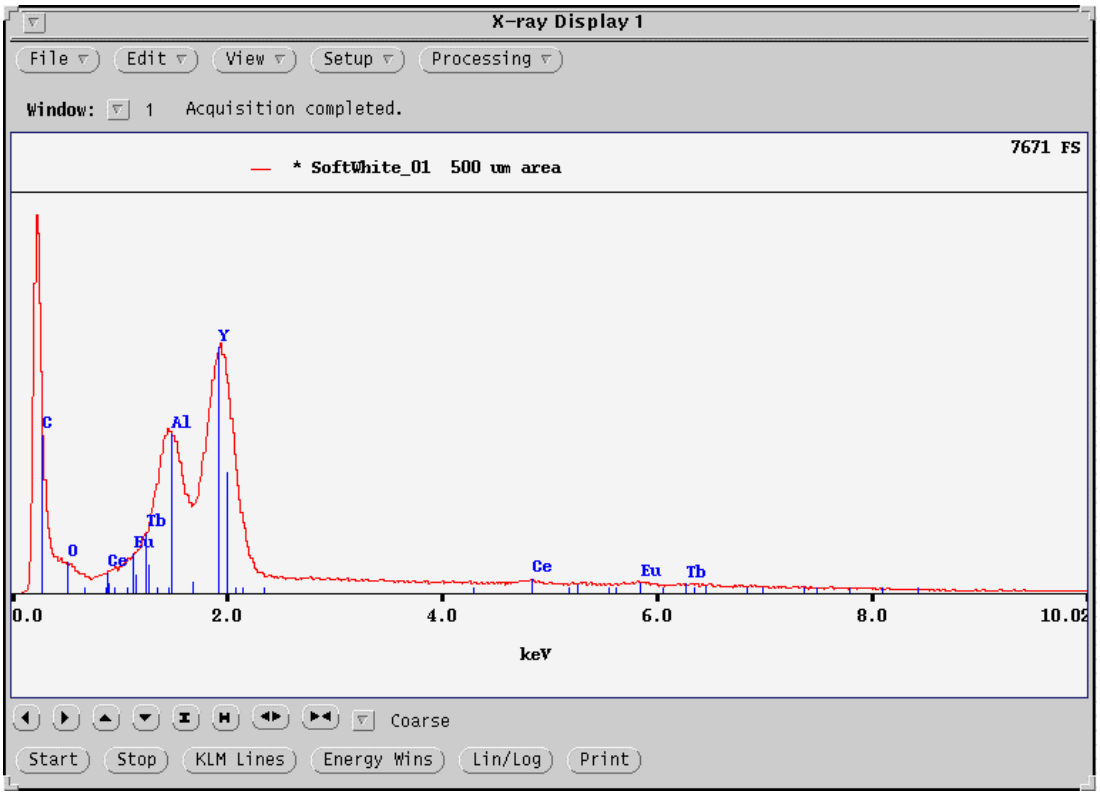

Figure 40: Electron microprobe analysis of tri-color phosphor powder from a soft white CFL.

Next, the phosphor powder was collected from CFLs and attempts to solubilize the REE, while limiting the Al content was completed. In order to do this we completed experiments on the solubility of the white phosphor powder in different acidic media (HNO_3 and HF). For this procedure, 500 mg of phosphor powder was added to 10 mL of the acidic media and mixed overnight at room temperature. The solid did not

completely dissolve under any circumstance. The solid was centrifuged and the top portion of the liquid was extracted for analysis via ICP-MS, as seen in Table 19. The concentration of each ion was determined and is listed in ppb. The higher the concentration in solution, the higher the solubility of the ion in the acidic media. The ideal case is the selection of an acidic media with the highest concentrations for Y, Tb, Eu, and Ce and the lowest for Al.

Table 19: Comparing dissolving media for the selected ions in CFL waste through use of concentration in ppb.

Dissolving Media	Concentration in ppb				
	Al	Y	Tb	Eu	Ce
Conc. HF	46,000	60	<0.1	5	<0.1
50% HF	50,000	30	0.3	2	<0.1
Conc. HNO_3	4,200	1,900	0.5	150	0.1
10% HNO_3	3,500	4,300	0.1	360	0.1

As seen from Table 19, Al, Y, and Eu are the primary elements present in HF and HNO_3. The best choice is 10% HNO_3 because the Al concentration is lowest and the Y, Eu concentrations are highest.

5.3 Ion Exchange Tests for Rare Earth Recovery

As part of the effort in recycling REE we have conducted uptake studies of typical REE present in CFLs, using our hybrid ion exchange materials. These ion exchange materials have the typical composition: $M(O_3PC_6H_4PO_3)_{1-x/2}(APO_4)_x \bullet nH_2O$, where M= Zr^{4+}, Sn^{4+}

and A = H, Na, K and x = 1. These samples have a 1:2 ratio of phosphonate ($O_3PC_6H_4PO_3$) : phosphate (HPO_4). Many of these materials have already been characterized.[13-16,18]

To determine potential application in this area, simulated ion solutions of Al^{3+}, Y^{3+}, Ce^{3+}, Eu^{3+}, and Tb^{3+} and other elements, at a concentration of $1x10^{-4}$ M at pH = 3, were tested to determine if uptake was possible with simplified single-ion solutions. The concentration was determined via Inductively Coupled Plasma-Mass Spectrometry (ICP-MS) before and after interaction with the ion exchange material. As seen in Table 20, uptake of common REE and Al present in CFLs was conducted with simulated, single-ion solutions, resulting in uptake of ions to be 90% or greater. This shows that our materials are able to complete separations of many REE and are not just limited to Y and Eu that are present in CFLs.

Table 20: Uptake of selected M^{3+} ions (%). Concentration is $1x10^{-4}$ M at pH = 3.

ID	Al^{3+}	Cr^{3+}	Y^{3+}	Ce^{3+}	Nd^{3+}	Sm^{3+}	Eu^{3+}	Tb^{3+}
H-Sn	98.6 ± 0.4	99.3 ± 0.1	99.1 ± 0.3	98.9 ± 0.6	99.1 ± 0.9	97.7 ± 2.7	98.2 ± 1.6	98.8 ± 1.1
Na-Sn	99.1 ± 0.7	99.6 ± 0.1	99.1 ± 0.2	99.3 ± 0.6	99.1 ± 0.5	99.6 ± 0.1	99.4 ± 0.4	99.4 ± 0.1
K-Sn	97.9 ± 2.5	99.7 ± 0.1	98.5 ± 1.0	99.7 ± 0.1	99.6 ± 0.1	99.2 ± 0.1	96.3 ± 2.2	99.5 ± 0.2
H-Zr	99.1 ± 0.2	98.2 ± 0.1	98.7 ± 0.3	99.0 ± 0.1	99.2 ± 0.2	99.4 ± 0.2	99.4 ± 0.1	99.5 ± 0.2
Na-Zr	97.9 ± 0.2	99.6 ± 0.1	98.3 ± 0.8	99.6 ± 0.2	99.3 ± 0.8	96.0 ± 5.4	99.2 ± 0.1	91.4 ± 3.7

To determine the preferential uptake with multiple ions in solution together from the phosphor powder, 100 mg of phosphor powder was mixed for 24 hours with 100 mL of

10% HNO_3. Afterward, the solid remained and was filtered off with a 0.2 µm Millipore filter. The liquid was then pH adjusted with NaOH to the range of 2-3 and the liquid remained colorless and transparent. 5 mL of the phosphor liquid was mixed with 200 mg of the ion exchange material for 24 hours and the concentration was compared by ICP-MS before and after addition of the ion exchange material. Table 21 shows the results of mixture with a neutral phosphor powder. Only the Na-Zr hybrid performed well, with 99% uptake of Y and Eu.

Table 21: Percent removal of ions from CFL neutral powder solution at pH ~ 3.

Hybrid Type	% Removal of Y^{3+}	% Removal of Tb^{3+}	% Removal of Eu^{3+}	% Removal of Al^{3+}	% Removal of Ce^{3+}
H-Sn x = 0	53.0	68.4	60.3	36.4	<1
H-Sn x = 1	21.1	52.6	27.2	<1	<1
H-Zr x = 0	9.0	<1	6.5	18.5	<1
H-Zr x = 1	3.4	36.8	1.1	<1	<1
Na-Zr x = 1	99.9	<1	99.9	95.4	<1
Conc of Ion Control [M]	$4.17x10^{-3}$	$5.98\ x10^{-7}$	$2.10x10^{-4}$	$7.80x10^{-4}$	$2.15x10^{-7}$

The concentrations of Tb and Ce were present in very limited quantities and results in large error for the concentration of Tb. Multiple studies have confirmed that the Ce and Tb concentrations are too low for consideration; therefore, all analysis will continue forward with Y, Eu, and Al. It should be noted that if the concentrations of Tb and Ce would have been higher, uptake would have been achieved much like what is seen for Eu. The only hybrid ion exchanger that performed well was the Na-Zr x = 1 hybrid. This

hybrid picked up 99.9% of the Y and Eu and 95.4% of the Al in solution. The K_d values for the Na-Zr hybrid uptake are shown in Table 22.

Table 22: A closer look at the performance of the Na-Zr hybrid with K_d (mL/g) and SF. Estimate of error < 5%

Hybrid	K_d of Y	K_d of Eu	K_d of Al	SF Y/Al	SF Eu/Al
Na-Zr x = 1	39,000	52,000	1,000	39	52
Conc of Ion Control [M]	4.17×10^{-3}	2.10×10^{-4}	7.80×10^{-4}	5.3	0.3

Not only is the Na-Zr x = 1 hybrid able to complete uptake of the ions, it has a preference for the Y and Eu over Al. The separation factors (SF) of Y/Al and Eu/Al in the actual solution were 5.3 and 0.3 but the preference of the ion exchanger shows separation factors of Y/Al and Eu/Al of 39 and 52. Fortunately for the goal of reclaiming REE, there is a clear preference for Y and Eu over Al.

5.4 Discussion of RMS Na-Zr Hybrid

The Na-Zr x = 1 hybrid was studied in depth by Burns et al.[13-16] Additional studies of the elemental content via EA and Microprobe were utilized to create a likely formula for the material used in these studies, as seen in Table 23.

Table 23: Analytical data from EA and microprobe for weight percent utilized to determine formula for Na-Zr x = 1 hybrid.

RMS Na-Zr (RMS-II-84)	EA Wt %		Microprobe Wt %			
	C	H	Na	Zr	P	Cl
Actual Values	8.21	1.92	6.12	27.13	15.69	0.10
Formula	$Zr(O_3PC_6H_4O_3P)_{0.387}(NaPO_4)_{0.905}(HPO_4)_{0.043}(OH)_{0.556}(H_2O)_{2.16}$					
Calculated Values	8.18	1.91	6.10	26.75	15.64	NA

The agreement of the calculated formula to the actual values determined from Microprobe and EA is quite good, with the largest difference being 1.4 percent error from Zr, which is comparable to the error in the weight percent measurement of Zr by Microprobe. In this formula, complete incorporation of $NaPO_4$ is nearly achieved.

5.5 Titration and pH Studies on Na-Zr Hybrid

Titrations were completed on this sample to monitor uptake of REE. A titration study with 0.0996 g of Na-Zr x = 1 hybrid, 25 mL of $1x10^{-3}$ M Eu^{3+} solution at pH 3.05 and 0.0958 M NaOH was completed. Much like in Chapter III, before titration began, the pH of the liquid was monitored before and after addition of the Na-Zr x = 1 material, with the pH changes shown in Table 24. For the initial pH change, no NaOH or acid was added; the pH increases because Eu is being removed from solution and Na^+ is being released. The Na-Zr x = 1 sample is the only known material that increases the pH due to the high sodium content.

Table 24: Change of pH from addition of Na-Zr x = 1 sample in $1x10^{-3}$ M Eu^{3+} solution.

pH Before Addition of Solid	3.05
pH at 15 Seconds After Addition	4.35
pH at 1 Minute After Addition	5.20
pH at 60 Minutes After Addition	7.28

After stirring the solid in the Eu solution for 1 hour, the solution appeared opaque and milky white. With constant monitoring of pH, 0.0958 M NaOH was manually added into the Eu/Hybrid liquid stirring below. The titration was quick as the pH was already above 7, after each drop the pH would slowly rise and fall. After the pH remained over 10, the titration was stopped. The graph of pH change versus addition of NaOH is shown in Figure 41.

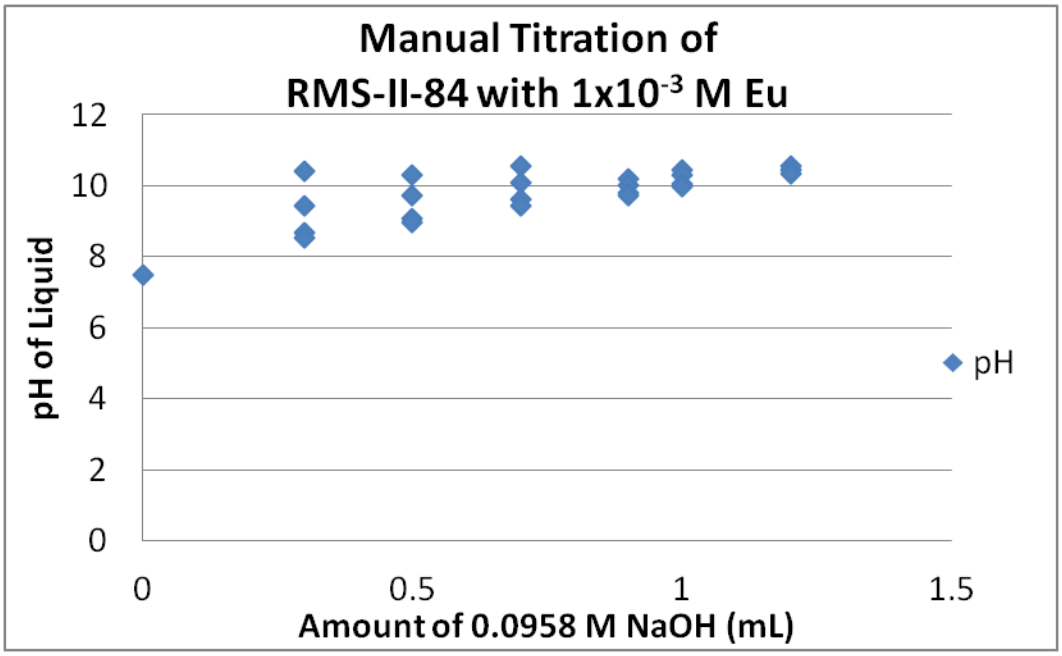

Figure 41: Titration curve for $1x10^{-3}$ M Eu and NaOH with Na-Zr hybrid x = 1.

The amount of NaOH added to achieve a pH well above 10 was used to determine the mmol of H+ present. Dividing the H+ mmol capacity by the amount of hybrid used in grams resulted in the capacity value (mmol/g), as shown in Table 25.

Table 25: Capacity study of Na-Zr x = 1 material with $1x10^{-3}$ M Eu^{3+} at pH = 7 and 0.0958 M NaOH.

x =	Amount of Sample (g)	Capacity Eu^{3+} (mmol/g)	Capacity H^{+} (mmol/g)
1	0.0996	0.32	0.96

The capacity is much lower because when the titration began the pH was above 7 for the Na-Zr x = 1 sample and the pH is below 3 for all other samples, as listed in Appendix A.

One question was why does the Na-Zr hybrid work in removing the REE from the CFL waste but the other hybrids do not? When the Na-Zr hybrid is added to a CFL ion solution at pH ~ 3, Na^{+} is released and the pH of the liquid increases. The concern here is that the pH can rise as high as 5-7, which may cause precipitation of the lanthanides and thus increase the perceived effectiveness of our hybrid materials. The other hybrid types exchange protons, which lower the pH into a region that would not cause lanthanide precipitation. Surprisingly, the Na-Sn hybrid also decreases the pH of the Eu solution because the incorporation of Na in the Na-Sn is less than in the Na-Zr hybrid, so mostly protons are released even in this material.

In order to see if it was possible to limit the increase in pH with the Na-Zr hybrid, a study was completed by adding the hybrid to the solution, followed by pH monitoring and adjustment with HNO_3. The results shown in Table 26 have large uptakes of Y, except for the sample with a pH below 1.5, which is expected for this material. The pH was adjusted before mixing for 24 hours but this had little effect on the overall pH after shaking. The pH of the adjusted solution should be near 2-2.5 to attempt for a pH less than 4 after shaking. What can be determined is that a pH above 4.5 definitely has 99.8+% uptake.

Table 26: Na-Zr hybrid uptake of Y with various pH values.

Sample ID	Weight of Hybrid (g)	Volume of Liquid (mL)	Concentration of Y in Sample (M)	Uptake of Y^{3+} (%)	K_d Value (mL/g)	pH Adjusted with HNO_3 Before Shaking	pH After 24 Hrs
RMS-IV-150-A2	0.0999	5	$2.52x10^{-6}$	99.9	75,000	4.54	6.36
RMS-IV-150-B2	0.1001	5	$2.16x10^{-6}$	99.9	87,000	3.48	5.90
RMS-IV-150-C2	0.1001	5	$9.22x10^{-7}$	99.9	200,000	3.78	6.31
RMS-IV-150-D2	0.1000	5	$4.75x10^{-6}$	99.9	40,000	3.15	5.86
RMS-IV-150-E2	0.1001	5	$8.37x10^{-6}$	99.8	22,000	2.82	4.74
RMS-IV-150-G2	0.1000	5	$2.79x10^{-3}$	25.7	20	1.31	1.07
RMS-IV-150-F2 (control)	no solid	5	$3.76x10^{-3}$	NA	NA	2.25	2.58

Unfortunately, the pH range for the experiment fell outside the preferred range of 2.5-4.0 after mixing for 24 hours, with most samples being above a pH of 4. This may also lead to precipitation; therefore, the experiment was repeated in order to achieve a pH range of 1.5-3.0, as shown in Table 27.

Table 27: Na-Zr hybrid uptake of Y with various pH values 1.4-3.0.

Sample ID	Weight of Hybrid (g)	Volume of Liquid (mL)	Concentration of Y in Sample (M)	Uptake of Y^{3+} (%)	K_d Value (mL/g)	pH Adjusted with HNO_3 Before Shaking	pH after 24 hrs
RMS-IV-170-A	0.0999	5	$2.20x10^{-3}$	33.8	30	1.30	1.40
RMS-IV-170-B	0.1001	5	$1.03x10^{-3}$	69.2	110	1.79	1.95
RMS-IV-170-C	0.1001	5	$2.49x10^{-4}$	92.5	620	2.20	2.57
RMS-IV-170-D	0.1000	5	$7.35x10^{-5}$	97.8	2,200	2.52	2.97
RMS-IV-170-E	no solid	5	$3.33x10^{-3}$	NA	NA	2.82	2.88

Microprobe analysis of RMS-IV-170-A-D was completed on the solid samples after uptake with Yttrium in order to determine Y content. Solid samples were collected and the weight is shown in Table 28.

Table 28: Collection of solid after uptake and ion exchange with yttrium.

Sample ID	Tare Weight (g)	Final Weight (g)	Actual Weight (g)
RMS-IV-170-A	6.0395	6.1394	0.0999
RMS-IV-170-B	6.0023	6.0761	0.0738
RMS-IV-170-C	5.9702	6.0519	0.0817
RMS-IV-170-D	6.0232	6.1166	0.0934

These samples were analyzed by electron microprobe. The samples are mostly homogeneous with a few white spots. There was a large amount of Y but no chlorine was present in the samples. The primary content of these samples is Zr/P, followed by Na/Y. Analyses of these samples were completed with oxygen being done by stoichiometry and carbon by difference. The weight percent content of each element is listed in Table 29.

Table 29: Microprobe analysis of elemental content in weight percent of solid samples.

Sample Type	Sample ID	Y Wt %	Na Wt %	P Wt %	Zr Wt %	C Wt %
Na-Zr x = 1 Grid Analysis	RMS-IV-170-A	0.78	1.5	18.26	29.89	3.99
	RMS-IV-170-B	1.44	1.42	16.81	30.25	4.56
	RMS-IV-170-C	1.96	1.19	17.78	28.99	4.33
	RMS-IV-170-D	1.91	1.37	17.22	28.34	4.87

The sample with the best uptake was RMS-IV-170-D, which had an Yttrium uptake of 97.8% from solution. This sample has 1.91 wt% Yttrium, which is similar to a sample with 92.5 % uptake from RMS-IV-170-C. The comparison and formulae for these samples are shown in Table 30.

Table 30: Elemental content of Zr/Y/Na/P from microprobe analysis.

Sample Type	Sample ID	Ratios
Na-Zr x = 1 Grid Analysis	RMS-IV-170-A	$ZrY_{0.03}Na_{0.20}P_{1.80}$
	RMS-IV-170-B	$ZrY_{0.05}Na_{0.19}P_{1.63}$
	RMS-IV-170-C	$ZrY_{0.07}Na_{0.16}P_{1.81}$
	RMS-IV-170-D	$ZrY_{0.07}Na_{0.19}P_{1.79}$

For all samples, the amount of Yttrium present in the solid sample is close to what was calculated as removed from the solution, as calculated by the concentration difference by ICP-MS. This does not mean that the sample could not have precipitated but the microprobe analysis indicates that the sample is moderately heterogeneous and there were no pockets of yttrium salts detected, leading to the belief that precipitation is not

the dominant mechanism for removal of Y from the solution. The Na-Zr hybrid ion exchanger is likely the dominant contributor to removal of Y from the liquid.

5.6 Conclusion

Recovery of REE from CFL tri-phosphor solutions was achieved by the Na-Zr x = 1 hybrid, which was able to remove 99.9% of Eu and Y. The material had a preference for Y and Eu over Al, with separation factors of Y/Al = 39 and Eu/Al = 52 at pH = 3. Studies at varying pH were conducted to determine if lanthanide precipitation was responsible for the results; however, solids analysis after ion exchange, indicates that precipitation was not the main cause of ion removal from solution and that ion exchange is responsible, as the amount of Y removed was similar to the amount of Na present in the solid. More work will be completed to determine the recyclability of these materials.

5.7 Materials

All chemicals were used as received without further purification. ICP-MS Trace Metals Grade HNO_3 and HCl were purchased from Fisher Scientific. Sodium hydroxide pellets (NaOH, 98%) and aluminum nitrate nonahydrate ($Al(NO_3)_3 \cdot 9H_2O$, 98%) were purchased from Aldrich. Yttrium nitrate hexahydrate ($Y(NO_3)_3 \cdot 6H_2O$, 99.9%), europium nitrate hexahydrate ($Eu(NO_3)_3 \cdot 6H_2O$, 99.9%), cerium nitrate hexahydrate ($Ce(NO_3)_3 \cdot 6H_2O$, 99.9%), and terbium chloride hexahydrate ($TbCl_3 \cdot 6H_2O$, 99.9%) were

purchased from Strem Chemicals. All ICP-MS standards were purchased from Inorganic Ventures. Phillips Soft White, Neutral and Cool White CFLs were purchased from Home Depot. They were opened in a laboratory hood and the white powder was extracted.

CHAPTER VI

CONCLUSIONS AND FUTURE WORK

6.1 Radioactive Separations

As part of our NEUP grant, continued work in this area will revolve around distinct separations of Ln^{3+} from oxidized An to become AnO_2^{+} or AnO_2^{2+}. The oxidants used for An previously have been 0.5 M $Na_2S_2O_8$ or $(NH_4)_2S_2O_8$ with addition of $Ca(OCl)_2$. The goal of this grant is to use our hybrid materials, to facilitate a separation of 3+ ions from those of lower charge 1+.

Completing a large scale separation of lanthanides from actinides has challenges. A large problem for ion exchange is that the best uptake of 3+ ions has been achieved at pH = 3; however, precipitation of the lanthanides and fission products is a critical dilemma at pH = 3. New Zr/Sn phosphonate materials have had better success with lanthanide uptake at pH near 2 but precipitation may still be an issue even at pH 2. What must be completed is a full study of the light and heavy lanthanides uptake at pH 1, 2, and 3, which would result in a simplified detection for which lanthanides have the poorest solubility at pH > 2. Additional studies on the solubility of the lanthanides with the addition of the oxidant (either $Na_2S_2O_8$ or $(NH_4)_2S_2O_8$) must be determined at pH > 2.

After looking at the solubility of the lanthanides, then the focus should be on the actinides at pH 1, 2, and 3, in both the 3+ ion and actinyl (1+, 2+) forms. Oxidation of

the An must be studied more in depth with $Na_2S_2O_8$ or $(NH_4)_2S_2O_8$, specifically looking at how long can multiple An in solution retain the $An(V)O_2^+$ state. The complex environment of multiple ions of different charge may make stability of the An(V) state a problem, especially if $An(VI)O_2^{2+}$ is present or disproportionation occurs.

Once there is a better understanding for lanthanide and actinide separations with the proper conditions, large scale separations will be carried out in collaboration with Linda Wang at Purdue University. Current work is being completed to prepare 20-50 grams of our phosphonate-phosphate hybrids to conduct a column scale separation attempt. Due to limitations of highly radioactive material, these column separation attempts will include U and the lanthanides, with $U(VI)O_2^{2+}$ being the likely oxidation state for U. This may not give a great separation because the U(VI) has an effective charge near 3, and might be removed with the lanthanides. A proof of concept would still be achieved if this oxidation took place at pH > 2 and no precipitation occurred. Recycling studies must also be attempted for the large scale separation attempt, as this has not been attempted previously. Typically, a 1 M HNO_3 solution is enough to remove the M^{3+} ions retained on the column.

Another important item for the NEUP proposal was to determine the structure of the materials. Structural characteristics are being analyzed in collaboration with Simon Billinge at Columbia/BNL. We have prepared samples with and without incorporation of a lanthanide in order to determine how ion exchange is occurring. The materials, which

are poorly crystalline, are being analyzed by PDF/EXAFS for more detailed information on the bond distances and coordination around the Zr, P, and lanthanide. This work is in progress and will continue throughout the next year.

6.2 Cr(VI) Uptake

As part of an investigation on securing a provisional patent on this removal more work must be completed to determine the mechanism for the removal of Cr(VI) with the H-Zr x = 0 material. First, a detailed study including Cr(III) versus Cr(VI) uptake must be attempted with monitoring of oxidation state and separations using traditional cation/anion exchange materials for comparison. This is to ensure that Cr(VI) is actually removed and is not being reduced to Cr(III). If both Cr(III) and Cr(VI) are removed, this would give cause to obtain a provisional patent. Secondly, the structural characteristics and formula for the H-Zr x = 0 material must be determined to better understand how removal is achieved. This would include PDF/EXAFS studies with Cr(VI) incorporated in the material to have a better understanding of how Cr(VI) is removed and how to classify this material as either a sorbent, ion exchange or other mechanistic process.

Another large detail to be determined is whether the material is recyclable. Will the Cr(VI) be easily removable? For Cr(III) removal, a solution of 1 M HNO_3 is rinsed through the column and this leads to a simple recyclable material. If ion exchange is not

taking place then Cr(VI) removal may be more challenging or nearly impossible. This must be investigated before securing a provisional patent.

6.3 Rare Earth Recovery from CFLs

A large problem is that if only the Na-Zr x = 1 hybrid is successful in removing Y and Eu from CFL waste, then what will be the recycling possibilities of this material once the Na is exchanged for Y and Eu? Once the Y and Eu are removed with 1 M HNO_3, the material will now be completely protonated, as opposed to saturated with Na and now be H-Zr x = 1. Can this new material be easily regenerated to the Na-Zr hybrid with simple addition of NaOH or will this require a complicated regeneration phase, which would undoubtedly raise the cost. This experiment must be completed to determine the feasibility and price for this material to complete separations of rare earths from CFL and other waste streams.

6.4 Summary

During my time at Texas A&M, I have been funded by the NEUP and Rare Earth Recovery grants. I was involved with drafting and submitting these grants along with Dr. Clearfield. The collaborations with Dr. Bluemel, SRNL, and LANL have resulted in three first-author publications. Additional work will be released as either a publication or provisional patent.

REFERENCES

(1) Clearfield, A.; Stynes, J. A. *J. Inorg. Nucl. Chem.* 1964, *26*, 117-129.

(2) Troup, J. M.; Clearfield, A. *Inorg. Chem.* 1977, *16*, 3311-3314.

(3) Silbernagel, R.; Díaz, A.; Steffensmeier, E.; Clearfield, A.; Blümel, J. *J. Mol. Catal. A: Chem.* 2014, *394*, 217-223.

(4) Kullberg, L.; Clearfield, A. *J. Phys. Chem.* 1981, *85*, 1585-1589.

(5) Díaz, A.; David, A.; Pérez, R.; González, M. L.; Báez, A.; Wark, S. E.; Zhang, P.; Clearfield, A.; Colón, J. L. *Biomacromolecules* 2010, *11*, 2465-2470.

(6) Díaz, A.; Saxena, V.; González, J.; David, A.; Casanas, B.; Carpenter, C.; Batteas, J. D.; Colón, J. L.; Clearfield, A.; Delwar Hussain, M. *Chem. Commun.* 2012, *48*, 1754-1756.

(7) Wu, H.; Liu, C.; Chen, J.; Yang, Y.; Chen, Y. *Polym. Int.* 2010, *59*, 923-930.

(8) Zhang, Q.; Du, Q.; Jiao, T.; Zhang, Z.; Wang, S.; Sun, Q.; Gao, F. *Sci. Rep.* 2013, *3*, 1-9.

(9) Guenther, J.; Reibenspies, J.; Blümel, J. *Adv. Synth. Catal.* 2011, *353*, 443-460.

(10) Hecker, S. S. *Los Alamos Science* 2000, *26*, 10-15.

(11) World Nuclear Association: http://www.world-nuclear.org/info/Nuclear-Fuel-Cycle/Nuclear-Wastes/Radioactive-Waste-Management/#Notes (accessed November 10, 2013), April 2012.

(12) Nash, K. L.; Lumetta, G. J.; Clark, S. B.; Friese, J. *Separations for the Nuclear Fuel Cycle in the 21st Century*; American Chemical Society, 2006; Vol. 933.

(13) Burns, J. D.; Clearfield, A.; Borkowski, M.; Reed, D. T. *Radiochim. Acta* 2012, *100*, 381-387.

(14) Burns, J. D.; Borkowski, M.; Clearfield, A.; Reed, D. T. *Radiochim. Acta* 2012, *100*, 901-906.

(15) Burns, J. D.; Shehee, T. C.; Clearfield, A.; Hobbs, D. T. *Anal. Chem.* 2012, *84*, 6930-6932.

(16) Burns, J. D. Dissertation, Texas A&M University, 2012.

(17) Cahill, R. S., B.; Peng, G.-Z.; Bortun, L.; Clearfield, A. In *Separation of F-Elements*; Nash, K. L. C., G. R. , Ed.; Plenum Press: New York, 1995, p 165-176.

(18) Silbernagel, R.; Martin, C. H.; Clearfield, A. *Inorg. Chem.* 2016, *55*, 1651-1656.

(19) Silbernagel, R.; Shehee, T. C.; Martin, C. H.; Hobbs, D. T.; Clearfield, A. *Chem. Mater.* 2016, *Accepted*.

(20) Barrera-Díaz, C. E.; Lugo-Lugo, V.; Bilyeu, B. *J. Hazard. Mater.* 2012, *223–224*, 1-12.

(21) *Critical Materials Strategy*, Department of Energy December 2010.

(22) Barbaro, P.; Liguori, F. *Heterogenized Homogeneous Catalysts for Fine Chemicals Production*; Springer: Heidelberg, 2010.

(23) Blümel, J. *Coord. Chem. Rev* 2008, *252*, 2410-2423.

(24) Hartley, F. R. *Supported Metal Complexes*; Reidel D. Publ. Co.: Dordrecht, The Netherlands, 1985.

(25) DeVos, D. E.; Vankelecom, I. F. J.; Jacobs, P. A. *Chiral Catalyst Immobilization and Recycling*; Wiley-VCH: Weinheim, 2000.

(26) Rothenberg, G. *Catalysis: Concepts and Green Applications*; Wiley-VCH: Weinheim, 2008.

(27) Vansant, E. F.; VanDer Voort, P.; Vrancken, K. C. *Characterization and Chemical Modification of the Silica Surface*; Elsevier: Amsterdam, 1995.

(28) Scott, R. P. W. *Silica Gel and Bonded Phases*; John Wiley and Sons: New York, 1993.

(29) Blümel, J. *J. Am. Chem. Soc.* 1995, *117*, 2112-2113.

(30) Behringer, K. D.; Blümel, J. *J. Liq. Chromatogr. Relat. Technol.* 1996, *19*, 2753-2765.

(31) Merckle, C.; Blümel, J. *Chem. Mater.* 2001, *13*, 3617-3623.

(32) Reinhard, S.; Behringer, K. D.; Blümel, J. *New J. Chem.* 2003, *27*, 776-778.

(33) Reinhard, S.; Soba, P.; Rominger, F.; Blümel, J. *Adv. Synth. Catal.* 2003, *345*.

(34) Merckle, C.; Blümel, J. *Adv. Synth. Catal.* 2003, *345*, 584-588.

(35) Merckle, C.; Blümel, J. *Top. Catal.* 2005, *34*, 5-15.

(36) Merckle, C.; Haubrich, S.; Blümel, J. *J. Organomet. Chem.* 2001, *627*, 44-54.

(37) Beele, B.; Guenther, J.; Perera, M.; Stach, M.; Oeser, T.; Blümel, J. *New J. Chem.* 2010, *34*, 2729-2731.

(38) Posset, T.; Blümel, J. *J. Am. Chem. Soc.* 2006, *128*, 8394-8395.

(39) Posset, T.; Guenther, J.; Pope, J.; Oeser, T.; Blümel, J. *Chem. Commun.* 2011, *47*, 2059-2061.

(40) Pope, J. C.; Posset, T.; Bhuvanesh, N.; Blümel, J. *Organometallics* 2014, *33*, 6750-6753.

(41) Cluff, K. J.; Bhunvanesh, N.; Blümel, J. *Chem. Eur. J.* 2015, *21*, 10138-10148.

(42) Yang, Y.; Beele, B.; Blümel, J. *J. Am. Chem. Soc.* 2008, *130*, 3771-3773.

(43) de Vries, J. G.; Elsevier, C. J. *The Handbook of Homogeneous Hydrogenation*; 1st ed.; Wiley-VCH: Weinheim, 2007; Vol. 1-3.

(44) Ertl, G.; Knözinger, F.; Schüth, J. *Handbook of Heterogeneous Catalysis*; 2nd ed.; Wiley-VCH: Weinheim, 2008.

(45) Wende, M.; Meier, R.; Gladysz, J. A. *J. Am. Chem. Soc.*, *123*, 11490-11491.

(46) Knowles, W. S. *Adv. Synth. Catal.* 2003, *345*, 3-13.

(47) Noyori, R. *Adv. Synth. Catal.* 2003, *345*, 15-32.

(48) Crépy, K. V. L.; Imamoto, T. *Adv. Synth. Catal.* 2003, *345*, 79-101.

(49) Heinekey, D. M.; Lledós, A.; Lluch, J. M. *Chem. Soc. Rev.* 2004, *33*, 175-182.

(50) Li, P.; Thitsartarn, W.; Kawi, S. *Ind. Eng. Chem. Res.* 2009, *48*, 1824-1830.

(51) Qingshan, Z.; Chen, D.; Li, Y.; Zhang, G.; Zhang, F.; Fan, X. *Nanoscale* 2013, *5*, 882-885.

(52) Bischoff, S.; Kockritz, A.; Kant, M. *Top. Catal.* 2000, *13*, 327-334.

(53) Bae, J. W.; Park, S. J.; Woo, M. H.; Cheon, J. Y.; Ha, K. S.; W., J. K.; Lee, D. H.; Jung, H. M. *ChemCatChem* 2011, *3*, 1342-1347.

(54) Joshi, R.; Chudasama, U. *Ind. Eng. Chem. Res.* 2010, *49*, 2543-2547.

(55) Mosby, B. M.; Díaz, A.; Bakhmutov, V.; Clearfield, A. *Appl. Mater. Interfaces* 2014, *6*, 585-592.

(56) Ortiz-Avila, C. Y.; Clearfield, A. *Inorg. Chem.* 1985, *24*, 1773-1778.

(57) Casciola, M.; Capitani, D.; Donnadio, A.; Munari, G.; Pica, M. *Inorg. Chem.* 2010, *49*, 3329-3336.

(58) Pica, M.; Donnadio, A.; Troni, E.; Capitani, D.; Casciola, M. *Inorg. Chem.* 2013, *52*, 7680-7687.

(59) Pica, M.; Donnadio, A.; Capitani, D.; Vivani, R.; Troni, E.; Casciola, M. *Inorg. Chem.* 2011, *50*, 11623-11630.

(60) Nakayama, H. *Phosphorus Res. Bull.* 2009, *23*, 1-9.

(61) Díaz, A.; Mosby, B. M.; Bakhmutov, V. I.; Martí, A. A.; Batteas, J. D.; Clearfield, A. *Chem. Mater.* 2013, *25*, 723-728.

(62) Mejia, A. F.; Díaz, A.; Pullela, S.; Chang, Y.-W.; Simonetty, M.; Carpenter, C.; Batteas, J. D.; Mannan, M. S.; Clearfield, A.; Cheng, Z. *Soft Matter* 2012, *8*, 10245-10253.

(63) Sommer, J.; Yang, Y.; Rambow, D.; Blümel, J. *Inorg. Chem.* 2004, *43*, 7561-7563.

(64) Blümel, J. *Inorg. Chem.* 1994, *33*, 5050-5056.

(65) Posset, T.; Rominger, F.; Blümel, J. *Chem. Mater.* 2005, *17*, 586-595.

(66) Hilliard, C. R.; Bhuvanesh, N.; Gladysz, J. A.; Blümel, J. *Dalton Trans.* 2012, *41*, 1742-1754.

(67) Sun, L.; Boo, W. J.; Sue, H.-J.; Clearfield, A. *New J. Chem.* 2007, *31*, 39-43.

(68) Fyfe, C. A. *Solid-State Nmr for Chemists*; C.F.C. Press: Guelph, Canada, 1983.

(69) Duncan, T. M. *A Compilation of Chemical Shift Anisotropies*; Farragut Press: Chicago, IL, 1990.

(70) Wong, M.; Guenther, J.; Sun, L.; Blümel, J.; Nishimura, N.; Sue, H.-J. *Adv. Funct. Mater.* 2012, *22*, 3614-3624.

(71) Pica, M.; Donnadio, A.; Capitani, D.; Vivani, R.; Troni, E.; Casciola, M. *Inorg. Chem.* 2011, *50*, 11623-11630.

(72) Dines, M. B.; Cooksey, R. E.; Griffith, P. C.; Lane, R. H. *Inorg. Chem.* 1983, *22*, 1003-1004.

(73) Dines, M. B.; DiGiacomo, P. M. *Inorg. Chem.* 1981, *20*, 92-97.

(74) Dines, M. B.; Digiacomo, P. M.; Callahan, K. P.; Griffith, P. C.; Lane, R. H.; Cooksey, R. E. In *Chemically Modified Surfaces in Catalysis and Electrocatalysis*; American Chemical Society: 1982; Vol. 192, p 223-240.

(75) Alberti, G.; Casciola, M.; Vivani, R.; Biswas, R. K. *Inorg. Chem.* 1993, *32*, 4600-4604.

(76) Alberti, G. In *Comprehensive Supramolecular Chemistry*; Alberti, G., Bein, T., Eds.; Pergamon Elsevier: Tarrytown, N.Y., 1996; Vol. 7, p 151-188.

(77) Alberti, G.; Casciola, M.; Costantino, U.; Vivani, R. *Adv. Mater.* 1996, *8*, 291-303.

(78) Wang, J. D.; Clearfield, A.; Guang-Zhi, P. *Mater. Chem. Phys.* 1993, *35*, 208-216.

(79) Clearfield, A.; Demadis, K. *Metal Phosphonate Chemistry: From Synthesis to Applications*; Royal Society of Chemistry: Cambridge, U.K., 2012.

(80) Clearfield, A. *Chem. Mater.* 1998, *10*, 2801-2810.

(81) Clearfield, A.; Wang, Z. *J. Chem. Soc., Dalton Trans.* 2002, 2937-2947.

(82) Cocke, D. L.; Clearfield, A. *Design of New Materials*; Springer US: Plenum Press, New York, 1987.

(83) Luca, V.; Hanna, J. V. *Hydrometallurgy* 2015, *154*, 118-128.

(84) Veliscek-Carolan, J.; Hanley, T. L.; Luca, V. *Sep. Purif. Technol.* 2014, *129*, 150-158.

(85) Clearfield, A. *Dalton Trans.* 2008, *44*, 6089-6102.

(86) Medoukali, D.; Hubert Mutin, P.; Vioux, A. *J. Mater. Chem.* 1999, *9*, 2553-2557.

(87) Poojary, M. D.; Hu, H. L.; Campbell, F. L., III; Clearfield, A. *Acta Crystallogr., Sect. B: Struct. Sci* 1993, *B49*, 996-1001.

(88) Stuart, B. H. In *Infrared Spectroscopy: Fundamentals and Applications*; John Wiley & Sons, Ltd: 2005, p 71-93.

(89) Kim, H.-N.; Keller, S. W.; Mallouk, T. E.; Schmitt, J.; Decher, G. *Chem. Mater.* 1997, *9*, 1414-1421.

(90) Hilliard, C. R.; Kharel, S.; Cluff, K. J.; Bhuvanesh, N.; Gladysz, J. A.; Blümel, J. *Chem. Eur. J* 2014, *20*, 17292-17295.

(91) Hirao, T.; Masunaga, T.; Yamada, N.; Ohshiro, Y.; Agawa, T. *Bull. Chem. Soc. Jpn.* 1982, *55*, 909-913.

(92) Alberti, G. *Acc. Chem. Res.* 1978, *11*, 163-176.

(93) Alberti, G.; Costantino, U.; Szirtes, L. *Radiat. Phys. Chem.* 1997, *50*, 369-376.

(94) Frey, B. L.; Hanken, D. G.; Corn, R. M. *Langmuir* 1993, *9*, 1815-1820.

(95) Gomez-Alcantara, M. d. M.; Cabeza, A.; Olivera-Pastor, P.; Fernandez-Moreno, F.; Sobrados, I.; Sanz, J.; Morris, R. E.; Clearfield, A.; Aranda, M. A. G. *Dalton Trans.* 2007, 2394-2404.

(96) Gallios, G.; Vaclavikova, M. *Environ. Chem. Lett.* 2008, *6*, 235-240.

(97) Guo, F.-y.; Liu, Y.-g.; Wang, H.; Zeng, G.-m.; Hu, X.-j.; Zheng, B.-h.; Li, T.-t.; Tan, X.-f.; Wang, S.-f.; Zhang, M.-m. *RSC Adv.* 2015, *5*, 45384–45392.

(98) Lei, Z.; Zhai, S.; Lv, J.; Fan, Y.; An, Q.; Xiao, Z. *RSC Adv.* 2015, *5*, 77932-77941.

(99) Wang, H.; Yuan, X.; Wu, Y.; Chen, X.; Leng, L.; Zeng, G. *RSC Adv.* 2015, *5*, 32531-32535.

(100) Tandukar, M.; Huber, S. J.; Onodera, T.; Pavlostathis, S. G. *Environ. Sci. Technol.* 2009, *43*, 8159-8165.

(101) Augustynowicz, J.; Grosicki, M.; Hanus-Fajerska, E.; Lekka, M.; Waloszek, A.; Koloczek, H. *Chemosphere* 2010, *79*, 1077-1083.

(102) Barikbin, B.; Mortazavi, S. B.; Moussavi, G. *Desalin. Water Treat.* 2015, *53*, 1895-1901.

(103) Kusku, O.; Rivas, B. L.; Urbano, B. F.; Arda, M.; Kabay, N.; Bryjak, M. *J. Chem. Technol. Biotechnol.* 2014, *89*, 851-857.

(104) Yang, J.; Yu, M.; Qiu, T. *J. Ind. Eng. Chem.* 2014, *20*, 480-486.

(105) Xiao, K.; Han, G.; Li, J.; Dan, Z.; Xu, F.; Jiang, L.; Duan, N. *RSC Adv.* 2016, *6*, 5233-5239.

(106) Anger, G.; Halstenberg, J.; Hochgeschwender, K.; Scherhag, C.; Korallus, U.; Knopf, H.; Schmidt, P.; Ohlinger, M. In *Ullmann's Encyclopedia of Industrial Chemistry*; Wiley-VCH Verlag GmbH & Co. KGaA: 2000.

(107) Du, X.; Graedel, T. E. *Environ. Sci. Technol.* 2011, *45*, 4096-4101.

(108) Haxel, G. B.; Hedrick, J. B.; Orris, G. J.; USGS: http://pubs.usgs.gov/fs/2002/fs087-02/, 2002, p 1-4.

(109) Janeway, K. In *Consumer Reports* http://www.consumerreports.org/cro/news/2011/04/despite-mercury-concerns-few-people-recycle-their-cfls/index.htm, 2011.

(110) Solvay Press Release 2012. http://www.solvay.com/en/media/press_releases/20120927-coleopterre.html (accessed February 1, 2016).

APPENDIX A

COMPOUND CATALOG

A.1 Immobilized Catalyst Work

Included in Figure 42 are all the compounds listed in Chapter II.

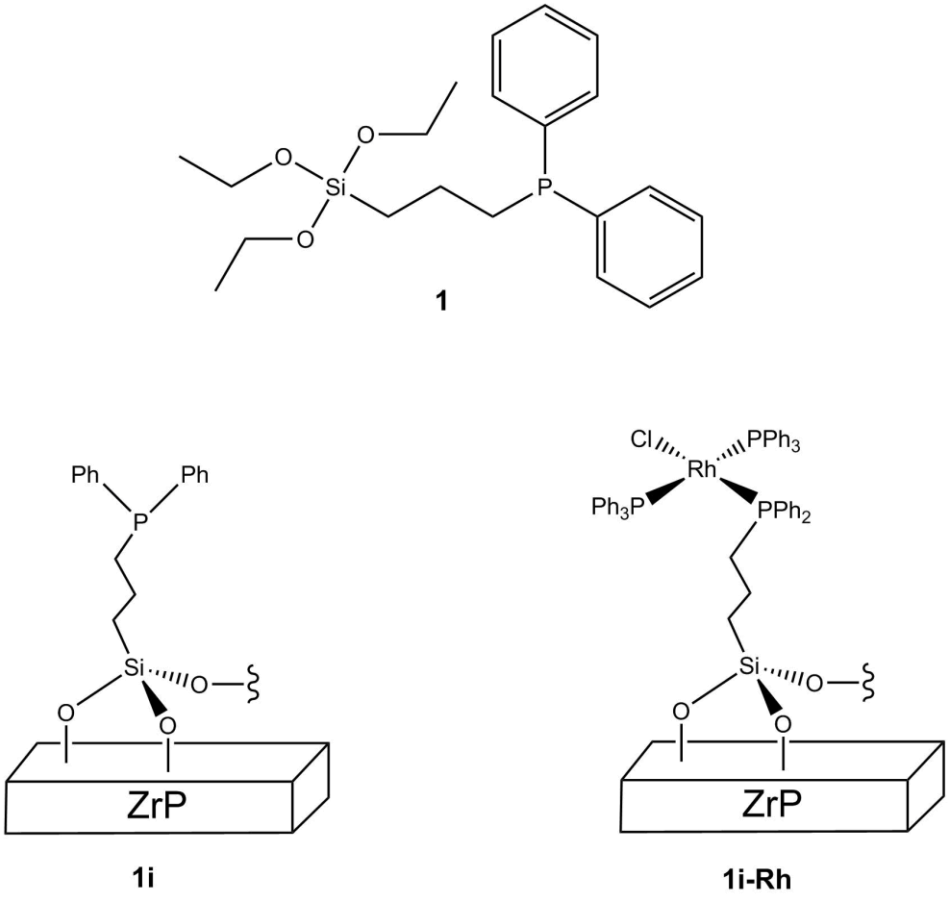

Figure 42: Schematic of compounds from Chapter II.

A.2 Table of Materials Prepared

Many samples were prepared for work related to Chapters III, IV, and V. A whole range of materials were newly prepared and some were synthesized for comparison to previous published works.[13-16]

Sample IDs are listed for easy reference from thesis to the lab notebook. The basic formula for these materials is $M(O_3PC_6H_4PO_3)_{1-x/2}(APO_4)_x \bullet nH_2O$, where M= Zr^{4+}, Sn^{4+}; A = H, Na, K; and x = 0, 0.5, 0.8, 1, 1.33, 1.6, as listed in Table 31.

Elemental analysis was completed by Robertson Microlit, microprobe analysis was completed at Texas A&M, and TGA with 90% Air / 10% N_2 on the Clearfield TA unit. These analyses were completed on unaltered bench-top samples (the samples were not dried beforehand), unless otherwise specified.

Table 31: Zr or Sn phosphonate-phosphates prepared and their analytical data.

Sample Type	Notebook ID	TGA Weight Loss %		Microprobe Analysis Wt%				Elemental Analysis Wt%	
		200 C	1000 C	Zr or Sn	P	Cl	Na or K	C	H
H-Zr x = 0	CHM-I-15-A	8.92	27.18	22.8752	14.6421	0.2443	NA	17.71	2.23
H-Zr x = 0.5	CHM-I-15-B	9.83	25.35	25.6958	16.1091	0.2805	NA	14.46	2.35
H-Zr x = 0.8	CHM-I-15-C	9.46	24.4	28.2495	17.2174	0.1108	NA	12.25	2.12
H-Zr x = 1	RMS-II-54	12.54	24.89	28.8752	16.7731	1.14	NA	7.90	2.38
H-Zr x = 1.33	CHM-I-15-D	7.49	18.02	30.4734	18.058	0.1751	NA	7.52	1.98
H-Zr x = 1.6	CHM-I-15-E	7.05	18.92	31.9613	18.1563	0.0578	NA	4.67	1.86
Na-Zr x = 0.5	CHM-I-21-A	10.83	26.22	25.8576	16.8693	0.0357	0	14.23	2.11
Na-Zr x = 0.8	CHM-I-21-B	8.92	20.89	25.7738	16.2597	0.058	3.9256	NA	NA
Na-Zr x = 1	RMS-II-84	7.61	18.13	27.1292	15.6919	0.0988	6.1191	8.21	1.92
Na-Zr x = 1.33	CHM-I-21-D	7.32	11.32	31.9058	14.104	0.0173	8.6139	NA	NA
Na-Zr x = 1.6	CHM-I-21-E	11.9	13.85	38.6699	10.6574	0.0086	8.1725	NA	NA
H-Sn x = 0	CHM-I-2-A	10.73	29.09	31.002	14.9594	1.5431	NA	16.93	2.51
H-Sn x = 0.5	CHM-I-2-B	9.74	25.66	32.7896	15.1414	1.6981	NA	13.15	2.46
H-Sn x = 0.8	CHM-I-2-C	8.84	22.3	34.1649	15.8421	0.6689	NA	11.1	2.32
H-Sn x = 1	RMS-II-65	13.92	27.85	35.011	14.585	2.44	NA	9.02	2.47
H-Sn x = 1.33	CHM-I-2-D	8.86	19.75	36.7462	16.067	0.9379	NA	6.59	1.99
H-Sn x = 1.6	CHM-I-2-E	11.3	55.87	37.345	15.3808	1.6946	NA	4.08	1.78
Na-Sn x = 0.5	RP-I-1-A	7.44	23.83	32.4803	15.0304	2.4103	0.3337	NA	NA
Na-Sn x = 0.8	RP-I-1-B	6.94	21.04	31.12	14.39	1.40	0.62	NA	NA
Na-Sn x = 1	RMS-II-74	10.39	23.21	35.2505	15.0753	0.9487	0.7253	8.99	2.42
Na-Sn x = 1.33	RP-I-1-D	10.08	21.26	38.1686	14.5675	1.4788	0.6173	NA	NA
Na-Sn x = 1.6	RP-I-1-E	7.62	17.33	44.92	11.6519	1.325	3.2451	NA	NA
K-Sn x = 0.5	CHM-I-9-A	9.85	25.64	32.2067	15.9013	1.4293	0.4845	13.14	2.07
K-Sn x = 0.8	CHM-I-9-B	9.51	23.18	33.6752	15.892	0.8079	0.6202	11.22	2.23
K-Sn x = 1	RMS-II-126	9.48	21.87	36.0898	14.6886	0.3227	0.7767	9.44	2.24
K-Sn x = 1.33	CHM-I-9-C	9.21	18.71	37.2682	15.6342	0.1292	1.5375	4.36	1.09
K-Sn x = 1.6	CHM-I-9-D	8.08	15.44	40.7273	14.4183	0.0305	3.4262	4.47	1.59

A.3 PXRD and TGA Data for Samples

PXRD and TGA Comparisons between H-Zr, Na-Zr, H-Sn, Na-Sn, and K-Sn x= 0, 0.5, 0.8, 1.33, 1.6 can be seen in Figures 43-52.

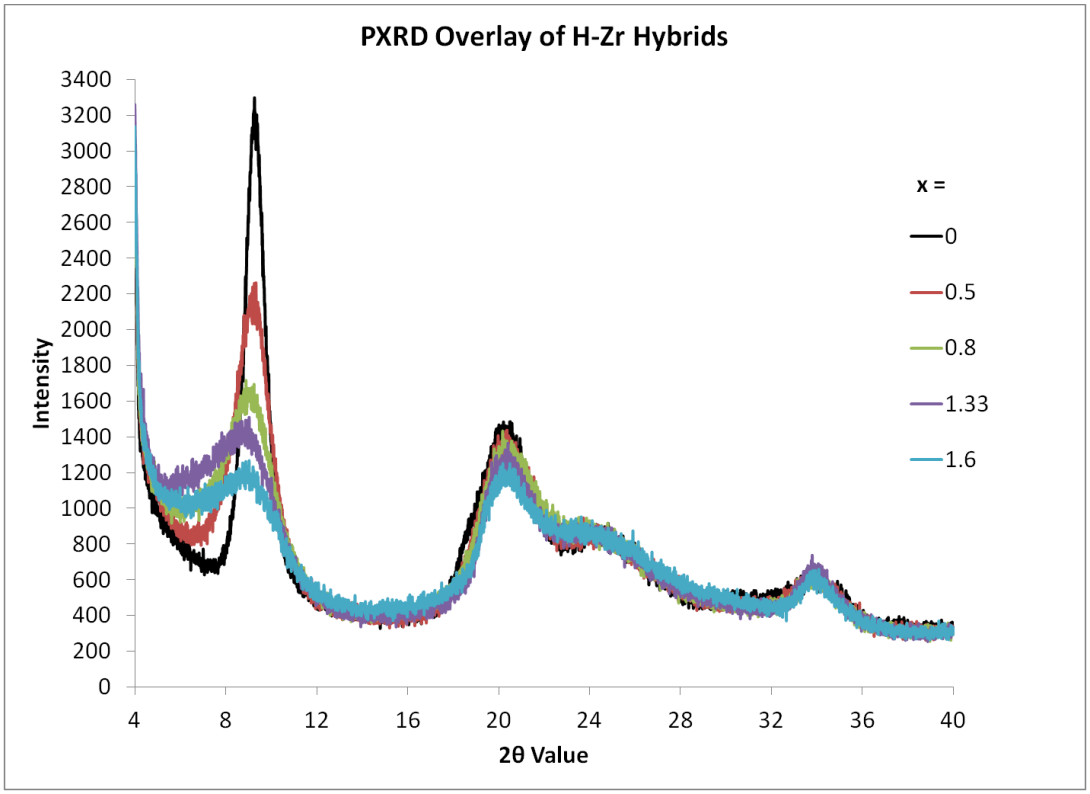

Figure 43: PXRD overlay of H-Zr x = 0, 0.5, 0.8, 1.33, 1.6 samples.

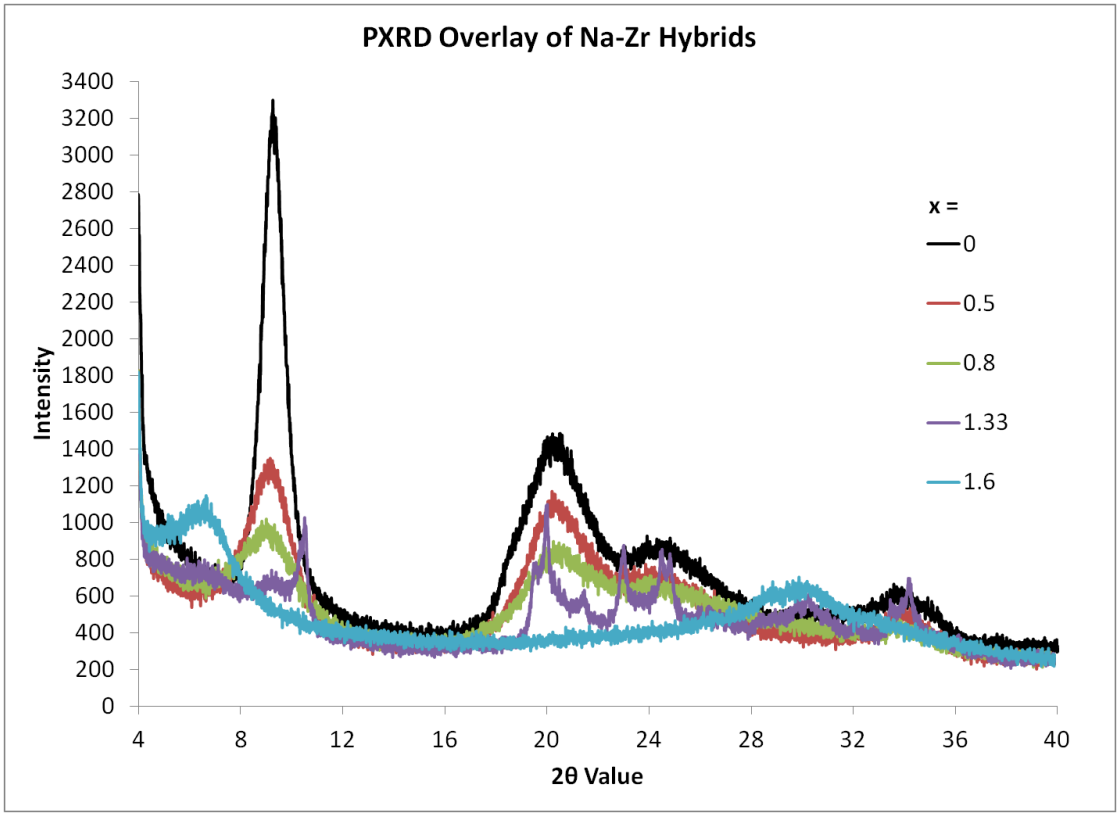

Figure 44: PXRD overlay of Na-Zr x = 0, 0.5, 0.8, 1.33, 1.6 samples.

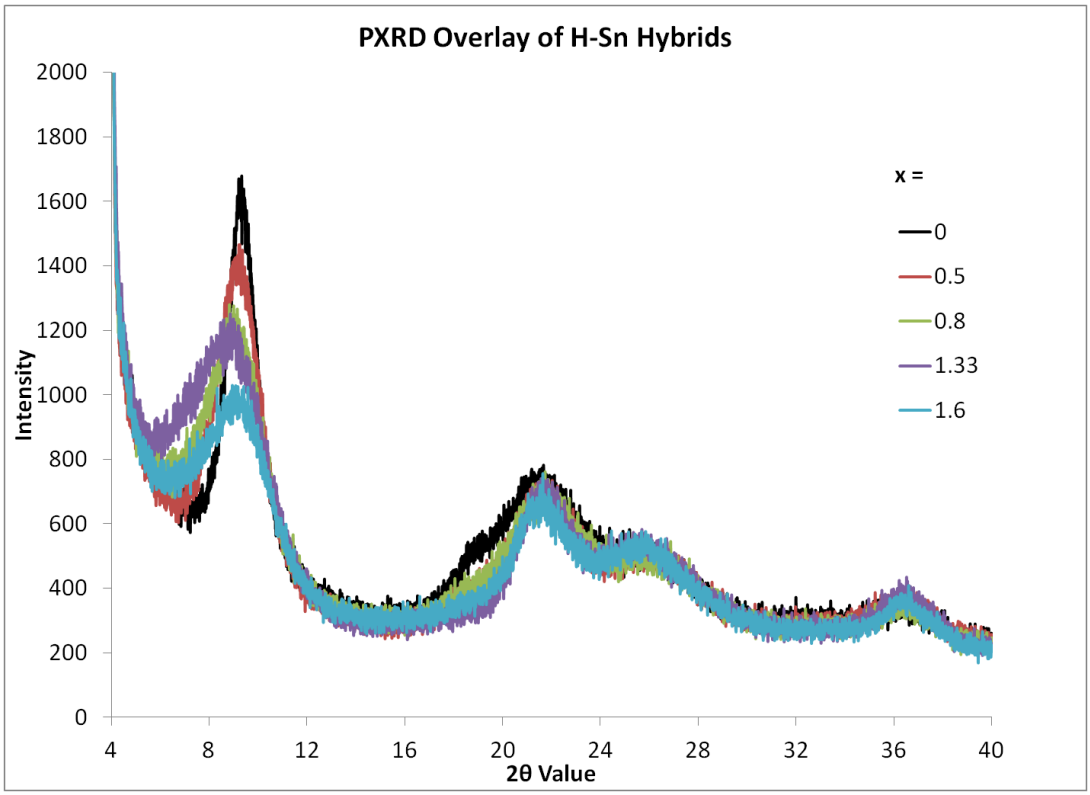

Figure 45: PXRD overlay of H-Sn x = 0, 0.5, 0.8, 1.33, 1.6 samples.

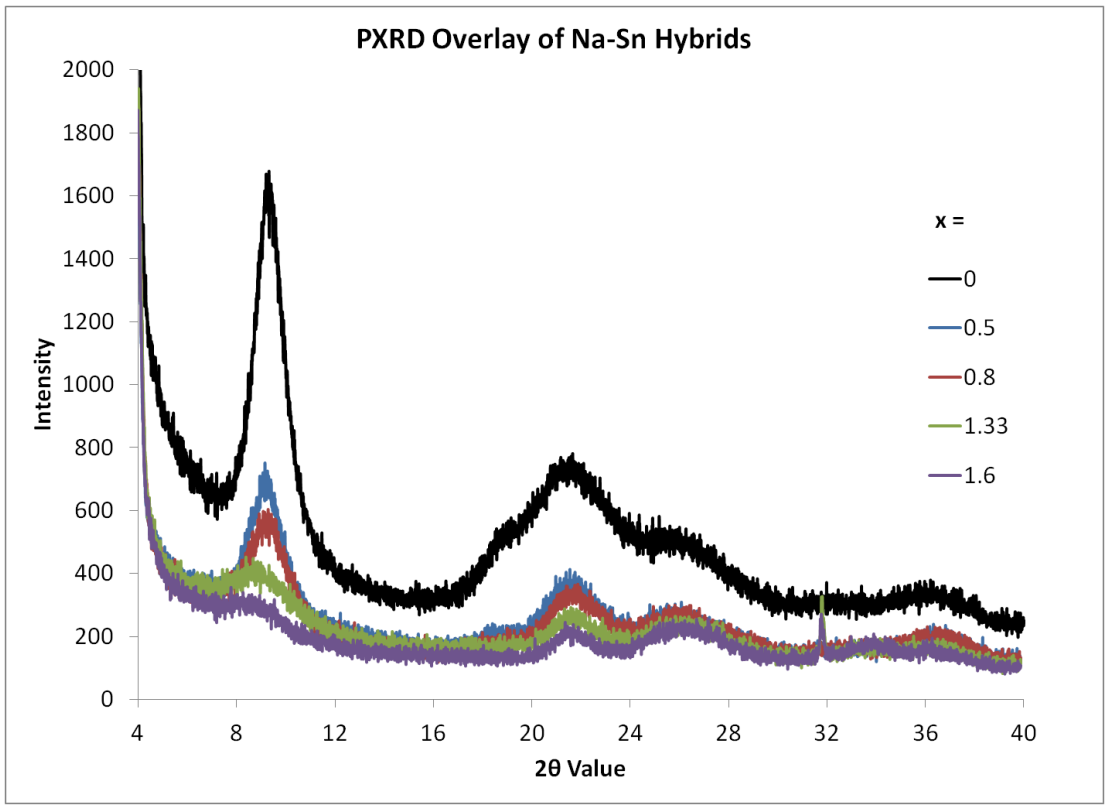

Figure 46: PXRD overlay of Na-Sn x = 0, 0.5, 0.8, 1.33, 1.6 samples.

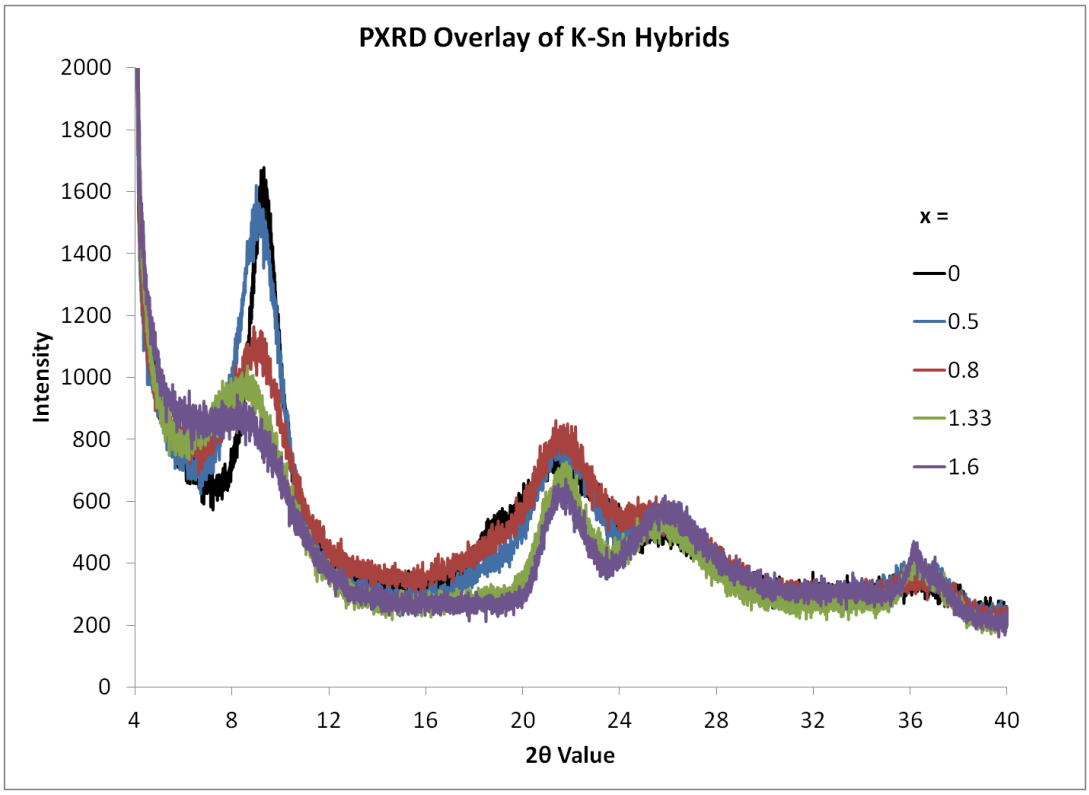

Figure 47: PXRD overlay of K-Sn x = 0, 0.5, 0.8, 1.33, 1.6 samples.

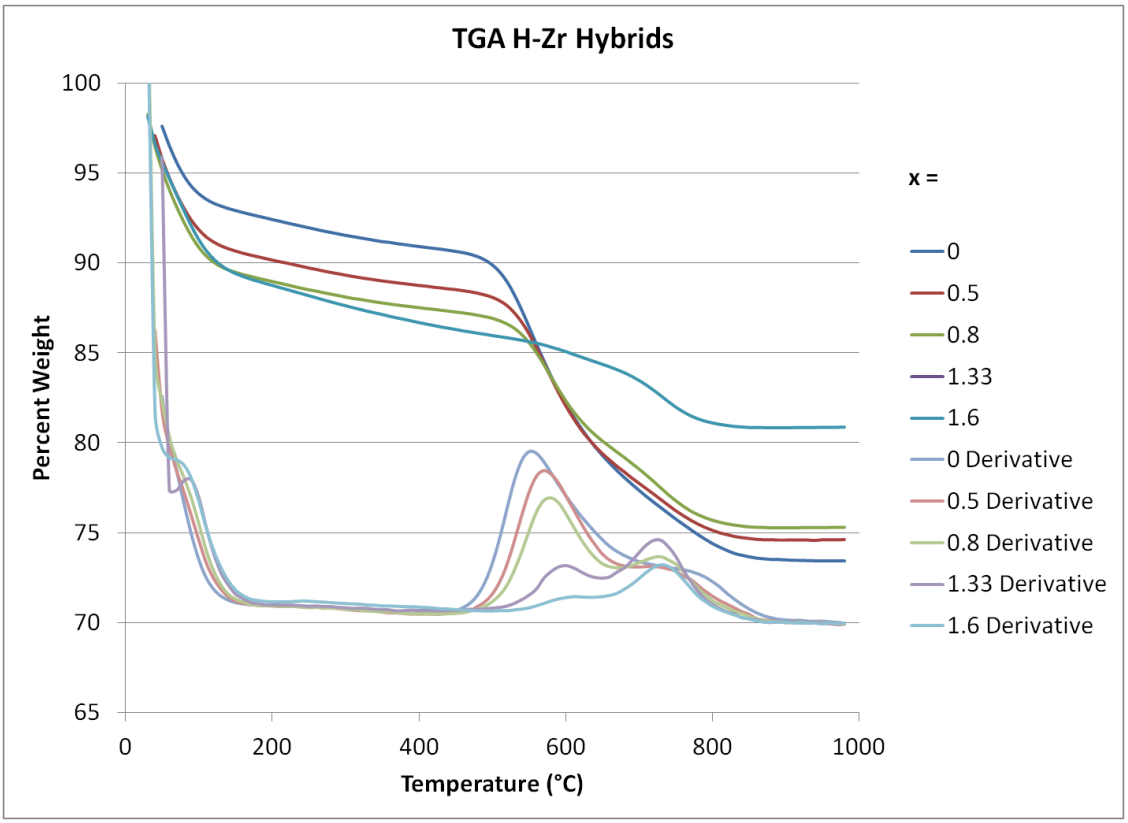

Figure 48: TGA overlay of H-Zr x = 0, 0.5, 0.8, 1.33, 1.6 samples.

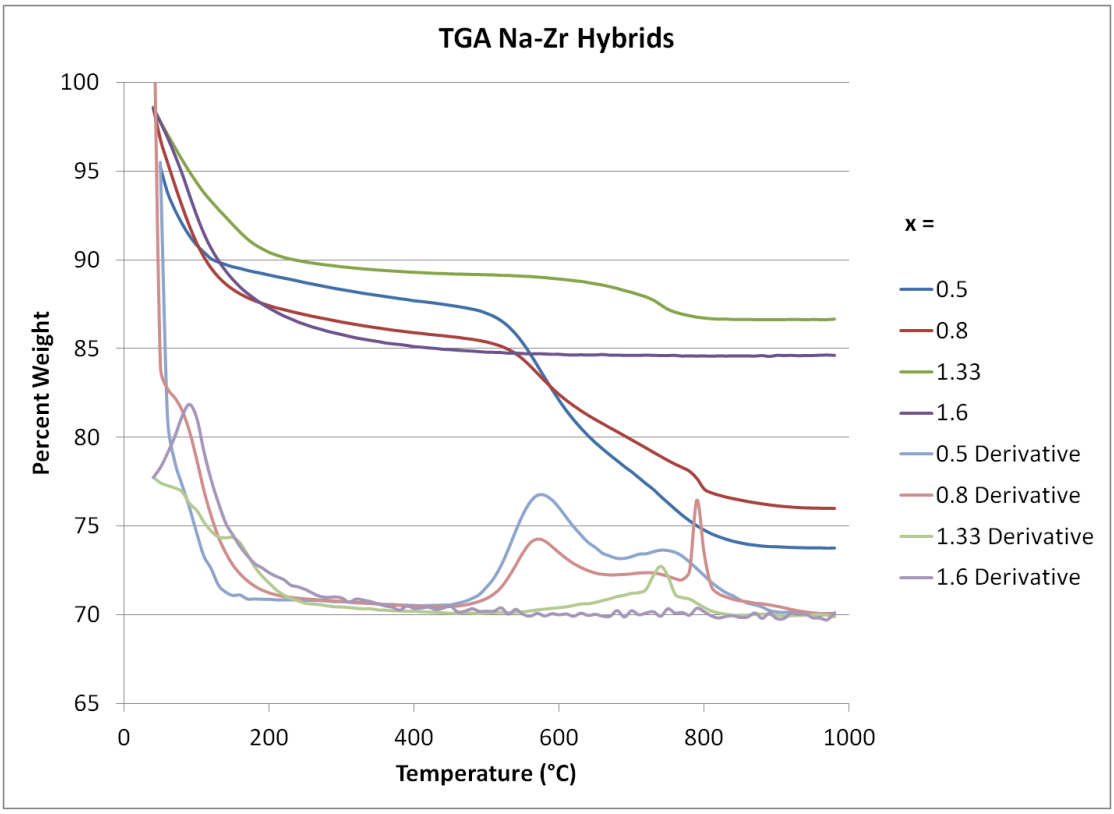

Figure 49: TGA overlay of Na-Zr x = 0.5, 0.8, 1.33, 1.6 samples.

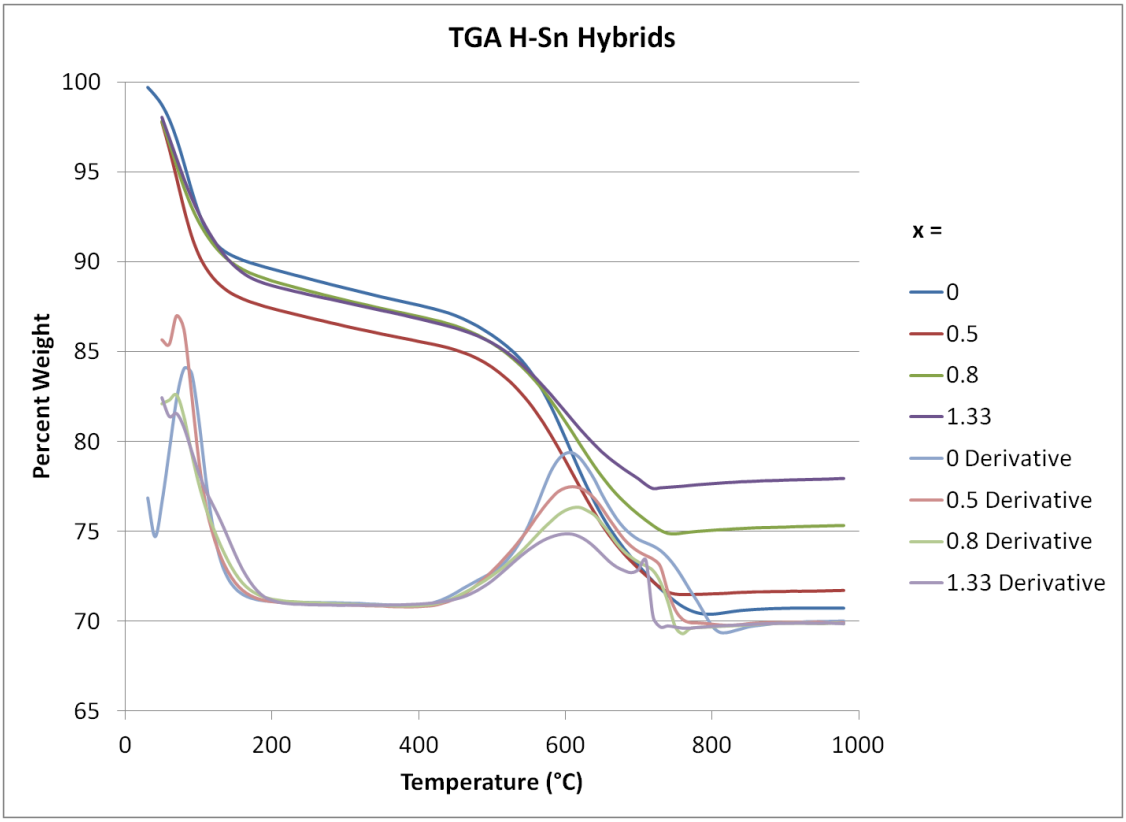

Figure 50: TGA overlay of H-Sn x = 0, 0.5, 0.8, 1.33 samples.

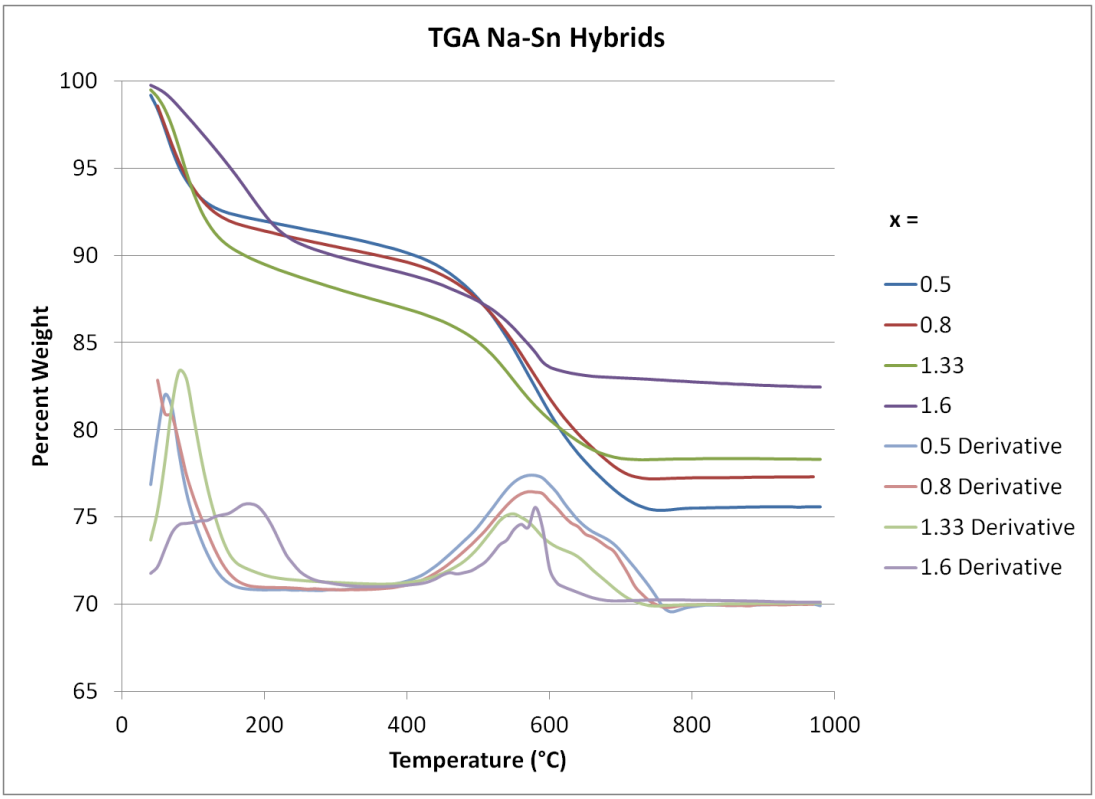

Figure 51: TGA overlay of Na-Sn x = 0.5, 0.8, 1.33, 1.6 samples.

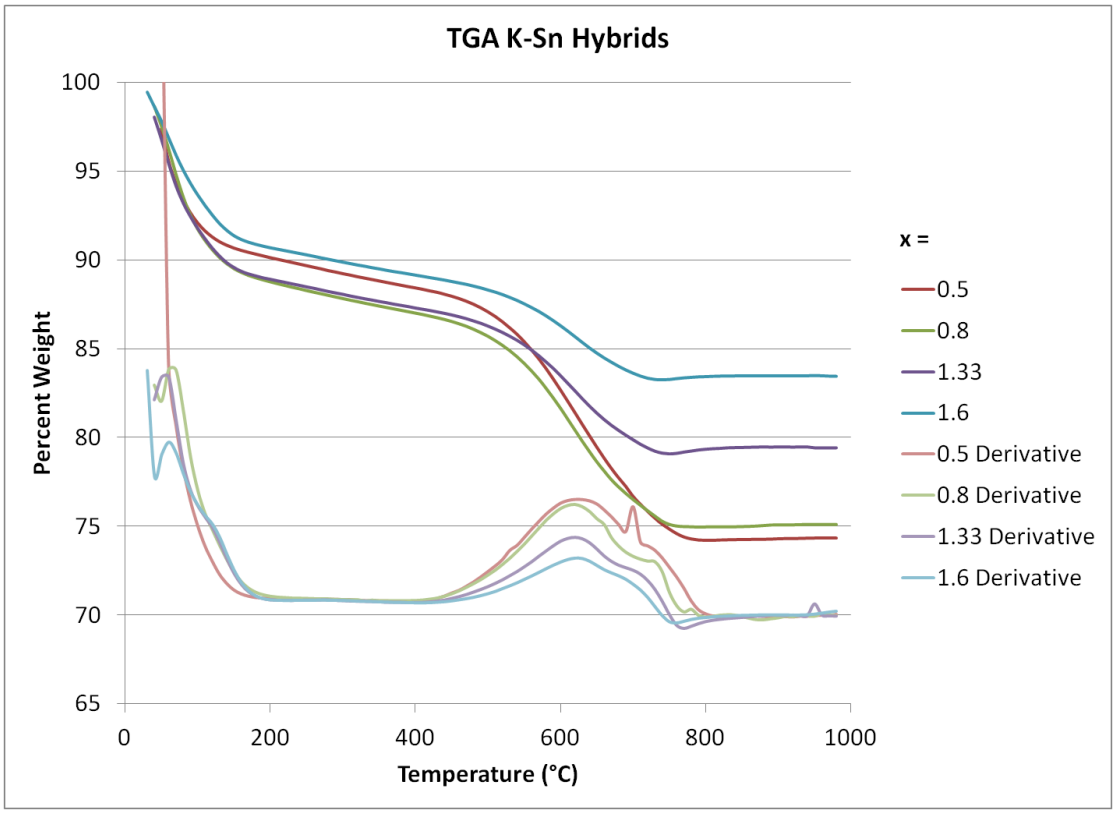

Figure 52: TGA overlay of K-Sn x = 0.5, 0.8, 1.33, 1.6 samples.

A.4 Capacity Studies on H-Zr, Na-Zr, H-Sn, and Na-Sn x = 1 Samples

Capacity studies on H-Zr and H-Sn samples were included in Chapter III and IV. Titration studies were completed with other samples to provide additional information on previously published materials. Traditionally, the Na-Sn x = 1 hybrid incorporates a small amount of Na compared to the Na-Zr x = 1 variety. This is verified from the materials prepared by RMS, where the Na-Sn x = 1 sample has 0.74 wt% Na and the Na-Zr x = 1 hybrid has 6.12 wt% Na, as seen in Table 31.

Titrimetry was completed on H-Zr, Na-Zr, H-Sn, and Na-Sn x = 1 samples. First, ion exchange with 25 mL $1x10^{-3}$ M Eu^{3+} solution was achieved by stirring the solid (~0.1 g) for 1 hour, as the pH was monitored, as shown in Table 32. As discussed previously in Chapter V, the Na-Zr hybrid is the only material where the pH increases after addition of the Eu solution. For the other samples, the pH decreases as protons are exchanged for Eu, thus lowering the pH of the solution. Due to the low Na content in the Na-Sn x = 1 sample, protons are still predominately released over Na ions.

Table 32: Change of pH from addition of samples in $1x10^{-3}$ M Eu^{3+} solution.

Before Titration, Monitoring pH	x = 1			
	H-Zr	Na-Zr	H-Sn	Na-Sn
Amount of Hybrid (g)	0.1001	0.0996	0.1001	0.0998
pH Before Addition of Solid	3.04	3.05	3.06	3.05
pH at 15 Seconds After Addition	2.56	4.35	2.74	2.91
pH at 1 Minute After Addition	2.48	5.20	2.62	2.83
pH at 60 Minutes After Addition	2.40	7.28	2.33	2.49

After stirring the solid in the Eu solution for 1 hour, the solution appeared opaque and milky white. With constant monitoring of pH, 0.0958 M NaOH was manually added into the Eu/Hybrid liquid stirring below. The typical scenario involved a sharp increase in the pH followed by a delayed increase of pH above 8. After the pH remained over 10, the titration was stopped. The amount of NaOH added to achieve a pH well above 10 was used to determine the mmol of H+ present. Dividing the H+ mmol capacity by the amount of hybrid used in grams resulted in the capacity value (mmol/g), as shown in Table 33.

Table 33: Capacity study of hybrids with $1x10^{-3}$ M Eu^{3+} at pH = 3 and 0.0958 M NaOH.

x = 1	Amount of Sample (g)	Capacity Eu^{3+} (mmol/g)	Capacity H^{+} (mmol/g)
H-Zr	0.1001	1.28	3.83
Na-Zr	0.0996	0.32	0.96
H-Sn	0.1001	1.37	4.12
Na-Sn	0.0998	1.18	3.55

Since the Na-Zr x = 1 hybrid is already at a pH above 7 before titration begins, the amount of NaOH required to reach 10 is small, which explains the lower value in Table 33.